Effects of Time-Doses and Cycle-Doses of Acute Vibration Exposure on Apoptotic Cell Death and TNF-α Signaling in the Vocal Fold Epithelium

By

Carolyn K. Novaleski

Dissertation

Submitted to the Faculty of the

Graduate School of Vanderbilt University

in partial fulfillment of the requirements

for the degree of

DOCTOR OF PHILOSOPHY

in

Hearing and Speech Sciences

August, 2016

Nashville, Tennessee

Approved:

Bernard Rousseau, Ph.D., Chair

Stephen M. Camarata, Ph.D.

Bruce D. Carter, Ph.D.

Preeti M. Sivasankar, Ph.D.

To my lab mates,

Tsuyoshi, Carla, Renee, Masanobu, Hongmei, Emily, Maria, and Takashi.

And for Edward “Ted” V. MacArthur

(1943–2016).

ACKNOWLEDGEMENTS

This research was supported by the National Institute on Deafness and Other Communication Disorders (NIDCD) of the National Institutes of Health (NIH) under Award Numbers F31DC014621 and R01DC011338. The content is solely the responsibility of the author and does not necessarily represent the official views of the NIH. Portions of this research were supported by a Vanderbilt University Graduate School Dissertation Enhancement Grant, Vanderbilt Institute for Clinical and Translational Research funded by the National Center for Advancing Translational Services of the NIH under the Clinical and Translational Service Award UL1TR000445, and Vanderbilt University Department of Otolaryngology.

Experiments and data analysis of transmission electron microscopy were performed through the use of the Vanderbilt University Medical Center Cell Imaging Shared Resource, which is supported by the NIH under Award Numbers CA68485, DK20593, DK58404, DK59637, and EY08126. Paraffin tissue embedding was performed through the use of the Vanderbilt University Medical Center Translational Pathology Shared Resource, which is supported by the National Cancer Institute of the NIH Cancer Center Support Grant 2P30 CA068485-14 and Vanderbilt Mouse Metabolic Phenotyping Center Grant 5U24DK059637-13.

I would like to acknowledge my mentors for their support during my journey. In particular, I will remain forever grateful to the chair of my dissertation committee, Professor Bernard Rousseau, Ph.D., CCC-SLP. Dr. Rousseau guided me for the past four years throughout my Ph.D. program and taught me that perfect is the enemy of good. As his first doctoral student, I most appreciate his passion to mentor others and desire to learn from others in the process. I am also thankful to the members of my dissertation committee, Dr. Stephen Camarata, Dr. Bruce

Carter, and Dr. Preeti Sivasankar, for offering substantial insight and recommendations that improved the quality of this project. Thank you to Dr. Masanobu Mizuta, Dr. Hongmei Wu, and Ms. Emily Kimball for technical assistance with portions of this work. Finally, I would like to thank my family and friends who supported me to pursue my goals, encouraged me to do what makes me happy, and reminded me of what is truly important in life.

TABLE OF CONTENTS

LIST OF TABLES

LIST OF FIGURES

Figure Page

LIST OF ABBREVIATIONS

3’-OH ..... hydroxyl ends

ANOVA ..... analysis of variance

Bcl-2 ..... B cell lymphoma 2

BSA ..... bovine serum albumin

DAPI ..... 4',6-diamidino-2-phenylindole

DN ..... deoxyribonucleic

DNase ..... deoxyribonuclease

F_0 ..... fundamental frequency

FITC ..... fluorescein isothiocyanate

HAS ..... hyaluronic acid synthase

HSD ..... Honestly Significant Difference

H&E ..... hematoxylin and eosin

PBS ..... phosphate buffered saline

PCR ..... polymerase chain reaction

qRT-PCR ..... quantitative real-time polymerase chain reaction

SCC ..... squamous cell carcinoma

SDHA ..... succinate dehydrogenase complex subunit A

tDt ..... terminal deoxynucleotidyl transferase

TEM ..... transmission electron microscopy

TNF-α ..... tumor necrosis factor-alpha

TUNEL ..... terminal deoxynucleotidyl transferase dUTP nick end labeling

CHAPTER I

INTRODUCTION

Voice disorders occur in nearly one-third of the population in the United States (Roy, Merrill, Gray, & Smith, 2005). Clinically, the hallmark symptom of a voice disorder is dysphonia, which refers to a listener's auditory perception of abnormal voice quality. For patients, dysphonia compromises communication function and quality of life (Behrman, Sulica, & He, 2004). In annual healthcare costs, voice disorders account for an estimated $11.9-13.5 billion in the United States alone (Cohen, Kim, Roy, Asche, & Courey, 2012). Moreover, the occupational impact of voice disorders includes absenteeism and decreased work productivity (de Medeiros, Assuncao, & Barreto, 2012). Voice disorders, therefore, pose a significant burden to patients, healthcare, and society[1].

The vocal folds are involved in producing sound during vibration (i.e., phonation). Phonation occurs through the coordinated effort of air from the lungs passing through the approximated vocal folds, which results in repeated cycles of vibration. Listeners then internally synthesize the physical production of the voice signal, which is perceived as normal or dysphonic voice quality (Kreiman & Sidtis, 2011). An overarching objective of research in voice science is to understand the underlying vocal fold tissue changes that lead to dysphonia. The work in this dissertation will expand the current state of knowledge regarding apoptosis, a type of programmed cell death, in the epithelial tissue that covers the vocal folds. This study

[1] The challenges associated with voice disorders have received significant attention. Specifically, the National Institute on Deafness and Other Communication Disorders identified the health-related impact of voice disorders as a high priority area (*National Institute on Deafness and Other Communication Disorders 2012-2016 Strategic Plan*).

begins to investigate the effects of increasing durations of vocal fold vibration exposure on apoptosis signaling. Findings will serve as an important foundation for future studies designed to examine the role of normal and abnormal apoptosis in vocal fold disease. Long-term, this study may lead to the development of novel approaches for the prevention, diagnosis, and management of voice disorders.

Problem Statement

The surface cell layer of the membranous true vocal folds is comprised of stratified squamous epithelium (Gray, 2000). Healthy epithelium is necessary for the vocal folds to vibrate and respond to changes in the external environment. In contrast, abnormal vocal fold epithelium presents clinically in many voice disorders. Common voice disorders that affect the epithelium include laryngeal squamous cell carcinoma (SCC) and benign lesions. Additionally, surgical and medical interventions for voice disorders can adversely interfere with the epithelial layer. The most notable interventions impacting the epithelium are phonomicrosurgery to remove vocal fold lesions and radiation therapy to treat head and neck cancer.

The vocal fold epithelium serves several important biological functions that contribute to maintaining an ideal environment for normal vibratory function. Among these functions, a major role of the epithelium is to protect the underlying tissue by forming a barrier. The epithelial barrier divides the boundary between the external environment from the underlying connective tissue (Ross, Kaye, & Pawlina, 2003). To promote a strong barrier against insults, an established property of epithelial tissue is rapid cell turnover, a process that involves cell death, division, and renewal (Hooper, 1956; Pellettieri & Sanchez Alvarado, 2007). Apoptotic cell death occurs in the vocal folds after biomechanical trauma (Bartlett et al., 2015; Gaston,

Quinchia Rios, Bartlett, Berchtold, & Thibeault, 2012; King, Guille, & Thibeault, 2015; Novaleski, Mizuta, & Rousseau, accepted for publication). These findings suggest that apoptosis may be a natural biological response to vocal fold vibration and may therefore contribute to maintaining a normal epithelial barrier. Nevertheless, while vibration causes apoptosis signaling in the vocal fold epithelium, it remains unknown whether this is a static response or if increasing vibration exposure leads to greater apoptosis.

Study Purpose

The purpose of the current study was to quantify the rate of apoptosis signaling in vocal fold epithelial cells in response to increasing durations and extrapolated cycles of vibration in an *in vivo* animal model. In addition, there is evidence of tumor necrosis factor-alpha (TNF-α) upregulation in response to biomechanical trauma in the vocal folds (King et al., 2014; Verdolini, Rosen, Branski, & Hebda, 2003). However, studies reveal inconsistencies regarding the effect of TNF-α on cell death in the vocal folds (Berchtold, Coughlin, Kasper, & Thibeault, 2013; Chen & Thibeault, 2010). To examine the relationship between TNF-α and apoptosis, a secondary purpose of this study was to investigate whether gene transcript and protein levels of TNF-α are upregulated with increasing durations of vibration exposure in the vocal folds.

Research Aims and Hypotheses

This study explores three research questions: 1) What is the effect of longer time-doses of vibration exposure on apoptosis signaling in the vocal fold epithelium?; 2) What is the effect of higher cycle-doses of vibration exposure on apoptosis signaling in the vocal fold epithelium?; and 3) What is the effect of longer time-doses of vibration exposure on TNF-α levels in the vocal

fold epithelium? Three specific research aims are addressed in this study, which are described below with corresponding hypotheses:

Aim 1: To measure the effects of increasing time-doses of vibration exposure on apoptotic cell death in the true vocal fold epithelium using terminal deoxynucleotidyl transferase dUTP nick end labeling (TUNEL)[2] method and transmission electron microscopy[3] (TEM).

Aim 1A Hypothesis: There is a significant increase in the mean intensity of TUNEL staining in the true vocal fold epithelium with increasing time-doses of vibration exposure.

Aim 1B Hypothesis: There is a significant decrease in the mean area of epithelial cell nuclei using TEM images of the true vocal fold epithelium with increasing time-doses of vibration exposure.

Aim 2: To determine the relationship between extrapolated cycle-doses of vibration exposure and apoptotic cell death in the true vocal fold epithelium using TUNEL method and TEM.

Aim 2A Hypothesis: There is a significant positive correlation between extrapolated cycle-doses of vibration exposure and the mean intensity of TUNEL staining in the true vocal fold epithelium.

Aim 2B Hypothesis: There is a significant negative correlation between extrapolated cycle-doses of vibration exposure and the mean area of epithelial cell nuclei using TEM images of the true vocal fold epithelium.

Aim 3: To measure the effects of increasing time-doses of vibration exposure on gene and protein expression of the pro-inflammatory cytokine TNF-α in the true vocal fold epithelium.

[2] Assay that labels DNA strand breaks to detect fragmented DNA in cells undergoing apoptosis.
[3] Gold standard technique of identifying apoptosis that provides high-resolution images of cell morphology.

Aim 3A Hypothesis: There is a significant increase in the gene transcript levels of TNF-α in the true vocal fold epithelium with increasing time-doses of vibration exposure.

Aim 3B Hypothesis: There is a significant increase in the mean intensity of TNF-α protein expression in the true vocal fold epithelium with increasing time-doses of vibration exposure.

To summarize Chapter I, Figure 1 provides a succinct overview of the general area of study beginning at the top of the funnel. Toward the bottom of the funnel, the structure narrows down to the purpose and specific aims of the present study.

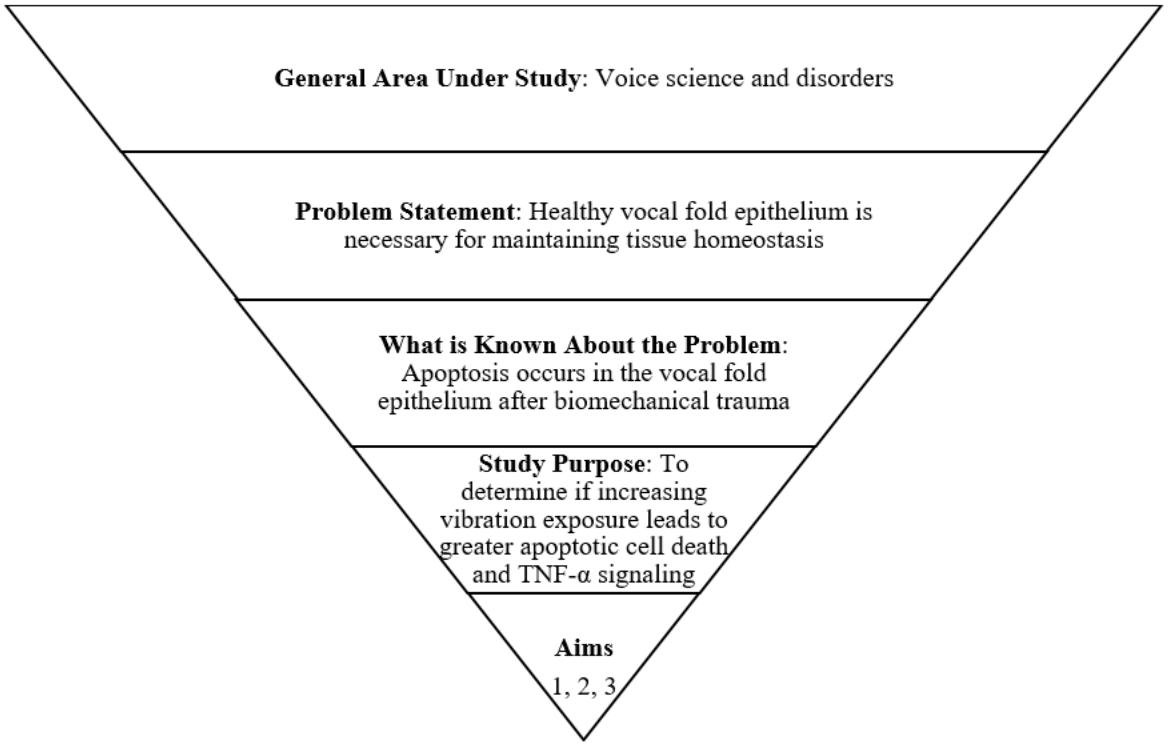

Figure 1. Funnel Structure Overview of Chapter I Leading to the Study Purpose.

Organization of the Study

The remainder of the dissertation is delineated into five chapters that include a literature review, pilot study, methodology, results, and discussion. Chapter II presents a review of the relevant literature regarding the current state of knowledge about vocal fold anatomy and physiology, epithelial tissue, apoptosis, and TNF-α research in the vocal folds. Chapter III presents a pilot study that established the methods used in this dissertation to evaluate dying vocal fold epithelial cells. Chapter IV describes the research design, materials, and methodology used to address the research aims. Data collection procedures included *in vivo* phonation, TUNEL method, TEM, extrapolation of cycle-doses, gene expression, and protein expression. Chapter V presents the results of the study that include pre-hypothesis testing, data analysis for the three research aims, and post-hoc analysis. Notably, the chapter highlights that TUNEL staining was significantly higher after 120 minutes of vibration exposure compared to the control condition, and mean intensity of TUNEL staining was positively correlated with mean intensity of TNF-α protein expression. Chapter VI summarizes the major findings of the study, additional commentary, and conclusion. Chapter VII provides a clinically relevant review of cell death and a theoretical framework regarding the potential role of cell death in diseases of the vocal folds. Finally, references and appendices are presented at the end.

CHAPTER II

REVIEW OF THE LITERATURE

Vocal Fold Anatomy and Physiology

The true vocal folds, a pair of membranous structures within the larynx[4], modulate airflow from the lungs to generate the audible sound of voice. Investigators have implemented a variety of approaches to study the mechanics of normal and abnormal vocal fold vibration. A traditional method relied on theoretical models to explain the physiology of phonation. According to the early work in van den Berg's (1958) myoelastic-aerodynamic theory[5], repeated cycles of vibration occur when exhaled air from the lungs flows through the approximated vocal folds, resulting in audible phonation. Although the theory initially proved useful, researchers later contended that it insufficiently described how vibration could be sustained. Thus, subsequent work on theories such as two-mass models, three-mass models[6], and flow separation vortices[7] enhanced van den Berg's original theory (Ishizaka & Flanagan, 1972; Khosla et al.,

[4] Positioned superior to the trachea, the larynx is an intricate structure in the upper respiratory tract that is comprised of cartilages, membranes, ligaments, and muscles. The valving nature of the vocal folds protects the lower respiratory tract during sensory-mediated airway reflexes such as coughing (Bruning et al., 2014). These mechanisms defend against noxious inhalants and prevent food and liquid from entering the lungs. Additional roles of the larynx include swallowing and breath-holding (Gates, Forrest, & Obert, 2013). While the larynx serves an important biological role to protect the airway, it also functions as part of the respiratory and phonatory systems during speech production.

[5] In this theory, laryngeal muscular forces bring the vocal folds together at midline, which obstructs airflow from the lungs. As subglottal pressure increases beneath the vocal folds, the folds eventually separate so that airflow passes through them. The cycle ends when the vocal folds return to the original approximated position via the Bernoulli effect and passive elasticity of the folds, whereby the vibratory cycle repeats (Jiang, Lin, & Hanson, 2000).

[6] Two-mass models incorporate the structural properties of the vocal folds into simulations. Specifically, the two-mass model considered the physical mass of the superficial vocal fold cover. Later, three-mass models extended this work by adding a third mass to simulate the vocal fold body, which is primarily muscle.

[7] According to Khosla et al. (2009), vortices refer to areas of concentrated rotational motion and are important during the opening and closing phases of vocal fold vibration.

2009; Story & Titze, 1995). Theoretical models served as a foundation for explaining how vocal fold vibration occurs.

The most significant contribution that theoretical models made was identifying the major types of mechanical stresses during phonation. As Titze (1994) explained, longitudinal or tensile stress occurs within the same direction of the anterior-posterior orientation of the fibers of the vocal ligament[8]. Shear stress, which is less damaging, occurs as the vocal folds move laterally in relation to one another. Finally, impact or collision stress occurs when the vocal fold surfaces directly contact one another in a transverse direction to the fibers of the vocal ligament (Jiang & Titze, 1994; Titze, 1994). In particular, it is believed that impact stress is most harmful to the vocal folds given that they experience the greatest collision during vibration. Determining the primary mechanical stresses in the vocal folds has proven useful in creating advanced vocal fold models.

In an effort to build upon theory, research progressed to computational and physical models to depict mechanical stress distributions during simulated vocal fold vibration. The advantage of such models is the ability to replicate and calculate the biomechanical stresses during phonation. As an example, a finite-elements model[9] created by Tao, Jiang, and Zhang (2006) included the input parameters of airflow and midline glottal[10] plane to obtain three-dimensional simulations of vibration. This group's simulations revealed that a narrow glottal configuration caused greater collision between the vocal folds, while a wider configuration reduced the amount of collision. Excised laryngeal models, on the other hand, use

[8] The vocal ligament includes the intermediate and deep layers of the lamina propria. Essential for changing vocal pitch, the vocal ligament is a well-designed structure for enduring longitudinal stresses while also helping maintain the integrity of the surrounding tissues.
[9] Finite-element computational models provide mathematical procedures for solving equations of continuum mechanics.
[10] Glottal refers to the opening between the vocal folds.

ex vivo[11] larynges to simulate controlled parameters of vocal fold vibration. For instance, Jiang and Titze (1994) attached one side of a hemi-sected excised canine larynx to a glass plate with holes representing common areas of vocal fold contact. Using a model diaphragm to simulate airflow, the intraglottal pressure was programmed to simulate an impact, preopen, and open phase of vibration. Results of their model agreed with the work by Tao and colleagues (2006) by demonstrating that smaller glottal width configurations resulted in greater impact stress (Jiang & Titze, 1994). In general, computational and excised laryngeal models have improved the complexity of describing vocal fold vibration.

Despite significant advances in simulating the mechanics of phonation, all modeling approaches rely on representations that are susceptible to inherent inaccuracies. A critical component of simulating vibration is ensuring a realistic representation of tissue geometry. However, computational models are not based on natural laryngeal anatomy, and therefore are unable to incorporate accurate structural details of the vocal folds. As such, altered representations of the vocal folds via computational formulae can undoubtedly affect the accuracy of vibratory output. Although *ex vivo* experiments preserve natural vocal fold anatomy, these models remove the *in vivo* components of phonation by separating a living organism from its natural environment. As such, theoretical, computational, and excised laryngeal models are limited in replicating the precise mechanical stresses during vibration.

In contrast to the aforementioned models, vibration dosimetry has bridged vocal fold tissue mechanics with clinically relevant metrics. Using an accelerometer[12] attached to the neck, vibration dosimetry estimates vibration-dose calculations during continuous speech. According

[11] *Ex vivo* experiments are performed on tissue(s) that are removed outside a living organism with attempts to minimize any disruptions to the natural tissue environment.
[12] An accelerometer is an instrument that detects and measures vibrations.

to Titze and Hunter (2015), common dosimetry calculations to measure daily voice use are time-dose, cycle-dose, and distance-dose. For instance, time-dose is the accumulated time of vibration exposure (i.e., voicing time), more specifically defined as the total duration in seconds that the vocal folds vibrate[13] (Titze, Svec, & Popolo, 2003). Another measure of interest is cycle-dose[14], which estimates the total number of vocal fold vibratory cycles and can be calculated from the fundamental frequency (F_0)[15] of vibration (Titze et al., 2003). Compared to time-dose that measures cumulative time that the vocal folds spend in vibration, cycle-dose measures how many times the vocal folds collide together[16]. As such, both estimates provide unique and important information regarding the mechanics of vibration.

Although the aim of vibration dosimetry is to find associations between human voice use and the predisposition to voice disorders, this method cannot explain the underlying tissue changes that cause dysphonia[17]. To fill this need, basic science approaches have gained increasing popularity to investigate the influence of vibration on direct structural damage to the vocal folds. Histologically, the vocal folds are comprised of epithelium, lamina propria, and muscle. First, stratified squamous epithelium constitutes the superficial cellular surface of the vocal folds (Gray, 2000). Underneath the epithelium is the basement membrane zone, a thin matrix that attaches basal[18] cells to the primarily non-cellular lamina propria (Titze, 1994).

[13] Time-dose can also be described as the percentage of voicing over time (Titze & Hunter, 2015).
[14] Cycle-dose was previously referred to as the vocal loading index.
[15] F_0 is the number of cycles of vocal fold vibration per second. F_0 is measured from the acoustic waveforms of voice recordings and corresponds to the perception of vocal pitch. F_0 ranges between 100-150 Hz for adult males, 180-220 Hz for adult females, and over 300 Hz for children (Awan, 2001).
[16] Distance-dose is defined as the distance that the vocal folds travel during vibration. Distance-dose is measured from both vocal intensity and F_0 (Mehta et al., 2015).
[17] Voice production involves complex interactions among neurological, aerodynamic, and phonatory mechanisms in which speakers frequently compensate for slight changes in phonation. Thus, it is difficult to experimentally induce trauma to the vocal fold tissue in humans and interpret obtained dosimetry values that reflect voice quality.
[18] Basal cells are innermost epithelial cells.

There are three layers of lamina propria which include a superficial, intermediate, and deep layer. Lastly, the bulk of the vocal fold is made up of the thyroarytenoid muscle.

The structure of the vocal fold lamina propria is important in determining tissue viscoelasticity and vibratory output (Long, 2010). Hirano (1974) introduced a foundational theory (i.e., body-cover theory) using histology to describe the role of the true vocal fold structure during vibration. This theory described the vocal folds as a double-structured vibrator in which the cover (i.e., epithelium, superficial, and intermediate layers) is loosely connected to the body (i.e., deep layer and thyroarytenoid muscle). While the intrinsic and extrinsic laryngeal muscles determine the mechanical properties of the cover and body, specific alterations to glottal configuration can change the shape, mass, and tension of the vocal fold tissue[19]. Because normal voice quality is characterized by periodic (i.e., regular) vocal fold vibration that depends on the integrity of the tissue, disruption to the histology results in irregular vibration and often leads to dysphonia.

To elucidate the relationship between the mechanical stresses of vibration and resulting damage to the vocal folds, scientists have utilized various *in vitro*[20] bioreactors. Bioreactors, which are tools that generate quantifiable vibrations to tissues, are most useful to investigate the responses of vocal fold cells to varying vibration doses (Klemuk, 2008). Mechanically-driven bioreactor designs apply mechanical stimulations to vocal fold cells via moving bars or specimen holders. In contrast, aerodynamically-driven bioreactor designs use hydrogel constructs to house vocal fold cells and apply controlled vibration frequencies using computer algorithms (Li, Heris,

[19] Vibratory parameters such as F_0 are related to the degree of coupling between the cover and body. The cover demonstrates flexibility during vibration, largely based on the elastin fibers that make up the intermediate layer of the lamina propria. In contrast, the body demonstrates greater stiffness and ability to contract during vibration because of collagen fibers in the deep layer that provide strength to the vocal fold (Gray, 2000; Jiang et al., 2000).
[20] *In vitro* experiments occur outside a living organism, such as cells in a test tube.

& Mongeau, 2013). Although *in vitro* studies demonstrate increased experimental control of vibration on vocal fold cell behavior, the results of these studies have poor external validity. In particular, it is unknown whether the experimental outcomes occur in the same way within the native vocal fold environment of an organism.

To overcome the limitations of *in vitro* experiments, *in vivo*[21] models are advantageous for studying vocal fold cell and tissue responses inside a living animal. In an effort to investigate tissue-level changes following *in vivo* vocal fold vibration, our laboratory established an *in vivo* rabbit phonation model. This model evokes physiologic (i.e., modal intensity) and phonotraumatic (i.e., raised intensity) vibration through direct neuromuscular stimulation to the laryngeal musculature and continuous controlled airflow through the glottis. The advantage of such a model is the ability to examine the real microarchitecture following trauma. After acute episodes of phonotraumatic vibration, Swanson and colleagues (2010) reported altered gene expression of interleukin-1 beta, transforming growth factor beta 1, and cyclooxygenase-*2* in the vocal folds. Moreover, studies have revealed that phonotraumatic vibration causes downregulated transcript levels of the tight junction proteins occludin and zonula-occludens-1, as well as downregulated transcript levels of the adherens junction protein E-cadherin (Kojima, Valenzuela, et al., 2014; Rousseau, Suehiro, Echemendia, & Sivasankar, 2011). In summary, our laboratory's work attests that the mechanical stresses during vibration lead to significant disruptions to the vocal fold tissue *in vivo*, therefore moving closer toward understanding the relationship between vocal fold tissue-level changes and dysphonia.

Given that the vocal fold is a multilayered tissue, researchers have chosen to examine multiple cell types in the vocal folds. For instance, the vocal folds consist of epithelial cells,

[21] *In vivo* takes place inside a living organism.

fibroblasts, macrophages, stellates, and myocytes (Klemuk, 2008). Cell types in the lamina propria have received the greatest attention because of their importance in maintaining normal vocal fold vibration. However, the outermost vocal fold epithelium is a particularly interesting histologic layer because its predominant role is to protect the underlying lamina propria. Thus, studying the epithelium can be useful to better understand the biological mechanisms underlying vocal fold diseases of epithelial origin and to ultimately determine the association between vocal fold tissue changes and dysphonia. The following section describes the major biological properties of epithelial tissue and the relevant literature regarding the vocal fold epithelium.

Epithelial Tissue

Epithelium is tissue that covers external body surfaces, primarily the epidermis[22]. Epithelium is composed of sheets of closely adjoined epithelial cells that are classified according to cell layer number and shape[23] (Ross et al., 2003). The organization of epithelial cell shape is related to the diverse roles of the tissue, which can include protection, secretion, and absorption (Ganz, 2002). Epithelial shape is also related to the biomechanical movement of the surface cells. For instance, stretching forces may flatten epithelial cells while contracting forces increase cell height (Maximow & Bloom, 1952). Given that epithelial tissue constitutes many different types of surfaces and internal cavities, it is necessary to consider the primary function of the epithelium when evaluating normal versus abnormal tissue homeostasis.

[22] Epithelium also forms glands and lines internal cavities of the respiratory, digestive, reproductive, and urinary tracts (Ganz, 2002).

[23] Specifically, simple epithelium has one layer and stratified epithelium is made of two or more layers. When categorized by cell shape, squamous epithelium demonstrates a flattened morphology, cuboidal epithelium is relatively symmetric in shape, and columnar epithelium has greater cell height than width (Ross et al., 2003).

Special properties distinguish epithelial cells from other cells in the body. These characteristics include planar cell polarity, cell-to-cell adhesion, and rapid cell turnover (Martini, 1998; Ross et al., 2003). First, epithelial cells demonstrate planar cell polarity, in which three cell membrane domains diverge in predetermined directions (Macara, Guyer, Richardson, Huo, & Ahmed, 2014). Each cell domain demonstrates structural and functional differences. The apical[24] or free domain orients to the lumen of internal cavities or external body surfaces. The lateral domain is located inferior to the apical surface, followed by the innermost basal domain that faces the basement membrane (Ross et al., 2003). Planar cell polarity directs cell movement and allows specific functions to correspond to these three respective domains (Rodriguez-Boulan & Macara, 2014; Ross et al., 2003).

Another property of epithelial tissue is cell-to-cell adhesion via the assembly of cell junctions[25]. The apical junctional complex seals the paracellular pathways[26] via tight junctions (Marchiando, Graham, & Turner, 2010). Tight junctions are two partially fused epithelial cell membranes that regulate which substances diffuse into the cell membrane and between other cells (Martini, 1998). Tight junctions primarily consist of the intracellular proteins zonula occludens (e.g., occludin, zonula occludin-1, claudin). By adhering epithelial cells closely to one another, tight junction proteins inhibit substances from moving between adjacent cells, thereby preventing paracellular flux[27] (Al-Sadi et al., 2011; Kimura, Teranishi, Kawamoto, & Nishida, 2011). At the lateral domain, the adherens junction is made of zonula adherens and desosomes[28] that assist with assembling the tight junctions. Finally, connexons or membrane proteins adhere

[24] Apical refers to the apex or tip.
[25] Cell junctions are created by cell adhesion molecules, transmembrane proteins that bind together, and proteoglycans (Martini, 1998).
[26] Paracellular pathways are pathways between epithelial cells.
[27] Flux refers to the movement of molecules across a membrane.
[28] Desosomes are strong cell junctions that connect opposing epithelial cell membranes. They are important in overcoming or resisting extreme movement of cells.

two epithelial cells together via the gap junctions. The narrowness of the gap junction pathway prohibits large molecules from entering, but allows small molecules and ions to pass between epithelial cells (Martini, 1998).

The entire junctional complex requires a carefully regulated degree of penetration that depends on the function of the tissue. On one end of the continuum, a highly permeable apical junctional complex may threaten the underling tissue by allowing unwanted toxins to pass through neighboring structures. For instance, increased permeability of tight junction proteins has been linked to pulmonary inflammation and edema, intestinal disease, and cerebral ischemia (Jiao, Wang, Liu, Wang, & Xue, 2011; Marchiando et al., 2011; You et al., 2012). Contrastively, an impermeable apical junctional complex can lead to impaired nutrient absorption in organs such as the small intestine (Marchiando et al., 2010). Within epithelial cells, the cell membrane is responsible for prohibiting the majority of hydrophilic[29] solutes from passing through the epithelium (Marchiando et al., 2010). Overall, the role of the junctional complex is to adhere epithelial cells tightly together.

Finally, in addition to cell polarity and cell-to-cell adhesion, epithelial tissue is characterized by rapid cell turnover. Cell turnover refers to continual cell self-renewal and is a lifespan cycle involving cell death, division, and renewal (Pellettieri & Sanchez Alvarado, 2007). In epithelial tissue, frequent cell turnover promotes a strong barrier against insults from the external environment (Hooper, 1956; Pellettieri & Sanchez Alvarado, 2007). Cell death terminates differentiated epithelial cells from the apical surface. As apical cells detach, basal

[29] Hydrophilic refers to a strong affinity for water or to mix with water.

cells proliferate[30] in the deeper layers[31] (Hooper, 1956). As a result, rapidly renewing cells assist with maintaining normal epithelial tissue homeostasis.

Scientists have described major features of the epithelium of the vocal folds. Non-keratinized, stratified squamous cell epithelium constitutes the surface cell layer of the membranous true vocal folds (Gray, 2000). First, unlike the dry surface of the epidermis that is waterproof, non-keratinizing apical epithelial cells are living. Therefore, these cells must maintain moisture or would otherwise dry out (Martini, 1998). Non-keratinized epithelium is generally resistant to moderate damage caused by mechanical trauma. Second, stratified squamous epithelium is thick and most flattened at the superficial layer (Maximow & Bloom, 1952). Stratified squamous epithelium typically covers structures that undergo more severe forms of biomechanical trauma (Martini, 1998). Similar to the vocal folds, structures that undergo mechanical trauma such as the pharynx, vagina, and anus are also covered with non-keratinized stratified squamous epithelium (Martini, 1998). In addition to tolerating trauma, Gray (2000) speculated that the vocal fold epithelium provides shape to the underlying lamina propria.

Because a major role of the vocal fold epithelium is to protect, epithelial cells must form a selective barrier. This epithelial barrier divides the boundary between the external environment from the underlying connective tissue (Ross et al., 2003). The primary function of the epithelial barrier is to prohibit water, ions, and large solutes from freely passing through the barrier (Marchiando et al., 2010). In the vocal folds, tight junctions function as the defending barrier between cells. It has been established that the vocal fold epithelial barrier is maintained by the

[30] Proliferating cells reproduce rapidly.
[31] In certain tissues, the rate of cell turnover may serve a functional purpose. For instance, endometrial epithelial cells undergo higher rates of cell turnover during phases of the menstrual cycle corresponding with uterine lining shedding (Ellis, Yuan, & Horvitz, 1991).

tight intercellular junctional complex, which includes tight junction proteins located at the apical-most junctions of the epithelium (Levendoski, Leydon, & Thibeault, 2014). To facilitate barrier integrity, the intercellular junctional complex comprises basolaterally located adherens junction proteins that connect cell-to-cell cytoskeletal filaments or cells to extracellular matrix (Levendoski et al., 2014; Rousseau et al., 2011). As Levendoski and colleagues (2014) speculated, the junctional complex may be especially necessary for maintaining structural stability during vocal fold vibration.

There are several noted functions that are particularly special for the vocal fold epithelium. Undoubtedly, chemosensory receptor function is the most critical characteristic of the epithelium covering the vocal folds. That is, epithelial chemosensory receptors serve as a defense mechanism against irritating stimuli to the airway. The mucosal surfaces of the larynx are composed of solitary chemosensory cells[32] that detect chemical irritants from the external environment (Sbarbati et al., 2004). When chemical irritants are exposed to the larynx, this results in laryngeal chemoreflex or laryngospasm[33] (Gates et al., 2013). Without such chemosensory receptor function, the airway would be significantly compromised.

Because the vocal folds are sensitive to the effects of hydration, another important function is ion channel transport. Ion channels are pores in the cell membrane that allow ion flux across membranes[34]. Hydration is important for optimal vocal fold vibration because surface

[32] Chemosensory cells in the laryngeal epithelium are innervated by the trigeminal nerve. When stimulated, this triggers the sensation of irritation or pain, followed by the activation of sensory-mediated defense mechanisms (Bruning et al., 2014; Tizzano, Cristofoletti, Sbarbati, & Finger, 2011).

[33] The laryngeal chemoreflex results in laryngeal constriction, coughing, apnea, retching, gagging, vomiting, and swallowing (Bradley, 2000; Bucca et al., 2011; Tizzano et al., 2011).

[34] There are other mechanisms in which solutes pass (e.g., transporters). Overall, these are passageways in the cell membrane that determine whether water, solutes, ions, and water-soluble materials may move across the membrane. Leak channels allow the movement of selected substances through the cell membrane. In contrast, gated channels carefully regulate ion transport through the membrane via intermittent opening and closing (Martini, 1998). The intracellular environment is typically characterized as high in potassium, while the extracellular environment is high in sodium (Bortner, Hughes, & Cidlowski, 1997). Cell volume is highly regulated by ionic channel activity, as ion

liquid on the tissue assists with biomechanical properties of vocal fold vibration (Leydon, Sivasankar, Falciglia, Atkins, & Fisher, 2009). Several ion channels, epithelial Na+ channel and cystic fibrosis transmembrane conductance regulator chloride channel, have been discovered in vocal fold epithelial cells (Leydon et al., 2009). Na^+/K^+ ATPase is believed to be responsible for the regulation of vocal fold hydration (Fisher, Telser, Phillips, & Yeates, 2001).

Vocal fold hydration has long been recognized as an important factor in maintaining vocal fold health and optimal phonation. Conversely, dehydration is believed to reduce vibratory function. The effects of dehydration on phonatory performance have been examined in animal models. As one example, after exposing canine larynges to dry air for five minutes, airflow and phonation threshold pressure[35] significantly increased compared to exposure to hydrated air (Jiang, Verdolini, Aquino, Ng, & Hanson, 2000). In human subjects, Patel, Walker, and Sivasankar (2015) introduced dehydrating conditions that included low humidity levels and oral breathing. Following dehydration, a high-speed laryngeal imaging measure (i.e., speed quotient) was significantly reduced compared to baseline measures, suggesting greater tension and stiffness of the vocal folds. An acoustic perturbation measure, jitter percentage, also decreased compared to baseline, which indicated more vocal instability (Patel et al., 2015). These studies, among others, support the notion that brief periods of dehydration can have detrimental effects on vocal fold vibration.

In the vocal folds, it remains unknown what the optimal degree of epithelial permeability is. In healthy vocal fold tissue, epithelial cells are relatively impermeable because the tight and

---

transport initiates changes in cell volume (Panayiotidis, Bortner, & Cidlowski, 2006). To maintain cell volume constancy, osmotic pressure across the cell membrane must remain balanced by restricting water from moving in or out of the cell. This equilibrium of solutes on both sides of the cell membrane is the result of the Na^+/K^+ ATPase pump.

[35] Phonation threshold pressure is a measure of the amount of subglottal pressure needed to initiate phonation (Zhuang et al., 2009).

adherens junction proteins effectively seal the paracellular spaces (Levendoski et al., 2014). Such a degree of impermeability restricts the unwanted passage of substances and solvents across the epithelial barrier. However, increased permeability from disrupted junctional proteins can lead to a higher risk of paracellular flux that could threaten the integrity of the epithelial barrier. The barrier must remain highly regulated to determine whether to permit or restrict external substances from passing internally across the barrier (Ross et al., 2003). Thus, there is a constant balance between permitting substances to aid in vocal fold hydration and restricting substances to prevent pathogen invasion.

Researchers have speculated that the vocal fold epithelium is primarily responsible for protecting the underlying connective tissue. However, there is emerging evidence that the vocal fold epithelium contributes to vibratory function. As a recent example, Tse, Zhang, and Long (2015) evaluated vocal fold vibratory function following epithelial removal in two excised human larynges. Larynges were positioned in an *ex vivo* airflow setup to evoke phonation at baseline and following nearly complete unilateral and bilateral removal of the epithelial tissue after treatment using the enzyme trypsin. High-speed imaging revealed that de-epithelialization led to increased airflow rate in addition to reduced glottal closure, resistance, and closed quotient. Qualitative assessment of vibration indicated disorganized mucosal wave and asymmetric vibration (Tse et al., 2015). Other researchers have advocated for the potentially important role of the epithelium during vibration. Xuan and Zhang (2014) speculated that the epithelium assists with complete glottal closure. Additionally, Murray and Thomson (2012) maintained that creating a thin, durable epithelial layer superior to a lamina propria in a synthetic model helps facilitate pliability during mucosal wave movement. Collectively, these

observations demonstrate that the vocal fold epithelium may be an active layer during vibration and could directly contribute to vibratory function.

As with other epithelia, vocal fold epithelial cells are polarized[36] and assembled with an intercellular junctional complex. The vocal fold epithelium also protects the airway and balances an optimal degree of permeability for hydration. However, research on cell turnover in the vocal fold epithelium has received limited attention. Given that the vocal folds undergo significant mechanical trauma during vibration, it is important to understand how cell turnover may assist with maintaining vocal fold tissue homeostasis. A logical mechanism to examine during turnover is cell death, given that the regulation and dysregulation of cell death is indicated in a variety of human diseases. The next section provides a review of the most commonly studied form of cell death, apoptosis, and research on apoptosis in the vocal folds.

Apoptosis

Cells throughout the body continually self-renew via turnover. To maintain tissue morphology and function, differentiated[37] cells are regularly replaced with proliferating cells (Denecker, Vercammen, Declercq, & Vandenabeele, 2001). Specifically, epithelial tissue maintains homeostasis and self-organizes by cell death, or the physiological elimination of cells (Macara et al., 2014). The most commonly studied type of programmed cell death[38] is apoptosis. Apoptosis is a genetically regulated mechanism that determines which cells are eliminated (Ashkenazi & Dixit, 1998; Denecker et al., 2001; Elmore, 2007). Apoptosis is considered

[36] All epithelial cells are polarized. Although no empirical research has addressed polarization of vocal fold epithelial cells, markers for cytokeratin 13, cytokeratin 14, involucrin, and nerve growth factor receptor have distinguished three separate layers in the human vocal fold epithelium. Cytokeratin 13 is expressed throughout most of the stratified squamous portion of the vocal fold epithelium, with the exception of basal cells (Dowdall et al., 2015).
[37] Differentiation is a process in which a cell matures and becomes specialized to perform pre-determined functions.
[38] An intracellular death program mediates programmed cell death.

intentional cell death or physiological cell suicide. This notion is emphasized by the Greek origin of the term apoptosis (*apo* meaning "from" and *ptosis* meaning "a fall") that provides imagery of leaves falling naturally from a tree (Majno & Joris, 1995). Macroscopically, cell death is most obvious during desquamation[39] of the superficial layer of the epidermis (Hooper, 1956). During the induction phase, a stimulus triggers apoptosis via transmitting signals to the cell. Conversely, the cell recognizes an internal defect (e.g., DNA damage) and initiates apoptosis. As the cell identifies the signal to die, it subsequently commits to apoptosis during the detection phase. Next is the effector phase in which downstream effectors and caspases activate. Lastly, the removal phase permanently eliminates the cell (Rai, Tripathi, Sharma, & Shukla, 2005).

Apoptosis is considered an organized method of cellular degradation for several reasons. During apoptosis, the plasma membrane is maintained and cellular constituents of apoptotic cells are not disbursed throughout the surrounding tissue. As such, apoptosis generally does not initiate an inflammatory response. The process of phagocytosis[40] occurs relatively quickly, thereby reducing the chances of reactive necrosis. Additionally, there are no pro-inflammatory cytokines[41] associated with cells during phagocytosis (Elmore, 2007). Apoptosis generally affects only single or small clusters of cells (Elmore, 2007). Additional forms of cell death include necrosis, programmed necrosis, secondary necrosis, autophagy, and aponecrosis[42].

---

[39] Desquamation is the shedding of the outermost layer of tissue. An example of macroscopic desquamation is the peeling of the epidermis after a sunburn.
[40] Phagocytosis is the process in which a cell engulfs a solid particle.
[41] Although macrophages do not release pro-inflammatory cytokines during phagocytosis, Gregory and Devitt (2004) reported that macrophages are related to the production of anti-inflammatory cytokines.
[42] Necrosis (i.e., oncosis), or accidental cell death, is viewed as a disordered manner in which cells die and is associated with an inflammatory reaction (Elmore, 2007; Denecker et al., 2001). Necrosis is characterized by cellular swelling, karyolysis or complete disbanding of chromatin caused by enzymatic destruction by endonucleases, plasma membrane rupturing, and eventual dispersing of cytoplasmic contents into the surrounding tissue (Denecker et al., 2001; Elmore, 2007). In contrast, signaling pathways intentionally regulate programmed necrosis (i.e., necroptosis, necrapoptosis) (Edinger & Thompson, 2004). Next, secondary necrosis can occur after

Despite that researchers continue to expand the study of different types of cell death, apoptosis remains the most commonly studied form of cell death.

Morphological criteria typically identify the type of cell death. Apoptosis begins with cellular shrinking and increased cell density (Majno & Joris, 1995). During the early phases of apoptosis, another readily identifiable feature is pyknosis in which chromatin condenses and becomes more concentrated. Next, a budding phenomenon results in rupturing of the cell nucleus or karyorrhexis. The cell extrudes fragments via plasma membrane blebbing (Majno & Joris, 1995) and these cellular fragments subsequently transform into apoptotic bodies. Apoptotic bodies consist of cytoplasm with tightly organized organelles along with an intact plasma membrane that maintains the integrity of the organelles. Phagocytosis removes the apoptotic bodies by surrounding cells that include macrophages, parenchymal cells, or neoplastic cells (Elmore, 2007; Majno & Joris, 1995).

Cysteine-aspartic proteases or caspases control apoptosis. Caspases are a family of cysteine proteases, or enzymes that degrade proteins, and are cell death proteases. When a single caspase is activated, a chain reaction activates multiple caspases (Cory & Adams, 2002). An initiator caspase is first activated to trigger the apoptotic cascade, which activates downstream effector caspases (i.e., caspase-3, caspase-7). Effector or executioner caspases cause the morphological signs of apoptosis (Fiers, Beyaert, Declercq, & Vandenabeele, 1999). Apoptosis

---

apoptosis is initiated when apoptotic bodies are unable to be cleared by neighboring cells. If surrounding cells are unavailable or defective, secondary necrosis is activated via autolysis. Autolytic degradation, or self-digestion, of the dying cell then completes the process of cell death (Silva, 2010). Autophagy or Type II cell death is non-apoptotic and refers to cellular self-eating. Finally, aponecrosis demonstrates morphological characteristics of both apoptosis and necrosis and is identified by decreased adenosine triphosphate (Formigli et al., 2000; Papucci et al., 2004).

is activated by intrinsic and extrinsic signaling pathways that both conclude with the execution pathway of caspase-3 cleavage[43].

In the intrinsic apoptosis signaling pathway[44], B cell lymphoma 2 (Bcl-2) family of proteins is the primary regulator (Lalaoui, Lindqvist, Sandow, & Ekert, 2015). Bcl-2 proteins that promote apoptosis include a group that shares all four Bcl-2 homology domains (i.e., BAX, BAK, BOK) and a group that shares only the Bcl-2 homology-3 domain (i.e., BIM, PUMA, BID, BAD, NOXA, BIK, HRK, BMF) (Lalaoui et al., 2015). Bcl-2 family proteins balance whether a cell's fate is to survive or die. If a cell is programmed to survive, anti-apoptotic (i.e., pro-survival) Bcl-2 family members bind to the pro-death factors to neutralize and ultimately prevent their action (Walensky, 2006). However, a cell is committed to undergo apoptosis when BAX and BAK are activated. BAX and BAK create pores in the mitochondrial membrane to allow the release of proteins such as cytochrome *c*. Cytochrome *c* combines with Apoptosis protease activating factor (i.e., Apaf1), which recruits caspase-9 to form a protein complex termed the apoptosome. Once the complex is formed, caspase-9 becomes active, subsequently activating caspase-3 and caspase-7. The caspases cleave their substrates[45], one of which is the Inhibitor of Caspase-Activated Deoxyribonuclease (DNase). Cleaving the Inhibitor of Caspase-Activated DNase activates Caspase-Activated DNase and this step causes the hallmark characteristic of DNA fragmentation in cells undergoing apoptosis (Lalaoui et al., 2015). In fact, DNA fragmentation is the foundation for many experimental approaches to detect apoptosis via the intrinsic apoptosis signaling pathway. Figure 2 depicts the overall schematic of the intrinsic apoptosis signaling pathway.

[43] Cleavage refers to splitting or dividing a cell. An enzyme such as a caspase cleaves a protein.
[44] The intrinsic signaling pathway is also known as the mitochondrial pathway.
[45] Substrate is a substance on an enzyme.

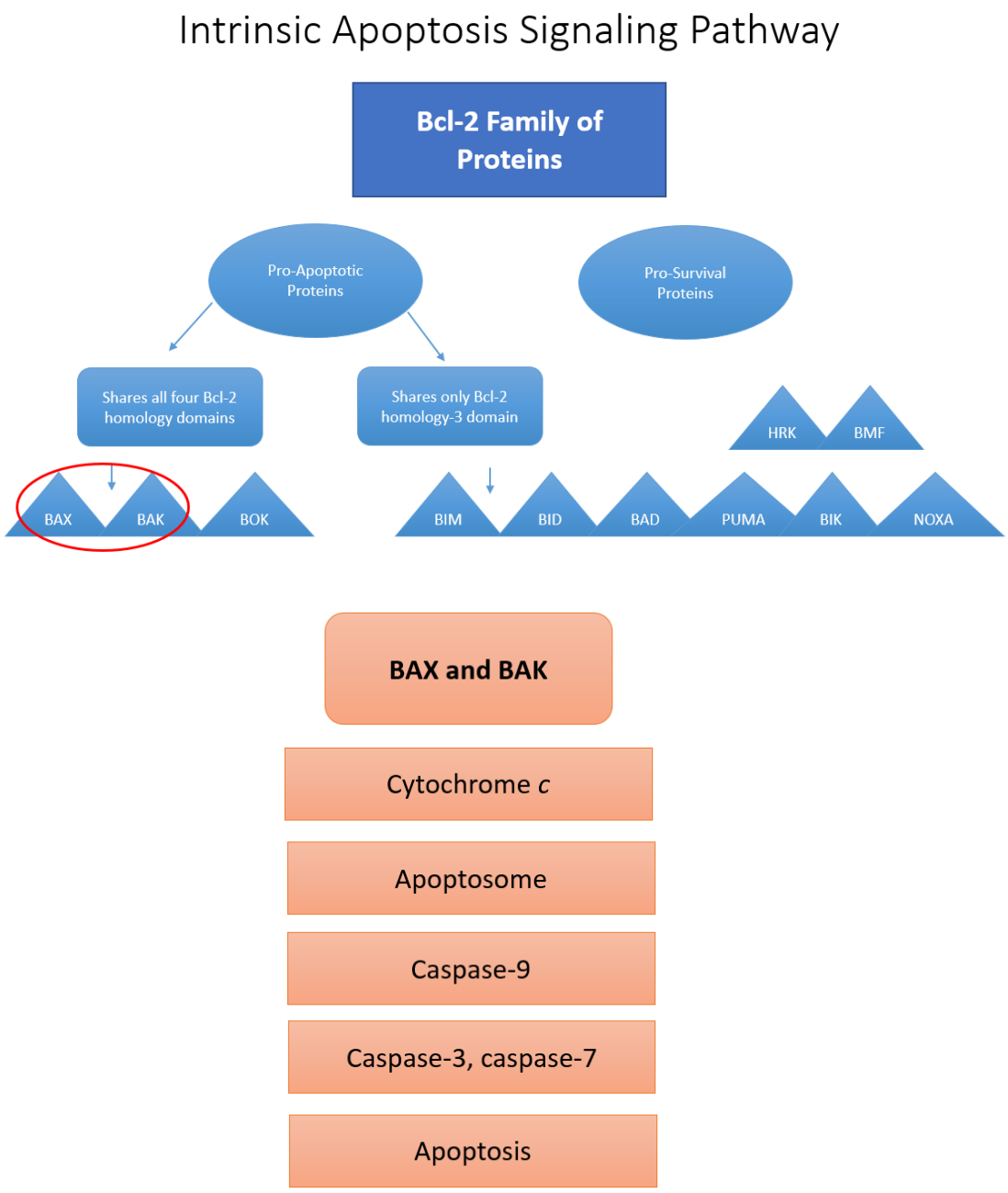

Figure 2. Schematic of the Intrinsic Apoptosis Signaling Pathway.

In contrast, the extrinsic apoptosis signaling or death receptor pathway involves a subcategory of death receptors. Death receptors are cell surface receptors that belong to the TNF receptor gene superfamily (Fiers et al., 1999). For instance, triggering the death receptor CD95 (i.e., Fas, Apo1) ultimately leads to the generation of the death inducing signaling complex (Lalaoui et al., 2015). Following CD95 ligation, death domain receptors cluster and an adaptor protein Fas-associated death domain binds to the clustered death receptor domains. Fas-associated death domain contains a death effector domain that recruits caspase-8 to activate by self-cleavage, triggering downstream effector caspases. Activing these caspases also results in forming mitochondrial membrane pores by BAX oligomerization, releasing cytochrome *c* and further activating effector caspases. This is the point at which the cell is committed to undergo apoptosis (Ashkenazi & Dixit, 1998). Figure 3 depicts the overall schematic of the extrinsic apoptosis signaling pathway.

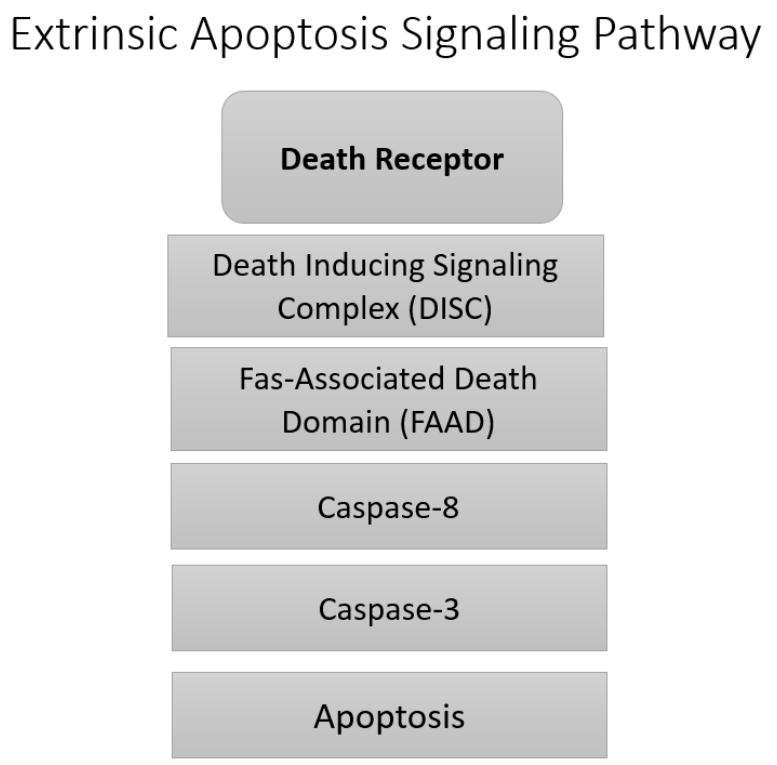

Figure 3. Schematic of the Extrinsic Apoptosis Signaling Pathway.

Many environmental insults cause apoptosis. Biomechanical trauma is a common injury that induces apoptosis to maintain homeostasis in a number of biological systems. For instance, corneal epithelium is subjected to mechanical injury such as eye blinking, eye rubbing, and poorly fitted contact lenses (Wilson & Kim, 1998). Using an *in vitro* rabbit model to simulate eyelid blinking, Ren and Wilson (1997) induced shear stresses to corneal epithelia via magnetic stirring in tear solution or static tear solution as the control. Results revealed that the mean rate of apoptosis in corneas exposed to shear stresses was significantly higher than the control. The rate of apoptosis significantly increased with increasing time-doses, suggesting that biomechanical stresses caused the epithelial surface to exfoliate and remove a greater number of

cells[46] (Ren & Wilson, 1997).

Although limited research is available regarding apoptosis in the vocal folds, Gray (2000) descriptively indicated that vocal fold epithelial cells undergo cell turnover. He described the morphological signs of desquamation of the true vocal fold epithelium along the apical surface. The process was characterized by a loss of cellular attachments (i.e., the cells no longer adhered tightly to one another) between superficial desquamated cells and differentiated cells underneath. Gray (2000) suggested that desquamated cells were no longer functional (i.e., dead) in comparison to the cells underneath with intracellular organelles. Additionally, it has been established that apoptosis occurs during normal vocal fold development. During murine embryologic development, apoptosis is responsible for terminating vocal fold epithelial cells (Lungova, Verheyden, Herriges, Sun, & Thibeault, 2015). Apoptosis also occurs as a result of mechanical trauma to the vocal folds. Using a bioreactor King et al. (2015) evaluated the effect of vibration on the rate of cell death in cultured *in vitro* human vocal fold fibroblasts. Findings showed that following vibration, 2-7% of fibroblasts underwent apoptotic cell death (King et al., 2015). Additional studies confirmed that cultured human vocal fold fibroblasts undergo apoptosis in response to biomechanical stimulation (Bartlett et al., 2015; Gaston et al., 2012).

[46] The cardiovascular system is also vulnerable to mechanical forces that include stretch and shear stresses. In animal models of hypertension, increased rates of apoptosis were present in the heart and brain (Wernig & Xu, 2002). In addition, apoptosis and necrosis was observed in neuronal cells following mechanical forces that simulated damage from traumatic brain injury (Serbest, Horwitz, Jost, & Barbee, 2006). The gastrointestinal tract is susceptible to frequent cell turnover. During turnover, apoptosis is a key process as the lining of the intestinal wall sheds (Que & Gores, 1996; Watson, Duckworth, Guan, & Montrose, 2009). Although there is disagreement regarding the precise functional role that apoptotic cell death plays during intestinal cell shedding, there are associations between apoptosis and epithelial barrier function in intestinal disease (Watson et al., 2009). Overall, it appears that regular damage from biomechanical trauma results in apoptosis. In contrast, severe mechanisms of injury such as radiation and toxins are more characteristic of necrosis. This indicates that tissues may signal cells to initiate apoptosis after sustaining mild damage in the form of biomechanical stress, which appears to be a critical component in maintaining normal tissue regulation.

As research continues to grow concerning apoptosis in the vocal folds, the study of apoptosis in vocal fold disease also deserves further investigation. The most notable vocal fold disease involving apoptosis is laryngeal SCC. Cancer involves the simultaneous interactions of uncontrolled cell proliferation and reduced apoptosis (Evan & Vousden, 2001). As such, incessant proliferating cells invade and destroy tissue. Apoptosis has been measured in primary tumor and resection biopsies from patients with laryngeal SCC and epithelial hyperplasia (Hellquist, 1997; Hirvikoski et al., 1999). In addition, patients with increased apoptotic events had a significantly poorer prognosis for survival than did patients with lower apoptotic events (Hirvikoski et al., 1999). These results indicate that apoptosis may be a potentially useful clinical biomarker to predict survival rate for laryngeal SCC. In contrast, Hellquist (1997) observed that the rate of apoptosis did not differ among epithelial hyperplastic laryngeal lesion types that included laryngeal SCC versus simple and abnormal hyperplasia. This finding suggests that a single apoptosis assay, such as TUNEL method, is insufficient alone to distinguish cancer from other laryngeal lesion types.

In contrast to directly detecting apoptosis in the vocal folds, researchers have frequently alluded to apoptosis. In particular, there have been descriptions of morphological features of cells in the vocal folds that are consistent with dying cells. For instance, benign vocal fold lesions were characterized by desquamating epithelial cells, shrinking nuclei, and altered chromatin (Dikkers, Hulstaert, Oosterbaan, & Cervera-Paz, 1993; Kotby, Nassar, Seif, Helal, & Saleh, 1988; Martins, Defaveri, Custodio Domingues, de Albuquerque, & Fabro, 2010; Martins, Defaveri, Domingues, & de Albuquerque e Silva, 2011). Research groups have also described desquamation in vocal fold epithelial tissues exposed to biomechanical trauma and inhaled pollutants (Gray & Titze, 1988; Marcelino & Oliveira, 2005; Rousseau et al., 2011). It is likely

that desquamating epithelial cells are in fact dying cells and that shrinking nuclei represent early phases of apoptotic cellular shrinking.

However, the aforementioned studies fail to confirm that such ultrastructural findings are evidence of vocal fold epithelial cell death. Despite this weakness, alluding to cell death provides insight into the potential role of apoptosis in the vocal folds. To more consistently describe damage to the vocal folds, it is necessary to implement gold standard approaches to confirm and effectively communicate key biological processes during the lifecycle of an epithelial cell. Novaleski and colleagues (accepted for publication) aimed to establish more systematic approaches to evaluate cell death in vocal fold epithelial cells and to investigate cell death in response to immobilization, approximation, and biomechanical vibration using an *in vivo* rabbit phonation model. The gold standard technique of TEM evaluated high-quality ultrastructural criteria of cell death and TUNEL method detected *in situ* staining of DNA strand breaks to confirm cell death signaling. Results revealed that ultrastructural characteristics of apoptotic cell death, specifically condensed chromatin and apoptotic bodies, were observed after vocal fold vibration and approximation. Although episodes of necrotic cell death were rare, few enlarged cell nuclei were present after vibration and approximation. The vocal fold expressed an immunohistochemical marker for apoptosis along the apical surface of the epithelium, as evidenced by TUNEL-labeled cells (Novaleski et al., accepted for publication) (see Chapter III: Pilot Study). This study is in agreement with the effects of mechanical trauma on cell death in vocal fold fibroblasts (Bartlett et al., 2015; Gaston et al., 2012; King et al., 2015).

Cell death occurs through complex signaling pathways that are responsible for deciding to allow cells to either die or survive. These decisions must take place through the coordinated interactions of many different cytokines. Cytokines are small proteins that coordinate localized

cell activities. Cells release cytokines to send messages to surrounding cells and regulate functions (Martini, 1998). The particular function of a cytokine varies depending on the circumstances, resulting in many diverse roles of cytokines. For this reason, cytokines are classified into several categories that include interleukins, interferons, chemokines, and TNF-α (Khan, 2008; Ross et al., 2003). The following section briefly explains the roles of the cytokine TNF-α and reviews the literature on TNF-α in the vocal folds.

Tumor Necrosis Factor-Alpha

The TNF family of cytokine receptors is derived from a mononuclear phagocyte and T-lymphocyte (Strieter, Kunkel, & Bone, 1993). The TNF protein superfamilies include the TNF superfamily and TNF receptor superfamily (Brenner, Blaser, & Mak, 2015). TNF is produced locally at relatively low concentrations to maintain physiologic homeostasis. On the other hand, TNF production substantially increases in response to local injury (Strieter et al., 1993). TNF-α is a cytokine that is important in initiating and directing the acute inflammatory response (McInnes, 2013). In addition to promoting, maintaining, and regulating pro-inflammatory responses, TNF-α is largely involved in cell death, proliferation, differentiation, and communication (Aggarwal, Gupta, & Kim, 2012; Brenner et al., 2015). TNF-α activates cell death among select receptors that carry a death domain (Lalaoui et al., 2015). Specifically, TNF receptor 1 (i.e., p55, CD120a) is a death receptor involved in the extrinsic apoptosis signaling pathway (Ashkenazi & Dixit, 1998; Lalaoui et al., 2015).

Given the multiple functions of TNF-α, changes to the structure of this protein have significant implications in human diseases. Faulty features in TNF-α can render the protein unable to perform critical regulatory functions throughout the body that are related to

inflammation and cell death (Brenner et al., 2015; Varfolomeev & Ashkenazi, 2004). Clinically, TNF has been implemented in the treatment for a number of inflammatory diseases. In particular, the primary therapeutic approach for inflammatory diseases is to block TNF-mediated signaling with the use of drugs such as antibodies. Successful clinical outcomes from the use of TNF as a biologic target have been demonstrated in inflammatory bowel disease and rheumatoid arthritis (Brenner et al., 2015).

Localized inflammatory responses occur in vocal fold injury and disease (Branski, Rosen, Verdolini, & Hebda, 2004, 2005). In particular, TNF-α is upregulated in the vocal fold after injury. After resecting[47] rat vocal folds, TNF-α gene expression significantly increased as early as 1 and 8 hours compared to normal tissue (Lim, Tateya, Tateya, Munoz-Del-Rio, & Bless, 2006; Welham, Lim, Tateya, & Bless, 2008)[48]. Moreover, TNF-α gene expression was significantly upregulated 3 days after resecting rabbit vocal folds and injecting a synthetic extracellular matrix biomaterial of hyaluronan compared to saline (Thibeault & Duflo, 2008)[49]. These studies suggest that increased TNF-α transcript levels in the early phases after vocal fold tissue resection and injection augmentation may be associated with an acute inflammatory process.

[47] A commonly induced injury in the animal wound healing literature is vocal fold stripping or resecting. Because there are many inconsistencies regarding the degree of resection, Imaizumi, Thibeault, and Leydon (2014) proposed a classification system that includes subepithelial, transmucosal, and transmuscular injury. During transmucosal injury, microforceps resect the epithelium and lamina propria without harming the underlying thyroarytenoid muscle (Imaizumi et al., 2014).

[48] Work by Lee and colleagues (2015) confirmed that similar to rats, TNF-α protein expression in rabbits significantly upregulated in the first day after vocal fold stripping compared to uninjured contralateral vocal folds. As expected, TNF-α signaling is upregulated after more severe surgical injury, as resecting the thyroarytenoid muscle by transmuscular injury significantly upregulated TNF-α gene expression up to 3 days in porcine vocal folds (King et al., 2015).

[49] King et al. (2014) maintained a similar finding at 3 days after embedding cultured mesenchymal stromal/stem cells derived from multiple human tissue sources with hyaluronic acid hydrogel constructs, which were subsequently co-cultured with macrophages. After 3 days, biomaterial constructs embedded with vocal fold-derived cells resulted in significantly increased TNF-α protein expression (King et al., 2014).

Similar to surgical injury, biomechanical trauma causes upregulated TNF-α protein expression in the vocal folds. In a case study of one normal female speaker, secretions collected from the vocal fold surface[50] demonstrated upregulated TNF-α protein expression following loud phonation produced almost continuously for 1 hour (Verdolini et al., 2003)[51]. There is evidence that TNF-α signaling may differ in normal and diseased tissue. For example, King, Chen, Jette, and Thibeault (2013) investigated the effects of biomechanical stimulation on inflammatory signaling of macrophages that were co-cultured with vocal fold fibroblasts. Fibroblasts were derived from healthy tissue and vocal fold pathology. Compared to normal fibroblasts, biomechanical stimulation of benign polypoid- and scar-derived fibroblasts led to significantly increased TNF-α protein expression (King et al., 2013). These findings revealed differential signaling of TNF-α from macrophages co-cultured with normal vocal fold fibroblasts versus fibroblasts obtained from pathology. Collectively, the aforementioned studies suggest that acute vibratory-induced biomechanical trauma increases TNF-α expression in the vocal folds.

Inconsistencies in the literature exist regarding the effect of non-biophysical challenges to the vocal folds on TNF-α signaling. Pathogenic injury, such as viruses and bacteria, upregulate TNF-α. Specifically, King et al. (2015) observed that lipopolysaccharide-induced injury caused increased TNF-α gene expression in porcine vocal folds after 1 and 5 days compared to intact controls. Conversely, other types of acute vocal fold challenges do not alter TNF-α levels. For instance, repeated acidified pepsin challenges to porcine vocal folds for 4 weeks revealed no significant differences in TNF-α gene expression compared to saline challenges (Durkes &

[50] To characterize inflammatory responses in humans, a method emerged involving either swabbing or suctioning tissue secretions from the surface of the vocal folds before and after vocal loading tasks (Verdolini Abbott et al., 2012).

[51] Li and colleagues (2008) continued this line of work with nine normal male and female speakers. Although the data were more variable between participants, one participant's vocal fold tissue secretions revealed a pattern of upregulated TNF-α protein expression immediately following 1 hour of vocal loading (Li et al., 2008).

Sivasankar, 2015)[52]. The discrepancy in TNF-α signaling among challenges suggests that perhaps the vocal folds are able to tolerate acute pepsin challenges without the initiation of an inflammatory cascade and therefore, may respond differently to biophysical versus pathogenic insults.

While changes in TNF-α have been examined in vocal fold injury, it is also important to consider the functional role of TNF-α. In the vocal folds, TNF-α serves several roles. First, TNF-α orchestrates additional inflammatory cytokine networks. Berchtold and colleagues (2013) confirmed this by treating cultured human vocal fold fibroblasts with TNF-α. After 24 hours, TNF-α caused significantly increased protein levels of the pro-inflammatory cytokines interleukin-1 beta, interleukin-6, and interleukin-8. In fact, inducing TNF-α in the vocal folds significantly upregulated its own protein expression (Berchtold et al., 2013). The findings that TNF-α initiates and mediates further inflammatory signaling are in congruence with TNF-α signaling in other tissue types (Brenner et al., 2015).

The role of TNF-α in the vocal folds extends beyond inflammation. TNF-α influences chemotactic signaling and may be involved in the remodeling process during vocal fold wound healing. For instance, TNF-α administration to cultured human vocal fold fibroblasts led to significantly higher chemokine levels for eotaxin and monocyte chemotactic protein-1, in addition to basic fibroblast growth factor (Berchtold et al., 2013). Researchers have speculated about the possible role of TNF-α from observing similar patterns of TNF-α expression with other wound healing events following vocal fold injury. For instance, given that the expression of TNF-α and extracellular matrix factor hyaluronic acid synthase (HAS) were upregulated at similar acute time points after vocal fold stripping, Lim et al. (2006) speculated that TNF-α may

[52] In addition, TNF-α protein expression did not significantly change in cultured human vocal fold fibroblasts exposed to cigarette smoke extracts (Berchtold et al., 2013).

be responsible for signaling HAS-1 and subsequently HAS-2. Welham et al. (2008) further substantiated this idea by speculating that the TNF-α signaling pathway induces HAS-1 in vocal fold fibroblasts based on the observations of upregulated TNF-α and HAS-1 expression 1 hour post-injury. Thus, these findings suggest that TNF-α affects not only inflammatory signaling during the initial stage of wound healing, but also subsequent remodeling in the vocal folds.

Cell proliferation and death are other important cell processes that involve TNF-α. However, studies reveal inconsistencies regarding the effect of TNF-α on cell death. Increased concentrations of administered TNF-α to cultured human vocal fold fibroblasts inhibited the rate of cell proliferation after 9 days (Chen & Thibeault, 2010). Based on this observation, the researchers affirmed that TNF-α demonstrates vocal fold tissue specificity in regulating other cell processes such as proliferation and death. It may be possible in this study that vocal fold fibroblasts failed to grow because of cell death. However, Berchtold et al. (2013) maintained that cell death was not evident after 24 hours following TNF-α administration to cultured human vocal fold fibroblasts. This noted discrepancy in the literature leads to a logical question concerning the association of apoptosis and TNF-α in the vocal folds. Thus, this gap demonstrates a need for further studies designed to investigate the possible role that TNF-α plays during apoptotic cell death in the vocal folds.

Summary and Dissertation Goals

In conclusion, apoptotic cell death occurs in the vocal fold epithelium after biomechanical trauma. The purpose of this study was to quantify the rate of apoptotic cell death signaling and TNF-α expression in vocal fold epithelial cells in response to increasing time-doses of vibration exposure in an *in vivo* animal model. This study also applied relevant calculations

of vibration dosimetry (i.e., extrapolated cycle-doses) to the *in vivo* phonation model. To summarize, the following three research aims were addressed:

Aim 1: To measure the effects of increasing time-doses of vibration exposure on apoptotic cell death in the true vocal fold epithelium using TUNEL method and TEM.

Aim 2: To determine the relationship between extrapolated cycle-doses of vibration exposure and apoptotic cell death in the true vocal fold epithelium using TUNEL method and TEM.

Aim 3: To measure the effects of increasing time-doses of vibration exposure on gene and protein expression of the pro-inflammatory cytokine TNF-α in the true vocal fold epithelium.

CHAPTER III

PILOT STUDY[53]: EVALUATION OF DYING VOCAL FOLD EPITHELIAL CELLS BY ULTRASTRUCTURAL FEATURES AND TUNEL METHOD

Introduction

The objective of this pilot study was to extend the current state of knowledge by establishing methods to evaluate dying vocal fold epithelial cells. In particular, this protocol focused on the gold standard technique of TEM for evaluating high-quality ultrastructural characteristics of cell death. A common immunohistochemical marker of cell death, TUNEL, was used to confirm these results. A secondary purpose was to investigate cell death in response to vocal fold immobilization, approximation, and biomechanical vibration. Immobilized vocal folds were harvested from normal rabbits, approximated vocal folds underwent intermittent adduction and abduction, and vibrated vocal folds underwent evoked phonation. Results indicated that just as in other tissues and as previously reported, epithelial cells of the vocal fold undergo cell death. In response to approximation and vibration, dying cells demonstrated morphological signs primarily consistent with apoptosis. However, few cells revealed ultrastructural evidence of necrosis after vibration. This study provides two standard techniques to more accurately evaluate the process of cell death in the vocal fold epithelium, which may serve as a foundation to better characterize the functional role of cell death in the vocal folds.

[53] The work in Chapter III is cited as the following:
Novaleski, C. K., Mizuta, M., & Rousseau, B. (accepted for publication). Evaluation of dying vocal fold epithelial cells by ultrastructural features and TUNEL method. *Cells Tissues Organs*.

Methodology

Animals

Laryngeal tissue specimens were obtained from 12 adult male New Zealand white breeder rabbits weighing 3-5 kg. Animals were anesthetized via intramuscular injections of ketamine (35 mg/kg), xylazine (5 mg/kg), and acepromazine (0.75 mg/km). To maintain anesthetic effects, ketamine (17.5 mg/kg) and acepromazine (0.375 mg/kg) were subsequently administered as necessary. During the entire experimental procedure, animal wellbeing was ensured by continually monitoring heart rate, oxygen saturation level, body temperature, and respiratory rate. The Vanderbilt University Institutional Animal Care and Use Committee approved the procedures used in this study. Procedures were performed in accordance with the Public Health Service Policy on Humane Care and Use of Laboratory Animals, National Institutes of Health Guide for the Care and Use of Laboratory Animals, and Animal Welfare Act (7 U.S.C. et seq.).

In Vivo Procedures

Cell death in the vocal fold epithelium was evaluated using three experimental conditions: immobilization, approximation, and vibration. First, normal larynges were harvested to assess cell death in the epithelium of immobilized vocal folds ($n = 2$). Normal tissue was chosen because rabbits do not spontaneously phonate, therefore minimizing the possibility of external vibratory damage. Next, a separate condition included approximated vocal folds at midline with no supplied airflow for 120 minutes ($n = 5$) to examine the effect of laryngeal movement via vocal fold adduction and abduction. To induce this condition, an *in vivo* surgical procedure was performed as previously described (Ge, French, Ohno, Zealear, & Rousseau, 2009; Kojima, Valenzuela, et al., 2014; Kojima, Van Deusen, et al., 2014; Rousseau et al., 2011).

In brief, the larynx and trachea were exposed by creating a midline incision from the hyoid bone to sternal notch. A stable airway was provided via a tracheostomy. Stainless-steel hooked electrodes were inserted into the laryngeal musculature to deliver electrical stimulation. Pulse trains were delivered every 10 seconds that included 3 seconds of electrical stimulation (i.e., adduction) and 7 seconds of rest (i.e., abduction).

Finally, a separate condition included vibrated vocal folds (i.e., evoked phonation) via approximation at midline with controlled airflow for 120 minutes (n = 5). This vibratory condition was selected based on our laboratory's previous findings which suggest that modal intensity phonation may best represent physiologic vibration. Modal intensity phonation, even up to 120 minutes, revealed no significant structural disruption to the basement membrane zone and no functional changes in transepithelial resistance (Kojima, Valenzuela, et al., 2014). To evoke phonation, the aforementioned surgical procedures were performed in addition to inserting a cuffed, inflated endotracheal tube into the trachea approximately 2 cm below the opening of the glottis. Compressed, humidified airflow was delivered at 37°C to the glottis. The combined neuromuscular stimulation and controlled airflow produced sustained, audible phonation of modal intensity. Laryngeal imaging was captured using a rigid endoscope and camera. To detect changes in vocal intensity and F_0, acoustic signals were recorded at baseline and in 15-minute intervals using a Perception 170 Condenser Microphone (AKG, Vienna, Austria) positioned approximately 10 cm from the opening of the endoscope. Mouth-to-microphone distance and amplitude gain were held constant. Recordings were digitized using Computerized Speech Lab Model 4500 (KayPENTAX, Montvale, NJ). Acoustic analysis focused on the most representative 1-second central portions of the waveforms. A repeated measures analysis of variance (ANOVA) revealed no significant difference in mean vocal intensity across 120

minutes of vibration, $F(8) = 0.60$, $p = .773$. As displayed in Figure 4A, stable intensity values ranged from 60.06-61.46 dB sound pressure level. Similarly, a repeated measures ANOVA revealed no significant difference in mean F_0 across 120 minutes of vibration, $F(8) = 1.94$, $p = .087$. Mean F_0 values ranged from 492-615 Hz (Figure 4B). At the end of all procedures, animals were sacrificed and larynges were excised. One vocal fold was used for TEM and the contralateral vocal fold was used for TUNEL method.

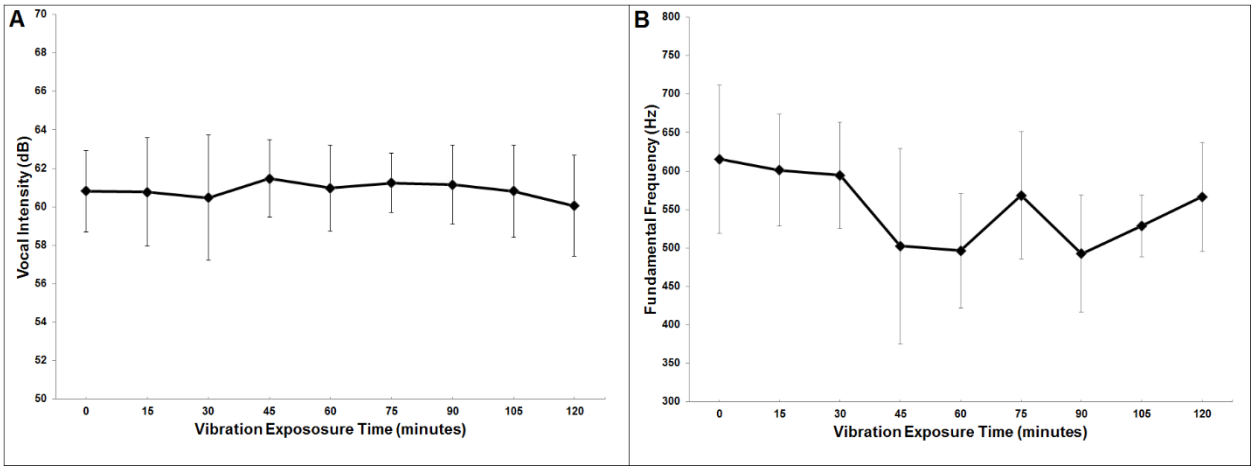

Figure 4. Stability of Acoustic Measurements Across 120 Minutes of Vibration Exposure Time (x-axis) for Animals that Underwent Evoked Phonation. Data points are A) mean vocal intensity in dB sound pressure level (y-axis) and B) mean F_0 in Hz (y-axis). Error bars represent standard deviations of the means.

Transmission Electron Microscopy

11 of the 12 vocal fold specimens were prepared for routine processing for TEM. One vocal fold in the normal condition was not prepared for TEM because this tissue had been used for a separate experiment. For primary fixation, tissue specimens were immersed in 2.5% glutaraldehyde in 0.1 M sodium cacodylate buffer (pH 7.4) and then rinsed with 0.1 M sodium

cacodylate buffer (5 minutes x3). For secondary fixation, tissue specimens were immersed in 1% osmium tetroxide in 0.1 M sodium cacodylate buffer (1 hour at room temperature) and then rinsed in 0.1 M sodium cacodylate buffer as before. An ethyl alcohol series was used for specimen dehydration. Specimens were immersed in 30%, 50%, 75%, 85%, and 95% ethyl alcohol for 15 minutes. Final dehydration occurred using 100% (x3) ethyl alcohol for 15 minutes, and then propylene oxide and 100% ethanol for 5 minutes, followed by incubation in 100% propylene oxide (x2) for 15 minutes each. Stepwise infiltrations were completed with Epon resin and specimens were embedded in flat molds and allowed to polymerize for 48 hours at 60°C. Thick sections (500 nm to 1 micron) were initially cut from each block, the region of interest was identified, and then ultrathin sections (70 nm) were cut and placed on 300 mesh copper grids. Grids were post-section stained with 2% uranyl acetate for 15 minutes and then with Reynold's lead citrate for 15 minutes. After TEM preparation, images were captured using a Philips/FEI T12 transmission electron microscope (FEI Company, Hillsboro, OR) at low and high magnifications to visualize the apical epithelial cell surface and internal cellular structures.

To initially assess the most common morphological features of cell death, the author (CN) performed a non-blinded evaluation of TEM images from selected vocal fold tissues that were immobilized (n = 1), approximated (n = 2), and vibrated (n = 3). This preliminary analysis involved subjective and qualitative descriptions of cellular features that are consistent with cell death. These data were used to create six categories for a subsequent rating task with TEM images from all 11 specimens. As displayed in Table 1 with corresponding justifications, the categories focused on cell size, cell morphology, and characteristics specific to cell death. These categories have previously been cited in the literature as evidence of dying cells under visualization by TEM (Elmore, 2007).

Table 1

Selected Ultrastructural Categories and Justifications for Ratings of Transmission Electron Microscopy Images

Category	Theme	Justification
Cells with small nuclei	Cell size	Apoptotic cells shrink in size
Cells with enlarged nuclei	Cell size	Necrotic cells swell in size
Cells with rounded shape	Cell morphology	Shrinking apoptotic cells appear more circular
Cells with elongated shape	Cell morphology	Healthy vocal fold epithelium is stratified squamous
Cells with condensed chromatin	Cell death	Chromatin in apoptotic nuclei becomes more concentrated
Cells with apoptotic bodies	Cell death	Apoptotic bodies extrude from cells before undergoing phagocytosis

Two blinded judges completed a rating task in which they were presented with TEM images. The order of image presentation was randomized. For each specimen, three distinct TEM images were included with the following criteria: images were captured at 4,400x magnification, showed a visible apical surface, and contained at least one identifiable epithelial cell nucleus. The judges were asked to count the total number of cells in each image and then count the number of cells in each of the following six categories: (1) small nuclei, (2) enlarged nuclei, (3) rounded cell shape, (4) elongated cell shape, (5) condensed chromatin, and (6) apoptotic bodies (Table 1). The number of cells in each category was divided by the total number of cells and converted to a percentage. Percentages were averaged across three TEM images per specimen for both judges (i.e., mean of 6 percentage values per specimen). The judges were permitted to refer to visual examples of each category, increase image

magnification, change previous responses, and take brief breaks to minimize the effects of fatigue. The first judge (CN) trained the second judge in the aforementioned procedures.

To determine if the judges internally rated the TEM images with consistency, intra-rater reliability was evaluated in which the judges repeated the rating task on 50% of the original TEM images. The order of image presentation was again randomized. For both judges, two separate paired samples *t*-tests and two separate Pearson product-moment correlation coefficients were computed. Inter-rater reliability was evaluated to determine if both judges rated the TEM images similarly to one another. An independent samples *t*-test and Pearson product-moment correlation coefficient were computed.

Terminal Deoxynucleotidyl Transferase dUTP Nick End Labeling

Cryosectioning of all 12 vocal fold tissues specimens was performed. Tissues were immersed in 4% paraformaldehyde for 24 hours, followed by immersion in sucrose for 24 hours. Specimens were coated in optimal cutting temperature compound embedding medium (Fisher HealthCare, Houston, TX), placed in liquid nitrogen, stored at -80°C, and sliced into 12-μm thickness. 12-μm section thickness was selected to ensure that the vocal fold epithelium was preserved during cutting and embedding, as thicker sectioning reduced episodes of damage to the tissue. TUNEL method was performed in cryosections (two sections per larynx) with the ApopTag® Fluorescein *In Situ* Apoptosis Detection Kit (EMD MILLIPORE International, Inc.). Post-fixed slides were washed with phosphate buffered saline (PBS). Slides were pretreated with precooled 30 ml ethanol and 15 ml acetic acid at -20°C for 5 minutes. Slides were drained and washed with PBS. Equilibration buffer was applied to each laryngeal specimen and incubated at room temperature for 10 seconds. Working strength terminal deoxynucleotidyl transferase (tDt) enzyme was applied to each specimen and incubated in a humidified chamber at 37°C for 1 hour.

Slides were agitated in working strength stop/wash buffer for 15 seconds and incubated at room temperature for 10 minutes. Slides were washed with PBS and working strength antidigoxigenin conjugate was added to the specimen surface area. Slides were incubated in a humidified chamber at room temperature for 30 minutes. Slides were washed and Fluoromount-G® mounting medium containing 4',6-diamidino-2-phenylindole (DAPI) was applied to the specimens and mounted under a glass coverslip.

Negative and positive controls were created. A negative control was performed using a vocal fold tissue specimen exposed to biomechanical vibration for 120 minutes. The aforementioned TUNEL procedures were performed without active tDt enzyme. For the positive control, a normal vocal fold tissue specimen was pretreated with deoxyribonucleic (DN) buffer consisting of 30 mM Trizma base, pH 7.2, 4 mM $MgCl_2$, and 0.1 mM *dithiothreitol* at room temperature for 5 minutes, and then 0.2 µl DNase was dissolved in 2 ml DN buffer. DNase solution was applied to the tissue section, incubated at room temperature for 10 minutes, and rinsed with distilled water. Fluorescent images were captured using a Nikon Eclipse 90i Microscope (NIS-Elements Basic Research, ver. 3.20). Images were acquired of the apical epithelial cell surface of the true vocal fold. Because the images were acquired at varying exposure times, formal quantification procedures were avoided to reduce the risk of error. In lieu of this, a rating task was performed to evaluate TUNEL staining.

The same two blinded judges completed a rating task in which they were presented with images of all 12 fluorescent TUNEL-stained vocal fold specimens at 20x magnification. The order of image presentation was randomized. The judges selected the degree of TUNEL-positive staining along the entire apical epithelial surface as one of the following classifications per image: no TUNEL-positive cells, minimal TUNEL-positive cells, moderate TUNEL-positive

cells, and abundant TUNEL-positive cells. TUNEL-positive cells were defined as the amount of visible green staining, as individual cells and/or continuous staining, along the epithelium. The epithelium was defined as approximately two or three layers of DAPI staining cells that marked a clear outline of the apical vocal fold. Counting discontinued when there was a gap in this region, as indicated by a reduction in cells that likely corresponded to the lamina propria. An example of this boundary distinction is shown in Figure 5. The judges were permitted to increase image magnification, change previous responses, and take brief breaks to minimize the effects of fatigue. No visual examples of images were provided. Following individual ratings, the first and second judge completed a final consensus rating with four images in which there were discrepancies.

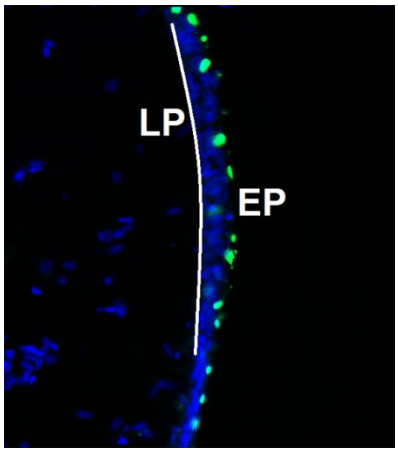

Figure 5. Image Illustrating Region Defined as Epithelial Layer of Vocal Fold during Rating Task for TUNEL Staining. On the right, the epithelium (EP) faces the apical surface. The white line demarcates the lamina propria (LP) on the left, as determined by a reduction in cells.

To determine if the judges internally rated the fluorescent TUNEL-stained images with consistency, intra-rater reliability was evaluated in which the judges repeated the rating task on

50% of the original images. The order of image presentation was again randomized. For both judges, two separate paired samples *t*-tests and two separate Pearson product-moment correlation coefficients were computed to investigate the strength of the associations between the original ratings and repeated ratings. Inter-rater reliability was evaluated to determine if both judges rated the images similarly to one another. An independent samples *t*-test and Pearson product-moment correlation coefficient was computed.

Results

Reliability: Ratings of TEM Images

For the first judge, there was no significant difference between the original ratings versus 50% of the repeated ratings, $t(101) = .32$, $p = .752$. Original and repeated ratings were strongly and positively correlated, $r(100) = .79$, $p = .000$. For the second judge, although there was a significant difference between the original versus repeated ratings, $t(101) = 2.52$, $p = .013$, original and repeated ratings were strongly and positively correlated, $r(100) = .87$, $p = .000$. For inter-rater reliability, there was no significant difference between ratings from the first judge and second judge, $t(394) = -.57$, $p = .572$. In addition, ratings from the first judge were positively correlated with ratings from the second judge, $r(196) = .21$, $p = .003$.

Reliability: Ratings of Fluorescent TUNEL-Stained Images

For the first judge, there was no significant difference between the original ratings versus 50% of the repeated ratings, $t(5) = -1.00$, $p = .363$. Original and repeated ratings were strongly and positively correlated, $r(4) = .86$, $p = .029$. For the second judge, there was no significant difference between the original versus repeated ratings, $t(5) = 0.00$, $p = 1.00$. Original and repeated ratings were strongly and positively correlated, $r(4) = .87$, $p = .024$. For inter-rater

reliability, there was no significant difference between ratings from the first judge and second judge, $t(22) = .351$, $p = .729$. In addition, ratings from the first judge were strongly and positively correlated with ratings from the second judge, $r(10) = .89$, $p = .000$.

Ultrastructural Evaluation by TEM

Table 2 summarizes the major ultrastructural characteristics of cell death across immobilized, approximated, and vibrated vocal folds. Normal immobilized vocal fold epithelium comprised approximately three layers of cells that demonstrated a flattened morphology consistent with stratified squamous cell shape. The apical membranes of polarized epithelial cells were distinctly outlined with microvilli protruding along the entire length of the surface facing the lumen. Cells showed well-defined nuclear envelopes and large, elongated nuclei. Cell nuclei contained a dark-staining nucleolus and chromatin in the form of tightly-coiled heterochromatin and loosely-coiled euchromatin (Figure 6A). The cytoplasm and organelles appeared structurally preserved. Adjacent cells were packed closely together, making it challenging to demarcate precise boundaries between cells along the basolateral membranes at lower magnification fields of view.

Table 2

Summary of Ultrastructural Characteristics of Cell Death in Immobilized, Approximated, and Vibrated Vocal Folds

Immobilized	Approximated	Vibrated
Flattened cell shape	Flattened cell shape	Small nuclei
Organized microvilli	Less organized microvilli	Irregular nuclear envelopes
Defined nuclear envelopes	Large nuclei	Uneven microvilli
Large, elongated nuclei	Euchromatin	Large extracellular space
Dark-staining nucleolus	Preserved organelles	Condensed chromatin
Heterochromatin	Reduced cell-to-cell contact	Preserved organelles
Euchromatin		Apoptotic bodies
Preserved organelles		Enlarged cells
Close cell-to-cell contact		Vacuolated cytoplasm
		Scarce organelles
		Poorly defined membranes

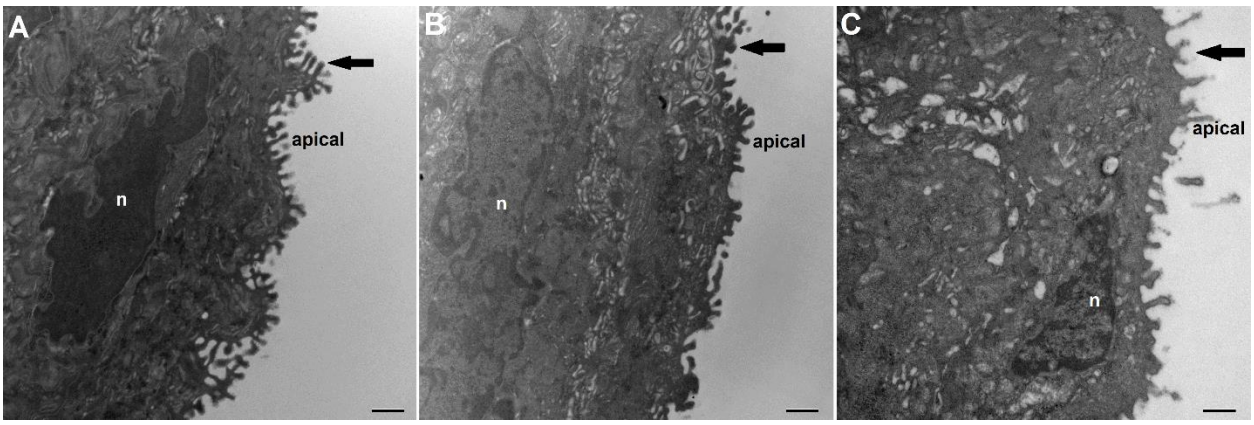

Figure 6. Analysis of Morphology of Vocal Fold Epithelial Cell Nuclei (n) by Transmission Electron Microscopy. The apical cell surface (right) is shown of the true vocal fold epithelium after A) immobilization, B) approximation for 120 minutes, and C) vibration for 120 minutes. Microvilli (arrows) show a regular shape in immobilized vocal fold tissue, but become increasingly irregular after approximation and vibration. Images were captured at 15,000x magnification.

Similarly, approximated vocal fold epithelial cells demonstrated a flattened shape. Microvilli of less uniform length covered the apical cell membranes. Large euchromatic nuclei were present (Figure 6B). Although preserved cytoplasm and organelles were appreciated, there was less cell-to-cell contact between the basolateral domains of the most superficial cells and the apical domains of the next layer of cells beneath. This loose connection appeared to be the result of increased expansion of the tight intercellular junctional complex. However, cell membranes and intercellular contents were maintained.

Finally, vibrated vocal fold epithelial cells were characterized by small nuclei and irregularly shaped dark-staining nuclear envelopes (Figure 6C). Uneven microvilli projected from the apical cell membranes. Large extracellular spaces separated adjacent cells. Cells showed a circular morphology and appeared to be shrinking inward. Cell membranes were relatively outlined, indicating that the membranes remained intact.

TEM images in Figure 7 illustrate the most common morphological features of apoptotic cell death in vocal fold epithelial cells. As shown in Figure 7A, apical epithelial cells had condensed, peripheralized chromatin. Organelles were still preserved, particularly mitochondria (Figure 7B). In some instances, cell nuclei began to break down into apoptotic bodies (Figures 7C and 7D). There was no evidence of engulfment of apoptotic bodies by neighboring cells or macrophages. In addition, several epithelial cells from one vibrated vocal fold showed features consistent with necrotic cell death (Figure 8). Necrosis was characterized by enlarged cells and nuclei compared to the basal epithelial cells located near the basement membrane zone. Necrotic cells had vacuolated cytoplasm, scarce organelles, and a poorly defined cell membrane, suggestive of initial membrane rupturing (Figure 8A). However, there were no apparent

observations of dispersed of cytoplasm into the extracellular space. Clusters of fragmented chromatin were also evident (Figure 8B).

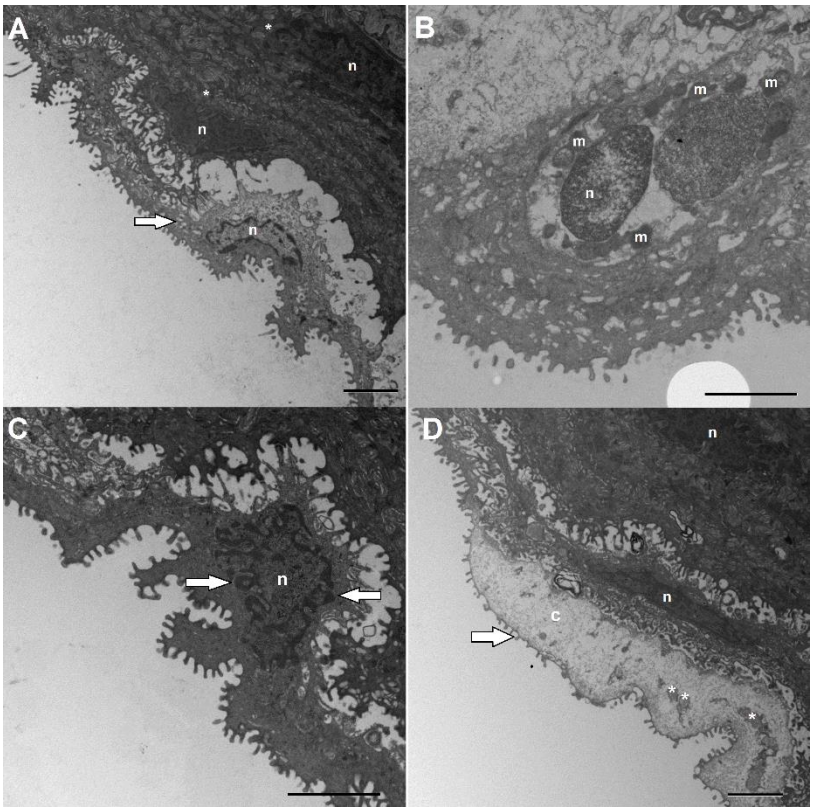

Figure 7. Evaluation of Ultrastructural Features of Different Stages of Apoptotic Cell Death in Vocal Fold Epithelial Cells after Biomechanical Vibration for 120 Minutes. A) Vital cells (asterisk) are located basolaterally with close boundaries between one another. An apical apoptotic cell (arrow) is shown with a large extracellular space between its neighboring vital cells. Examination of cell nuclei (n) reveals that the apoptotic cell is beginning to shrink in size compared to the vital cells. In the apoptotic cell nuclei, chromatin is condensed and peripheralized (6,500 x). B) Several mitochondria (m) are surrounding a pyknotic nucleus (n) of a cell undergoing apoptosis (11,000 x). C) An apoptotic cell nucleus (n) begins to break down into several apoptotic bodies (arrows) (11,000 x). D) A more advanced formation of apoptotic bodies (asterisk) is visible inside the cell cytoplasm (c) and intact plasma membrane of an apoptotic cell (arrow). At this phase, there is no evidence that apoptotic bodies are engulfed by a macrophage, as microvilli continue to protrude from the apoptotic epithelial cell membrane, the shape of which aligns with its neighboring vital cells with visible nuclei (n) (6,500 x).

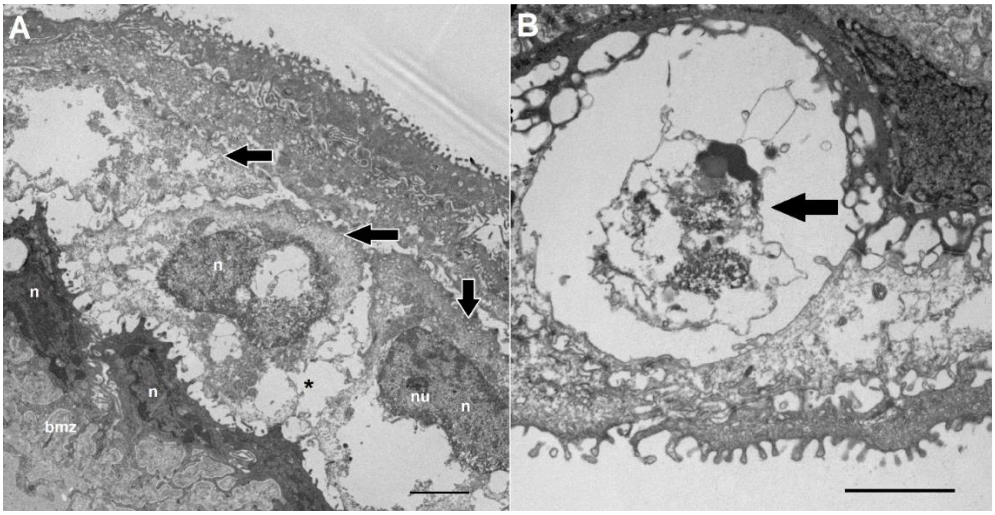

Figure 8. Evaluation of Ultrastructural Features of Different Stages of Necrotic Cell Death in Vocal Fold Epithelial Cells after Biomechanical Vibration for 120 Minutes. A) Necrotic cells (arrows) are visibly enlarged in comparison to vital basal epithelial cells located near the basement membrane zone (bmz). Necrotic cells are characterized by vacuolated cytoplasm and few organelles, while the swollen nuclei (n) and nucleolus (nu) remain identifiable. Large extracellular spaces surround the necrotic cells in contrast to vital basal cells which demonstrate closer boundaries to neighboring cells. There is evidence of an emerging ruptured cell membrane (asterisk) (6,500 x). B) High magnification microscopy image of an apical necrotic cell showing clusters of chromatin fragmentation (arrow). Edges of the cell membrane are less defined and might indicate the future vulnerability to increased cell membrane permeability (11,000 x).

The rating task of TEM images revealed that the mean percentage of vocal fold epithelial cells with small nuclei was similar across all three experimental conditions. As shown in Figure 9A, the epithelium from animals with immobilized vocal folds were rated as having the greatest percentage of small nuclei (30.60%), followed closely by vibrated (25.45%) and approximated vocal folds (24.60%). In contrast, enlarged cell nuclei were rarely observed ultrastructural features. Ratings of enlarged nuclei were indicated in only vibrated (9.44%) and approximated (4.60%) vocal folds. No epithelial cells in the TEM images of immobilized vocal folds were observed to have enlarged nuclei (0%; Figure 9B).

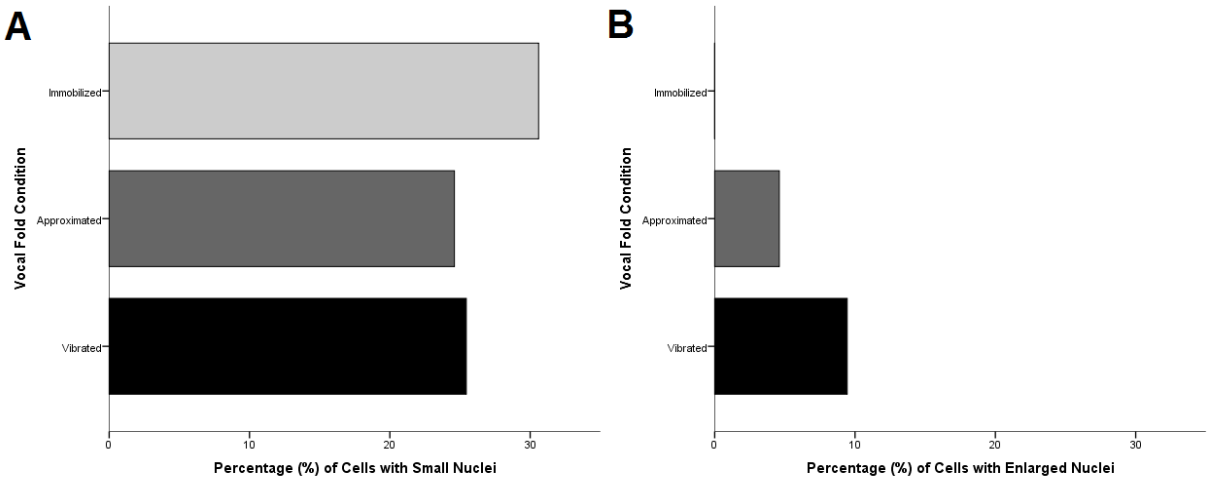

Figure 9. Mean Percentage of Vocal Fold Epithelial Cells (x-axis) Rated by Cell Size. Ratings are shown for immobilized (light grey bars), approximated (dark gray bars), and vibrated vocal folds (black bars) for A) small nuclei and B) enlarged nuclei.

Analysis of cell morphology showed that rounded cell shape was rated highest in cells of vibrated vocal folds (49.09%), with lower mean percentages for approximated (38.16%) and immobilized vocal folds (27.82%; Figure 10A). As expected, there was an inverse trend for the category of elongated cell shape. Specifically, Figure 10B shows that elongated cell shape was rated highest for immobilized vocal folds (59.96%) and continued to decrease for approximated (49.41%) and vibrated vocal folds (41.05%).

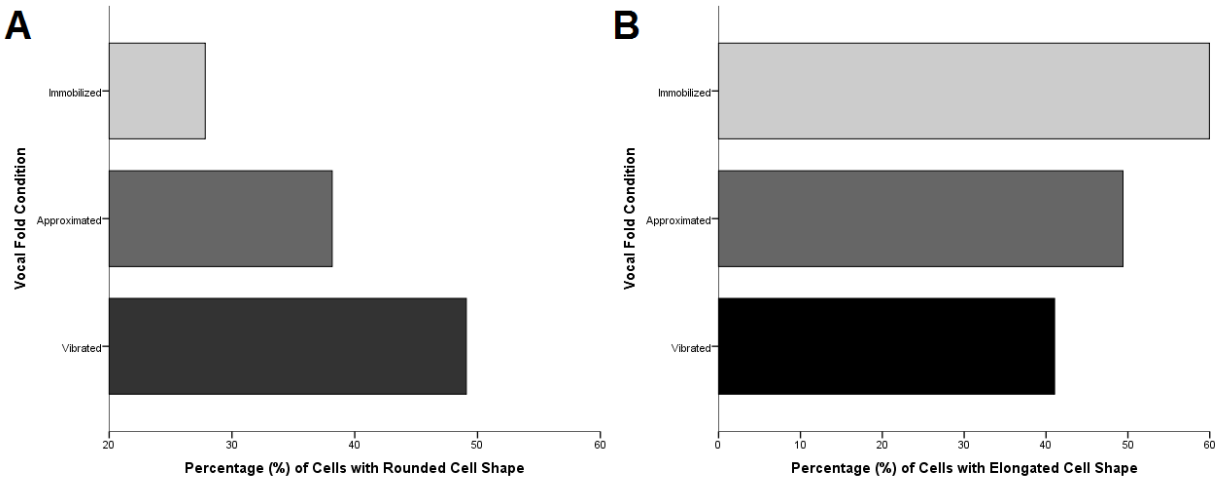

Figure 10. Mean Percentage of Vocal Fold Epithelial Cells (x-axis) Rated by Cell Morphology. Ratings are shown for immobilized (light grey bars), approximated (dark gray bars), and vibrated vocal folds (black bars) for A) rounded cell shape and B) elongated cell shape.

Categories related to cell death indicated that approximated and vibrated vocal folds had higher ratings of condensed chromatin (Figure 11A) and apoptotic bodies (Figure 11B) compared to immobilized vocal folds. In particular, the mean percentage of epithelial cells with condensed chromatin was rated highest for approximated (44.30%) and vibrated vocal folds (39.14%), while very few epithelial cells in the immobilized condition showed signs of condensed chromatin (6.61%). Likewise, the mean percentage of cells with apoptotic bodies was rated highest for approximated (24.50%) and vibrated vocal folds (22.25%), in comparison to only 3.52% of epithelial cells from animals with immobilized vocal folds.

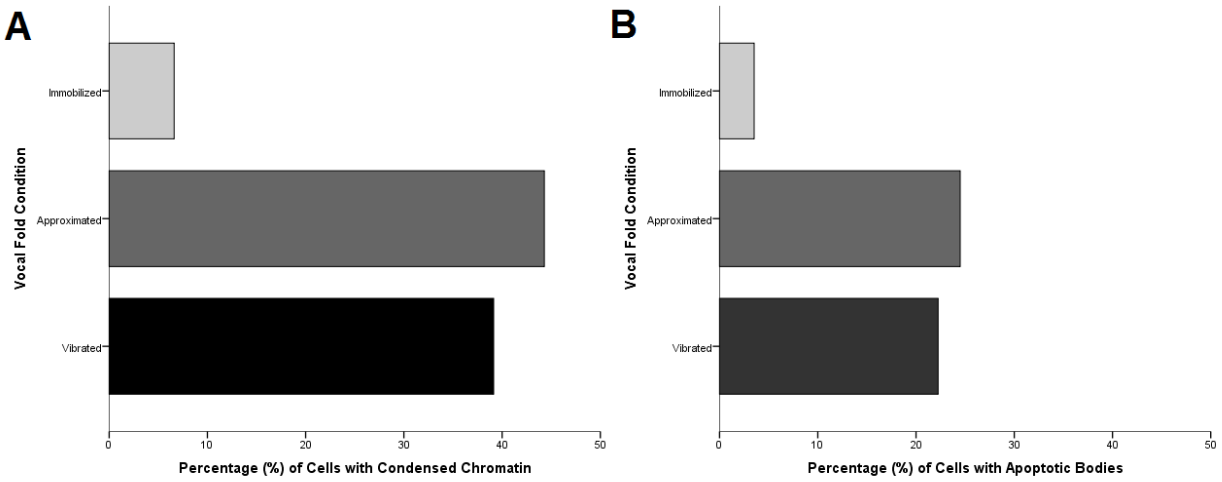

Figure 11. Mean Percentage of Vocal Fold Epithelial Cells (x-axis) Rated by Common Features of Cell Death. Ratings are shown for immobilized (light grey bars), approximated (dark gray bars), and vibrated vocal folds (black bars) for A) condensed chromatin and B) apoptotic bodies.

Immunohistochemical Detection by TUNEL Method

TUNEL method revealed the expression of cell death along the apical region of the true vocal fold epithelium. Figure 12 shows representative fluorescent TUNEL-stained vocal fold tissue sections after immobilization (Figure 12A), approximation (Figure 12B), and vibration (Figure 12C) acquired at 20x magnification. Table 3 displays the mean percentages of the degree of TUNEL-positive cells rated across the three experimental conditions. In the immobilized condition with $n = 2$, one-half of the fluorescent images (50%) were rated as no TUNEL-positive epithelial cells, while the remaining one-half (50%) were rated as moderate TUNEL-positive cells. The majority of florescent images of the approximated vocal folds were rated as no-to-minimal TUNEL-positive cells (40% rated as no TUNEL-positive; 40% rated as minimal TUNEL-positive). The majority of florescent images of the vibrated vocal folds were rated as moderate-to-abundant TUNEL-positive cells (40% rated as moderate TUNEL-positive; 40% abundant TUNEL-positive).

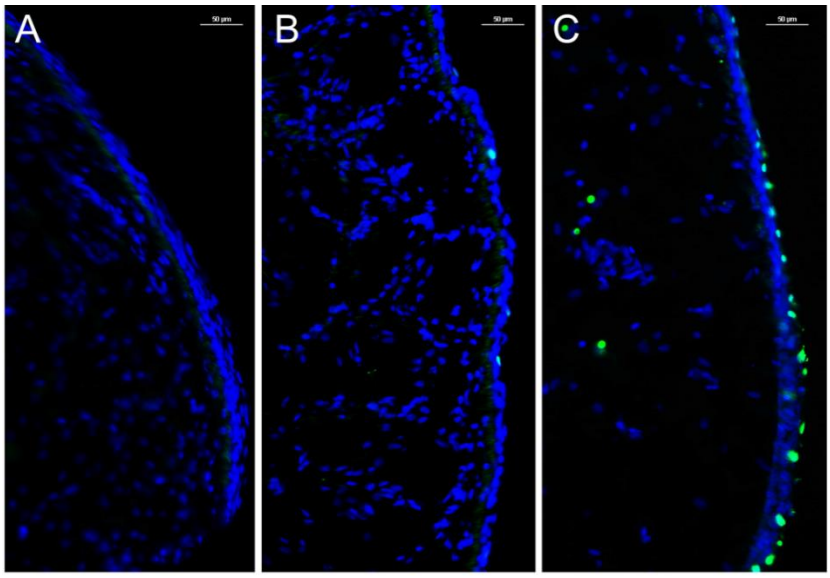

Figure 12. Fluorescent Stained True Vocal Fold Tissue Specimens using TUNEL Method. The apical cell surface (right) is shown of the true vocal fold epithelium after A) immobilization, B) approximation for 120 minutes, and C) vibration for 120 minutes. Images were acquired at 20x magnification.

Table 3

Mean Percentages of Rated Degree of TUNEL-Positive Staining in Immobilized, Approximated, and Vibrated Vocal Folds

Vocal Fold Condition	No TUNEL	Minimal TUNEL	Moderate TUNEL	Abundant TUNEL	Total
Immobilized (n = 2)	50%	0%	50%	0%	100%
Approximated (n = 5)	40%	40%	20%	0%	100%
Vibrated (n = 5)	0%	20%	40%	40%	100%

The negative control confirmed no presence of TUNEL staining (Figure 13A). To determine if TUNEL method properly worked, a positive control was used to induce cleavage of genomic DNA by DNase treatment. The positive control resulted in extensive nuclear fragmentation as indicated by the labeling of TUNEL in all vocal fold cell nuclei (Figure 13B). The majority of nuclear fragmentation was evident in epithelial cells, although scarce staining was also appreciated deeper in the primarily non-cellular lamina propria.

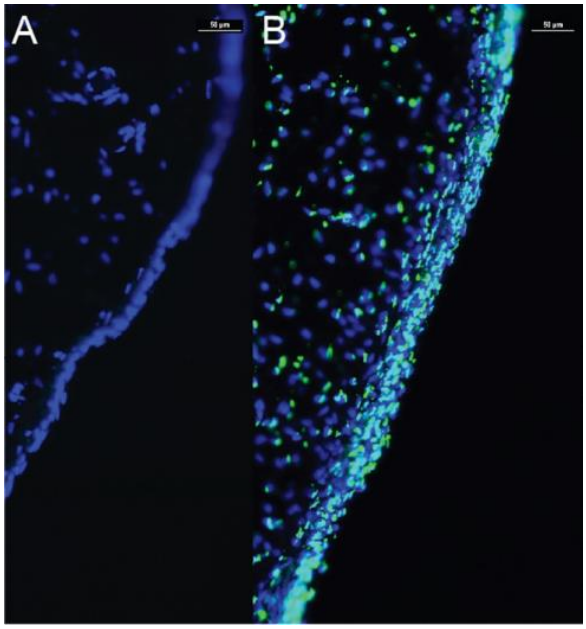

Figure 13. Positive and Negative Controls of Fluorescent Stained True Vocal Fold Tissue Specimens using TUNEL Method. The apical cell surface (right) is shown of A) a positive control of a normal vocal fold and B) negative control of a vocal fold specimen exposed to 120 minutes of biomechanical vibration. The apical epithelial surfaces are shown on the right. Images were acquired at 20x magnification.

Discussion

This pilot study aimed to establish more systematic approaches to evaluate cell death in vocal fold epithelial cells and to investigate cell death in response to immobilization, approximation, and biomechanical vibration. Cell death was detected by morphological signs using TEM and *in situ* staining of DNA strand breaks using TUNEL method. Ultrastructural evaluation revealed that apoptotic cell death is observed in the vocal fold epithelium of rabbits after undergoing approximation and vibration for 120 minutes. Movement- and vibratory-induced apoptosis is primarily characterized by pyknotic epithelial nuclei as indicated by condensed chromatin and apoptotic bodies. Although instances of necrosis are rare, morphological evidence of necrotic epithelial cells include cellular and organelle swelling (e.g., enlarged nuclei). Additionally, TUNEL method confirmed that the vocal fold expresses an immunohistochemical marker for apoptosis along the apical surface of the epithelium.

Two complementary methods were selected to measure vocal fold epithelial cell death. First, TEM was performed to provide high-resolution images of cellular structures. TEM was selected as the primary outcome because it serves as the gold standard technique for describing the ultrastructural features of cells committed to die (Elmore, 2007; Martinez, Reif, & Pappas, 2010). In conjunction with TEM, TUNEL method was performed on the laryngeal tissue sections. In cells undergoing apoptosis, caspase-activated DNase causes fragmented DNA that leads to a higher number of free 3' hydroxyl ends (3'-OH) in the nuclei. TUNEL is a common apoptosis assay that relies on labeling the 3'-OH with the tDt enzyme. While cells undergoing DNA fragmentation stain positive, normal or proliferating cells do not typically stain because they do not produce many 3'-OH. Collectively, our findings suggest that vocal fold epithelial cells undergo cell death, primarily apoptosis, in response to vocal fold movement via adduction

and abduction and biomechanical vibration. This is evidenced by observations of chromatin condensation and apoptotic bodies according to TEM ratings and positively stained DNA fragmentation by TUNEL method. When comparing individual results of TEM images with fluorescent TUNEL-stained images, approximately half of the laryngeal tissue specimens showed similar patterns. That is, there was a noted tendency for higher ratings of condensed chromatin and apoptotic bodies to correspond to moderate-to-abundant TUNEL-positive cells. Interestingly, the majority of specimens showing a consistent pattern between both analyses belonged to the vibration condition.

The two studied ultrastructural features of apoptotic cell death, condensed chromatin and apoptotic bodies, were rated as most prevalent following vocal fold approximation and vibration. These criteria indicate that multiple phases of apoptosis occurred. For instance, increased concentration of chromatin is an early stage of apoptosis in vocal fold epithelial cells, while a later stage is characterized by the formation of apoptotic bodies. A possible explanation for the occurrence of both features is that perhaps different locations of the epithelium may have undergone varying levels of biomechanical stresses that led to different stages of apoptosis. Interestingly, there were no identified inflammatory cells such as macrophages engulfing apoptotic bodies. This would be expected, given that the laryngeal tissues were harvested immediately after the experiments. Perhaps later stages of apoptosis would be observed with a longer delay between experimental procedures and tissue excision. In addition, necrotic cell death may be rarer after vocal fold movement and vibration, as few cells overall showed evidence of enlarged nuclei. However, episodes of some enlarged nuclei indicate that apoptosis is not be the only type of cell death in the vocal fold epithelium. It is possible that apoptosis and

necrosis may occur simultaneously or that given greater durations of trauma, apoptosis might eventually evolve into necrotic cell death.

In contrast, immobilized vocal folds were infrequently rated with features of cell death. Moreover, cell morphology of immobilized vocal fold epithelium suggests that cell shape was primarily elongated or flattened, which indicates that normal squamous epithelial cells remained intact. These findings in the immobilized experimental condition are not surprising given that rabbits are relatively quiet animals and are not susceptible to the biomechanical stresses that occur during phonation. As such, the regular exchange of airflow through the glottis during respiration and vocal fold adduction during swallowing may not be significant factors in initiating cell death. It is recognized that all epithelial cells in normal vocal folds must eventually die during turnover to promote a strong barrier. Moreover, it is likely that the rate of epithelial cell turnover occurs more gradually in normal vocal folds with during immobilization. This preliminary notion might be interesting to consider the effect of vocal fold epithelial cell turnover on wound healing in patients who are prescribed voice rest.

There are acknowledged differences between the preliminary TEM qualitative analysis and subsequent rating task of TEM images. Although the qualitative portion described reduced epithelial cell nuclei size in response to vibration, the rating task disagreed with this assessment. In fact, the size of epithelial cells was rated consistently across all experimental conditions and immobilized vocal folds revealed slightly greater occurrences of small nuclei. The discrepancy between the analyses could be explained by the inherent challenges with visual-perceptual judgements of electron microscopy images. Based on the current results, it is necessary to further explore alternative methods of measuring cell nuclei size to evaluate its role in vocal fold cell death with improved accuracy. Because the present findings suggest that rounded cell shape

may be common in vocal fold tissues exposed to vibration, it may be that vibrated vocal folds demonstrate early morphological signs consistent with cell shrinkage by becoming more circular.

Ratings using the TUNEL method revealed that vocal folds exposed to approximation tended to demonstrate no-to-minimal TUNEL-positive staining, while vocal folds exposed to vibration demonstrated moderate-to-abundant TUNEL-staining. These findings might be an initial indication that vibration leads to greater expression of cell death via TUNEL. However, the current rating procedure must be interpreted with caution given that the fluorescent images were captured at different exposure times. To determine whether the studied conditions induced more or less labeling of TUNEL-positive cells, future research is needed to objectively quantify the degree of staining.

Although previous studies alluding to vocal fold cellular degradation after injury or in vocal fold disease are highly suggestive of cell death (Dikkers et al., 1993; Gray & Titze, 1988; Kotby et al., 1988; Marcelino & Oliveira, 2005; Martins et al., 2010; Martins et al., 2011; Rousseau et al., 2011), it is not possible to confirm this without more concrete methods. The current results provide an important step toward better communicating the biochemical mechanism of cell death in the vocal fold. It is recognized that future research is necessary to quantify the rate of apoptosis with greater durations of damage exposure to determine if cell death increases or remains a static response. However, these findings lay a preliminary foundation for future studies to quantify cell death as it may relate to different degrees of vocal fold damage. The pilot study's current methods to measure apoptotic events may also become useful biomarkers for the diagnosis and prognosis of human vocal fold disease.

CHAPTER IV

METHODOLOGY

Overview

The purpose of the current study was to quantify the rate of apoptosis signaling in the vocal fold epithelium with increasing durations and extrapolated cycles of vibration exposure. A secondary objective was to investigate whether gene transcript and protein levels of TNF-α are upregulated in the vocal fold epithelium with increasing durations of vibration exposure. Table 4 summarizes the research questions, specific aims to address these questions, and corresponding hypotheses of the current study. Chapter IV presents the materials and methods, which is organized in the following sequence: research design, animals, data collection procedures, and statistical analysis.

Table 4

Research Questions, Specific Aims, and Hypotheses

Research Question	Research Aim	Hypothesis
1) What is the effect of longer time-doses of vibration exposure on apoptosis signaling in the vocal fold epithelium?	Aim 1: To measure the effects of increasing time-doses of vibration exposure on apoptotic cell death in the true vocal fold epithelium using TUNEL method and TEM.	Hypothesis 1A: There is a significant increase in the mean intensity of TUNEL staining in the true vocal fold epithelium with increasing time-doses of vibration exposure. Hypothesis 1B: There is a significant decrease in the mean area of epithelial cell nuclei using TEM images of the true vocal fold epithelium with increasing time-doses of vibration exposure.
2) What is the effect of higher cycle-doses of vibration exposure on apoptosis signaling in the vocal fold epithelium?	Aim 2: To determine the relationship between extrapolated cycle-doses of vibration exposure and apoptotic cell death in the true vocal fold epithelium using TUNEL method and TEM.	Hypothesis 2A: There is a significant positive correlation between extrapolated cycle-doses of vibration exposure and the mean intensity of TUNEL staining in the true vocal fold epithelium. Hypothesis 2B: There is a significant negative correlation between extrapolated cycle-doses of vibration exposure and the mean area of epithelial cell nuclei using TEM images of the true vocal fold epithelium.
3) What is the effect of longer time-doses of vibration exposure on TNF-α levels in the vocal fold epithelium?	Aim 3: To measure the effects of increasing time-doses of vibration exposure on gene and protein expression of the pro-inflammatory cytokine TNF-α in the true vocal fold epithelium.	Hypothesis 3A: There is a significant increase in the gene transcript levels of TNF-α in the true vocal fold epithelium with increasing time-doses of vibration exposure. Hypothesis 3B: There is a significant increase in the mean intensity of TNF-α protein expression in the true vocal fold epithelium with increasing time-doses of vibration exposure.

Research Design

A prospective between subjects factorial research design was used. Animals were randomized to three groups of time-doses of vibration exposure or one control group. As shown in Table 5, animals received 30 minutes (n = 5), 60 minutes (n = 5), or 120 minutes (n = 5) of modal intensity phonation as the experimental conditions, or 120 minutes of vocal fold approximation as the control condition (n = 5).

Table 5
Summary of Research Design

		Time Dose		
		30 minutes	60 minutes	120 minutes
Condition	Modal intensity phonation	n = 5	n = 5	n = 5
	Approximation (control)			n = 5
			Total *N*	**20**

The vibration magnitude of modal intensity phonation was selected based on previously reported morphological features of intact paracellular spaces and basement membrane, and a lack of functional tissue changes as measured by transepithelial resistance (Kojima, Valenzuela, et al., 2014). In contrast, raised intensity phonation was not studied due to evidence of pathologic damage, primarily epithelial tissue obliteration and upregulated inflammatory responses, which could lead to less viable tissue available for analysis (Kojima, Valenzuela, et al., 2014; Swanson et al., 2010). As such, modal intensity phonation is believed to be the best representation of physiologic vocal fold vibration.

The maximum time-dose of 120 minutes of vibration exposure was selected based on work by Solomon, Glaze, Arnold, and van Mersbergen (2003) that revealed decreased vocal

function after 120 minutes of loud speaking in human subjects. Subsequent work in our laboratory confirmed observations of structural and functional vocal fold tissue changes at 30-minute, 60-minute, and 120-minute time-doses of vibration exposure (Kojima, Valenzuela, et al., 2014; Kojima, Van Deusen, et al., 2014).

Vocal fold approximation with no supplied airflow for the maximum time-dose of 120 minutes was selected as the control condition. This control was selected to examine the effect of vocal fold movement via adduction and abduction on apoptotic cell death. Previous data revealed that approximated vocal folds for 120 minutes reveal morphological signs of cell death, specifically condensed chromatin and apoptotic bodies (Novaleski et al., accepted for publication). Thus, it is important in the current study to better differentiate the influence of movement (control condition) versus vibration (experimental condition) on cell death signaling. Normal vocal fold tissue was not evaluated in this study because preliminary data from Novaleski et al. (accepted for publication) revealed that normal vocal fold tissue infrequently showed ultrastructural signs of cell death (see Chapter III: Pilot Study). Thus, findings from normal tissue would be challenging to compare to experimental conditions and difficult to meaningfully interpret.

For research aim 1, laryngeal tissue specimens were evaluated for apoptosis by TUNEL and TEM. For research aim 2, extrapolated cycle-doses of vibration exposure were extrapolated based on mean F_0 values and correlated with TUNEL and TEM. For research aim 3, TNF-α gene transcript levels were measured using quantitative real-time polymerase chain reaction (qRT-PCR) and TNF-α protein expression was measured using immunofluorescent staining.

Animals

Animals were 27 adult male New Zealand white breeder rabbits weighing between 2.50-3.60 kg (M = 2.90, SD = 0.30). Animals were anesthetized via intramuscular injections of ketamine (35 mg/kg), xylazine (5 mg/kg), and acepromazine (0.75 mg/km). To maintain anesthetic effects, ketamine (17.5 mg/kg) and acepromazine (0.375 mg/kg) were subsequently administered as needed. Heart rate, respiratory rate, oxygen saturation level, and body temperature were monitored throughout the procedure to assess state of anesthesia and general wellbeing. A total of 20 animals were used for final data analysis. The remaining seven animals were excluded from analysis based on the following circumstances: two animals were unable to achieve phonation during the surgical procedures, four tissue specimens were destroyed during paraffin embedding, and one tissue specimen was destroyed during processing for TEM.

This study was performed in accordance with the Public Health Service Policy on Humane Care and Use of Laboratory Animals, National Institutes of Health Guide for the Care and Use of Laboratory Animals, and Animal Welfare Act (7 U.S.C. et seq.). The Vanderbilt University Institutional Animal Care and Use Committee approved the animal protocol (Appendix A).

Data Collection Procedures

In Vivo Phonation

To serve as the control condition, animals underwent vocal fold approximation at midline with no supplied airflow for 120 minutes (n = 5) to induce laryngeal movement via vocal fold adduction and abduction. An *in vivo* surgical procedure was performed as described previously (Ge et al., 2009; Kojima, Valenzuela, et al., 2014; Kojima, Van Deusen, et al., 2014; Rousseau et al., 2011; Swanson et al., 2010). Animals were placed on an operating platform in the supine

position. To prepare for surgery, the neck was shaved from the submentum to the chest. Local anesthesia of 4 mL 0.2% lidocaine was administered at the surgical site. A midline incision was made from the hyoid bone to the sternal notch to expose the larynx and trachea. A tracheostomy was created to provide a stable airway. The trachea was transected just proximal to the sternum and the lower portion of the trachea was suspended to the sternal fascia.

To supply electrical stimulation to the laryngeal musculature, stainless-steel hooked electrodes were used with a Grass S-88 stimulator (SA Instrumentation, Encinitas, CA) and constant current isolation unit (Grass Telefactor, model PSIU6; West Warwick, RI). One electrode was inserted into the belly of each cricothyroid muscle perpendicular to the muscle fibers (cathodes). One electrode was inserted into the cricothyroid membrane on each side at the intersection of a longitudinal line 1 mm lateral to midline and a transverse line 1 mm inferior to the thyroid cartilage (anodes). The total train duration was 10 seconds with 3 seconds of electrical stimulation (i.e., adduction) and 7 seconds of rest (i.e., abduction).

For the experimental conditions, animals underwent vocal fold vibration via approximation at midline with controlled airflow for 30 minutes (n = 5), 60 minutes (n = 5), or 120 minutes (n = 5). To evoke modal intensity phonation, the aforementioned surgical procedures were performed. In addition, a 3.5 cuffed endotracheal tube (Willy Rusch GmbH, Kernen, Germany) was inserted into the upper portion of the bisected trachea and positioned 2 cm below the glottal opening. The cuff of the endotracheal tube was inflated to seal off the trachea and deliver airflow. Continuous humidified airflow heated at 37°C was delivered to the glottis using a Gilmont Instruments flowmeter (GF-8522, Barrington, IL) and Conch Therm III humidifier (Hudson, RCI, Temecula, CA). The simultaneous neuromuscular electrical stimulation to the laryngeal musculature and controlled airflow evoked continuously sustained

audible phonation of modal intensity. Modal intensity phonation was elicited for 30, 60, or 120 minutes using stimulation currents of 0.20-0.60 mA above the phonation threshold, which represents the level necessary for producing sustained audible phonation (Swanson et al., 2009).

To confirm proper vocal fold positioning, laryngeal imaging was captured using a rigid endoscope and camera. The larynx was suspended using a 30° 2.7-mm rigid endoscope (Karl Storz Endoscopy-America, Inc., El Segundo, CA). Video imaging was captured using a Telecam-C camera (Karl Storz Endoscopy-America, Inc.). Acoustic signals were recorded during modal intensity phonation at baseline and in 15-minute intervals using a Perception 170 Condenser Microphone (AKG, Vienna, Austria) positioned approximately 10 cm from the opening of the endoscope. Mouth-to-microphone distance and amplitude gain were held constant. Recordings were digitized at a 44 kHz sampling rate using Computerized Speech Lab Model 4500 (KayPENTAX, Lincoln Park, NJ). Acoustic samples were later edited with focus on the most representative central 1-second portions of the waveforms. Acoustic parameters of F_0 (Hz) and vocal intensity (dB sound pressure level) were averaged across three trials for each time interval.

At the end of the phonation procedure, humidified airflow was discontinued. Animals were immediately sacrificed and larynges were harvested. The freshly excised larynx was dissected in half posteriorly to anteriorly. The right true vocal fold was placed in fresh 10% neutral buffered formalin solution for paraffin embedding for fluorescent staining using TUNEL method and TNF-α protein expression. The left true vocal fold was dissected under a microscope. The true vocal fold region was identified and dissected in the coronal section. The anterior to middle two-thirds portion of the left vocal fold was placed in 2.5% glutaraldehyde in 0.1 M sodium cacodylate buffer (pH 7.4) for TEM. The posterior one-third portion of the left

vocal fold was placed in RNA*later*® Stabilization Solution (Ambion, Thermo Fisher Scientific, Waltham, MA) for qRT-PCR.

Research Aim 1: Terminal Deoxynucleotidyl Transferase dUTP Nick End Labeling

After laryngeal excision, the right vocal fold tissue was fixed in fresh 10% neutral buffered formalin solution, pH 6.8-7.2 PFNBF-1000 (Azer Scientific, Morgantown, PA). The tissue was embedded in paraffin and 5-µm-thick sections were prepared in the coronal plane. TUNEL method fluorescent staining of formalin-fixed, paraffin-embedded tissue specimens was performed using the ApopTag® Fluorescein *In Situ* Apoptosis Detection Kit (S7110, EMD MILLIPORE International, Inc.). Post-fixed tissue sections were deparaffinized. Specimens were washed in 3 changes of xylene for 5 minutes each wash, 2 changes of 100% ethanol for 5 minutes each wash, 1 change of 95% ethanol for 3 minutes, 1 change of 70% ethanol for 3 minutes, and 1 change of PBS for 5 minutes. To enhance DNA exposure, tissue sections were pretreated with a protein digesting enzyme. 100 µL freshly diluted Proteinase K (20 µL/mL, IHC® Specific Proteinase K, EMD MILLIPORE International, Inc.) was applied to each tissue section and incubated for 15 minutes at room temperature. Slides were drained and washed in 2 changes of PBS for 2 minutes each wash. 50 µL equilibration buffer was applied to each tissue section and incubated for at least 10 seconds at room temperature. 55 µL working strength tDt enzyme (70% reaction buffer, 30% tDt enzyme) was applied to each tissue section and incubated in a humidified chamber for 1 hour at 37°C. Slides were agitated in working strength stop/wash buffer for 15 seconds and incubated for 10 minutes at room temperature. Slides were washed in 3 changes of PBS for 1 minute each wash. Tissue sections were treated with working strength anti-digoxigenin conjugate (53% blocking solution, 47% anti-digoxigenin) and incubated in a humidified chamber for 30 minutes at room temperature while avoiding exposure to light. Slides

were washed in 4 changes of PBS for 2 minutes each wash. Slides were mounted with DAPI Fluoromount-G® (SouthernBiotech Associates, Inc., Birmingham, AL) under glass coverslips.

Positive and negative controls using TUNEL method were created according to the procedures recommended in the ApopTag® Fluorescein *In Situ* Apoptosis Detection Kit (2012). For the positive control, a 5-μm-thick paraffin embedded tissue of rabbit tonsil was used to induce cleavage of genomic DNA by DNase treatment. After the post-fixed tissue section was deparaffinized, the section was pretreated with DN buffer consisting of 30 mM Trizma base, pH 7.2, 4 mM $MgCl_2$, and 0.1 mM *dithiothreitol* at room temperature for 5 minutes. 0.2 μl DNase was dissolved in 2 ml DN buffer and the solution was applied to the tissue section, incubated at room temperature for 10 minutes, and rinsed with distilled water. For the negative control, a true vocal fold tissue section exposed to the 120-minute phonation time-dose was used to confirm no presence of TUNEL staining. The tissue section received no tDt enzyme treatment.

Fluorescence microscopy image acquisition was performed using a 12-bit Hamamatsu Digital Camera C10600 ORCA-R^2 (Hamamatsu Corporation, Bridgewater, NJ) connected to a Nikon ECLIPSE 90i Microscope (Nikon Instruments, Inc., Melville, NY) on a Dell Optiplex 960 desktop computer running Windows 7 Enterprise (Microsoft Corporation, 2009). With the exception of the positive and negative controls, the experimenter was blinded to group assignment during data acquisition, quantification, and exportation. For each specimen, three distinct, non-overlapping fluorescent images were captured along the apical epithelial surface of the true vocal fold at 40x magnification at a constant exposure time (200 ms for DAPI, 500 ms for the fluorophore fluorescein isothiocyanate [FITC]). Microscopy quantification procedures were performed using Nikon Imaging Software Elements, Basic Research 3.22.00 (Nikon Instruments, Inc., Melville, NY) under Annotated Measurement Tools. To quantify the mean

intensity of fluorescence for TUNEL staining, a region of interest was selected in each image to identify only the vocal fold epithelium. The region of interest was defined as the entire length of the side facing the lumen (e.g., black) with several layers of closely-packed DAPI staining cells. The epithelium ended when the primarily non-cellular lamina propria was reached, which was determined by a significant reduction in the number of DAPI-staining cells. The mean intensity of the fluorophore FITC was captured and adjusted until it appeared that all TUNEL-labeled cells were visible. The mean intensity values for FITC were exported for analysis. For each specimen, the intensity values for FITC were averaged across three distinct images as the final data point. To obtain intra-rater reliability, the experimenter repeated the quantification procedures on 10% of the images (n = 6) that were selected at random.

Research Aim 1: Transmission Electron Microscopy

After laryngeal excision, the left vocal fold tissue was prepared for routine TEM processing. For primary fixation, tissue specimens were immersed in 2.5% glutaraldehyde in 0.1 M sodium cacodylate buffer (pH 7.4) and rinsed in 3 changes of 0.1 M sodium cacodylate buffer for 5 minutes each rinse. For secondary fixation, specimens were immersed in 1% osmium tetroxide in 0.1 M sodium cacodylate buffer for 1 hour at room temperature and rinsed in 3 changes of 0.1 M sodium cacodylate buffer for 5 minutes each rinse. An ethyl alcohol series was used for specimen dehydration. Specimens were immersed in 30%, 50%, 75%, 85%, and 95% ethyl alcohol for 15 minutes each. For final dehydration, specimens were immersed in 3 changes of 100% ethyl alcohol for 15 minutes each, propylene oxide for 5 minutes, and 100% ethanol for 5 minutes. Specimens were incubated in 2 changes of 100% propylene oxide for 15 minutes each. Stepwise infiltrations were completed with Epon resin and specimens were embedded in flat molds and allowed to polymerize for 48 hours at 60°C. Thick sections (500 nm to 1 micron)

were initially cut from each block, the region of interest of the vocal fold epithelium was identified, and ultrathin sections (70 nm) were cut and placed on 300 mesh copper grids. Grids were post-section stained with 2% uranyl acetate for 15 minutes and Reynold's lead citrate for 15 minutes.

TEM image acquisition was performed using a Philips/FEI T12 transmission electron microscope (FEI Company, Hillsboro, OR) to visualize the apical epithelial cell surface and internal cellular structures from 2,700x to 15,000x magnification. Images were captured under low-power magnification to visualize the location of the apical epithelial cell surface and high-power magnification to examine the morphology of individual epithelial cells. Microscopy quantification procedures were imported and performed using Nikon Imaging Software Elements, Basic Research 3.22.00 (Nikon Instruments, Inc., Melville, NY) under Annotated Measurement Tools. The experimenter was blinded to group assignment during data acquisition, quantification, and exportation. For each specimen, three distinct, non-overlapping TEM images at 4,400x magnification were selected for analysis. Images showed a visible apical epithelial surface and at least one identifiable epithelial cell nucleus. To measure the mean area of epithelial cell nuclei, area was defined as the number of pixels in a selected region. The outline of all nuclei were manually measured in each image. A nucleus was visually identified by showing dark contrast with evidence of chromatin or a nucleolus. Partial nuclei that were cut off, apoptotic bodies, and smaller fragmented pieces of nuclei were excluded from analysis. The number of identifiable nuclei ranged from one to six nuclei per image. For each image, the mean area values for all measured nuclei were exported for analysis. For each specimen, the area values were averaged across three distinct images as the final data point. To obtain intra-rater

reliability, the experimenter repeated the quantification procedures on 10% of the images (n = 6) that were selected at random.

Research Aim 1: Caspase-3

After laryngeal excision, the right vocal fold tissue was fixed in fresh 10% neutral buffered formalin solution, pH 6.8-7.2 PFNBF-1000 (Azer Scientific, Morgantown, PA). The tissue was embedded in paraffin and 5-µm-thick sections were prepared in the coronal plane. Immunohistochemical staining of formalin-fixed, paraffin-embedded tissue specimens was performed using the Anti-ACTIVE® Caspase-3 pAb Using Cy®3-Conjugated Secondary Antibody (Promega Corporation, Madison, WI). Post-fixed tissue sections were heated at 55°C for 30 minutes, cooled at room temperature for 30 minutes, and deparaffinized by being washed in 3 changes of Histo-Clear for 10 minutes, 10 minutes, and 30 minutes. Specimens were rehydrated by being washed in 3 changes of 100% ethanol for 5 minutes each wash, 2 changes of 95% ethanol for 5 minutes each wash, 1 change of 70% ethanol for 5 minutes, and 1 change of distilled water for 5 minutes.

For antigen retrieval, tissue sections were heated to boiling for 20 minutes in 10% Dako Target Retrieval Solution (pH 9, Agilent Technologies, Santa Clara, CA) and 90% distilled water and cooled at room temperature for 20 minutes. After briefly rinsing the slides in distilled water for several seconds, slides were washed in 1 change of PBS for 5 minutes. Dako Perxidase Blocking Solution was applied to the slides for 20 minutes at room temperature and washed in PBS for 5 minutes. For antigen blocking, 100 µL 1% bovine serum albumin (BSA) was applied to each tissue section. Slides were incubated in a humidified chamber at room temperature for 1 hour and 30 minutes. For primary antibody treatment, 1.0 µL Anti-ACTIVE® Caspase-3 antibody and 100 µL 1% BSA were applied to each specimen (dilution 1:100). Slides were

stored overnight at 4°C. The following day, slides were washed in 3 changes of PBS for 5 minutes each wash. For secondary antibody treatment, approximately three drops of Dako Labeled Polymer antibody were applied to tissue specimens and incubated in a humidified chamber for 15 minutes at room temperature. Slides were washed in 3 changes of PBS for 5 minutes each wash. Slides were treated with 75 μL chromagen and 25 μL substrate buffer and incubated in a humidified chamber for 20 minutes at room temperature. Slides were washed in 2 changes of PBS for 10 minutes each wash and rinsed in distilled water for at least 5 minutes. Slides were mounted with Mount Quick Mounting Medium (Newcomer Supply) under glass coverslips. Bright-field microscopy image acquisition was performed using a Nikon ECLIPSE 90i Microscope (Nikon Instruments, Inc., Melville, NY) on a Dell Optiplex 960 desktop computer running Windows 7 Enterprise (Microsoft Corporation, 2009). As shown in Appendix B, light microscopy images revealed strong, nonspecific staining of the vocal fold epithelium.

In an attempt to validate an alternative primary antibody for caspase-3, additional blocking mechanisms, antigen retrieval parameters, and antibody dilutions were implemented. Slides were placed on the Leica Bond Max IHC stainer. Heat-induced antigen retrieval was performed using both Epitope Retrieval 1 and 2 solution for 5 minutes, 10 minutes, and 20 minutes. Slides were placed in a Protein Block (DAKO, Ref# x0909) for 10 minutes, Rodent Block M (BioCare Medical, Ref# RBM961L, Concord, CA) for 60 minutes, Serum Block (Vector Laboratories, Ref# MP-2400, Burlingame, CA) for 60 minutes, and Mouse Detective Block (BioCare Medical, Ref# MD975 G,H, Concord, CA) for 75 minutes. These were initially tested separately and subsequently tested together. Slides were incubated with cleaved Caspase-3 (Cat. #ab2171, Abcam) for 1 hour at dilutions of 1:10, 1:25, 1:50, 1:75, and 1:100. Slides were incubated with the biotinylated secondary antibody anti-mouse (Cat. BA-9200, Vector

Laboratories, Inc.) for 15 minutes at dilutions of 1:200 and 1:1000. The Bond Polymer Refine detection system was used for visualization. Slides were dehydrated, cleared, and cover-slipped. Results revealed that strong, nonspecific staining of glandular epithelium and the squamous mucosa was consistently observed regardless of blocking mechanism, antigen retrieval parameters, and antibody dilutions (data not shown).

Research Aim 2: Extrapolation of Cycle-Doses

Mean vocal intensity (dB sound pressure level) and mean F_0 (Hz) were analyzed from the most representative central 1-second portions of the acoustic waveforms. To most accurately measure higher frequency phonations of rabbits, high pitch sensitivity was selected and F_0 range was set between 300-1,000 Hz. Subject 130653A had a missing acoustic recording at 120 minutes due to the inability to achieve stable phonation. To replace this missing data point, the previous time intervals between 0 and 105 minutes were averaged (57.75 dB and 546.17 Hz).

Time-dose was selected in the present study as the primary independent variable because it provides information about accumulated voicing time and reflects estimates of human phonation. Based on a previous definition of time-dose calculations using vibration dosimetry calculations (Titze, Hunter, & Svec, 2007; Titze et al., 2003), the current study's definition of time-dose was the total duration of time that the vocal folds underwent vibration exposure. Time-dose, measured in minutes, was divided into three levels of vibration exposure (i.e., 30 minutes, 60 minutes, 120 minutes). Additionally, because the number of cycles of vocal fold vibration per second can vary, it is important to consider the cycle-dose of vibration exposure. It is possible that cycle-dose may provide a more accurate metric related to vocal fold tissue damage as measured by apoptotic cell death. To more accurately determine the effect of vibrational damage on apoptotic events in the vocal fold, a quantified number of total

biomechanical stresses was obtained. Thus, this study calculated cycle-dose as the total number of cycles of vocal fold vibration and was measured as a raw number. Cycle-dose was extrapolated from mean F_0 values across phonation and an extrapolation calculation was performed. Because it was not feasible in the current study to record acoustic signals of phonation throughout the entire experiment, the cycle-dose measure was extrapolated based on mean F_0 values collected in 15-minute time intervals.

For each recorded trial of phonation, the total train duration was a total of 10 seconds, with 3 seconds of electrical stimulation (i.e., phonation) and 7 seconds of rest. To calculate the extrapolated cycle-doses per train duration, F_0 was multiplied by 3 seconds (cycle-dose train duration = mean F_0 x 3). Next, to calculate cycle-doses per minute based on 60 seconds in a minute, cycle-dose train duration was multiplied by 6 (cycle-dose per minute = cycle-dose train duration x 6). Finally, to calculate all cycle-doses within a 15-minute interval, cycle-dose per minute was multiplied by 15 (cycle-dose 15-minute interval = cycle-dose per minute x 15 minutes). In summary, for each mean F_0 value per 15-minute time interval, the following formula was computed: *[(F_0 at 0 minutes x 3) (6) (15)] + [(F_0 at 15 minutes x 3) (6) (15)] + [(F_0 at 30 minutes x 3) (6) (15)], … etc.* Table 6 describes the major components of the cycle-dose calculations.

Table 6
Cycle-Dose Extrapolation Calculations

Measurement	Calculation
Cycle-dose per train duration	Mean F_0 x 3 seconds of train duration
Cycle-dose per minute	Cycle-dose per train duration x 6 trains per minute
Cycle-dose per 15-minute interval	Cycle-dose per minute x 15 minutes per interval
Total extrapolated cycle-doses	Sum of all cycle-doses per 15-minute intervals

Research Aim 3: Quantitative Real-Time Polymerase Chain Reaction

After laryngeal excision, the left vocal fold tissue was prepared for qRT-PCR to measure gene expression of TNF-α. The tissue specimen was immersed in RNA*later*® Stabilization Solution (Ambion, Thermo Fisher Scientific, Waltham, MA) and stored overnight at 4°C. The following day, the tissue specimen was centrifuged, RNA*later* Stabilization Solution was removed, and the tissue was stored at -80°C. Vocal fold tissue specimens were homogenized using a Mixer Mill MM 301 (Retsch Inc., Pittsburgh, PA). Total RNA was isolated using an RNeasy Mini Kit (QIAGEN, Valencia, CA) and treated with ribonuclease-free DNase I (QIAGEN) to minimize contamination from genomic DNA. The quantity of total RNA was determined using the A260/A280 ratio. Electrophoresis was used to evaluate the quality based on the appearance of the 18S and 28S ribosomal RNA bands. Reverse transcription was performed using a High Capacity cDNA Reverse Transcription Kit (Applied Biosystems, Foster City, CA) using the manufacturer's recommended reaction protocol. Reactions were performed with a Biometra TGradient thermocycler (LABREPCO, Horsham, PA) using the following parameters: 25°C for 10 minutes, 37°C for 120 minutes, 85°C for 5 minutes, and 4°C for 5 minutes.

Rabbit-specific primers for TNF-α and succinate dehydrogenase complex subunit A (SDHA) were synthesized by Integrated DNA Technologies (Coralville, IA). The specific primer sequences for TNF-α and SDHA are displayed in Table 7. The primers generated a single polymerase chain reaction (PCR) band of the expected size. DNA sequencing was used to verify the PCR products. qRT-PCR was performed using the iQ SyBR Green Supermix Kit (BioRad, Hercules, CA) in a 20-µL volume reaction mixture composed of 500 nM primer 1, 500 nM primer 2, 12.5 µL iQ SyBR Green Supermix, 1 µL template complementary DNA, and 9 µL

ribonuclease-free water. The following protocol was used for real-time PCR: 1 cycle at 95°C for 3 minutes, followed by 40 cycles at 95°C for 15 seconds and 60°C for 60 seconds, and then 1 cycle at 60-95°C in 0.2°C increments to make a melting curve. An iCycler iQ Optical Syste, Software version 2.0, Bio-Rad was used to detect the PCR products. PCR products were separated by electrophoresis in 1% agarose gels containing 0.5 µg/mL ethidium bromide for verification according to fragment size. Standard curves were used to determine the relative ratio of gene expression. Target gene ratios from the experimental and control conditions were normalized using expression ratios of the internal control gene SDHA.

Table 7
Primer Sequences

Gene	Forward Primer	Reverse Primer
TNF-α	TCTTCTCTTTCCTGCTCGTG	TTGTTTGGGGACTGCTCTTC
SDHA	CATTTAGCAGAACTGAAGAC	CATTTAGCAGAACTGAAGAC

Note. TNF-α = tumor necrosis factor-alpha. SDHA = succinate dehydrogenase complex subunit A

Research Aim 3: TNF-α Protein Expression

After laryngeal excision, the right vocal fold tissue was fixed in fresh 10% neutral buffered formalin solution, pH 6.8-7.2 PFNBF-1000 (Azer Scientific, Morgantown, PA). The tissue was embedded in paraffin and 5-µm-thick sections were prepared in the coronal plane. Immunofluorescence staining of formalin-fixed, paraffin-embedded tissue specimens was performed using the TNFα Antibody (N-19): sc 1350 (Santa Cruz Biotechnology, Inc., Dallas, TX). Post-fixed tissue sections were heated at 55°C for 30 minutes, cooled at room temperature

for 30 minutes, and deparaffinized by being washed in 3 changes of Histo-Clear for 10 minutes, 10 minutes, and 30 minutes. Specimens were rehydrated by being washed in 3 changes of 100% ethanol for 5 minutes each wash, 2 changes of 95% ethanol for 5 minutes each wash, 1 change of 75% ethanol for 5 minutes, and 1 change of distilled water for 5 minutes.

For antigen retrieval, tissue sections were heated to boiling for 20 minutes in 10% Dako Target Retrieval Solution (pH 9, Agilent Technologies, Santa Clara, CA) and 90% distilled water and cooled at room temperature for 20 minutes. After briefly rinsing the slides in distilled water for several seconds, slides were washed in 1 change of PBS for 5 minutes. For antigen blocking, 100 µL 1% BSA was applied to each tissue section. Slides were incubated in a humidified chamber at room temperature for 1 hour and 30 minutes. For primary antibody treatment, 0.5 µL active TNF-α antibody and 100 µL 1% BSA were applied to each specimen (dilution 1:200). Slides were stored overnight at 4°C. The following day, slides were washed in 3 changes of PBS for 5 minutes each wash. For secondary antibody treatment, 0.5 µL secondary antibody Dnk pAb to Goat IgG conjugate (DyLight® 594, Abcam, ab96933, 0.5 mg/ml) and 100 µL 1% BSA were applied to each specimen (dilution 1:200). Slides were incubated for 1 hour at room temperature. Slides were washed in 3 changes of PBS for 5 minutes each wash. Slides were mounted with DAPI Fluoromount-G® (SouthernBiotech Associates, Inc., Birmingham, AL) under glass coverslips. Positive and negative controls were created using TNF-α protein expression. For the positive control, a 5-µm-thick paraffin embedded tissue of rabbit tonsil was used to determine that the TNF-α protein was expressed. Tonsil was selected because this is a tissue that is expected to express TNF-α. For the negative control, a true vocal fold tissue section exposed to the 120-minute phonation time-dose was used to confirm no presence of TNF-α staining. The tissue section received no primary TNF-α antibody treatment.

Fluorescence microscopy image acquisition was performed using a 12-bit Hamamatsu Digital Camera C10600 ORCA-R^2 (Hamamatsu Corporation, Bridgewater, NJ) connected to a Nikon ECLIPSE 90i Microscope (Nikon Instruments, Inc., Melville, NY) on a Dell Optiplex 960 desktop computer running Windows 7 Enterprise (Microsoft Corporation, 2009). With the exception of the positive and negative controls, the experimenter was blinded to group assignment during data acquisition, quantification, and exportation. For each specimen, three distinct, non-overlapping fluorescent images were captured along the apical epithelial surface of the true vocal fold at 40x magnification at a constant exposure time (200 ms for DAPI, 1 s for Texas Red). Microscopy quantification procedures were performed using Nikon Imaging Software Elements, Basic Research 3.22.00 (Nikon Instruments, Inc., Melville, NY) under Annotated Measurement Tools. To quantify the mean intensity of fluorescence for TNF-α staining, a region of interest was selected in each image to identify only the vocal fold epithelium. The region of interest was defined as the entire length of the side facing the lumen (e.g., black) with several layers of closely-packed DAPI staining cells. The epithelium ended when the primarily non-cellular lamina propria was reached, which was determined by a significant reduction in the number of DAPI-staining cells. The mean intensity of the fluorophore Texas Red was captured and adjusted until it appeared that all TNF-α-labeled cells were visible. The mean intensity values for Texas Red were exported for analysis. For each specimen, the intensity values for Texas Red were averaged across three distinct images as the final data point. To obtain intra-rater reliability, the experimenter repeated the quantification procedures on 10% of the images (n = 6) that were selected at random.

Exploratory Research Aim: Hematoxylin and Eosin Staining of Tracheal Tissue

Vocal fold vibration is the result of both airflow and muscular forces. An exploratory aim investigated a preliminary step toward determining the effect of aerodynamic forces on vocal fold tissue damage using the current *in vivo* phonation model. Hematoxylin and eosin (H&E) staining was performed to compare if longer durations of exposure to controlled humidified airflow damaged the superior portion of the tracheal epithelial tissue. At the time of laryngeal excision, the superior two rings of the trachea were excised from several animals that were selected at random (n = 5). Tracheal tissues belonged to animals from one control condition, one 30-minute phonation time-dose condition, two 60-minute phonation time-dose conditions, and one 120-minute phonation time-dose condition. The superior region of the trachea was selected to evaluate tissue damage due to exposure to controlled humidified airflow during *in vivo* phonation. The tracheal tissue was fixed in fresh 10% neutral buffered formalin solution, pH 6.8-7.2 PFNBF-1000 (Azer Scientific, Morgantown, PA). The tissue was embedded in paraffin and 5-μm-thick sections were prepared in the coronal plane.

H&E staining was performed using standard procedures. Slides were placed in 2 changes of xylene for 5 minutes each, 2 changes of 100% ethanol for 3 minutes each, and 2 changes of 95% ethanol for 3 minutes each. Slides were rinsed with water for 3 minutes. Slides were immersed in hematoxylin for 4 minutes, rinsed with water for 1 minute, immersed in clarifier for 1 minute and 30 seconds, rinsed in water for 1 minute, immersed in bluing for 30 seconds, and rinsed with water for 1 minute. Slides were immersed in 95% ethanol for 1 minute, eosin for 1 minute, 95% ethanol for 1 minute, 2 changes of 100% ethanol for 2 minutes each, and 2 changes of xylene for 2 minutes each. Slides with mounted under glass coverslips. Bright-field microscopy image acquisition was performed using a Nikon ECLIPSE 90i Microscope (Nikon

Instruments, Inc., Melville, NY) on a Dell Optiplex 960 desktop computer running Windows 7 Enterprise (Microsoft Corporation, 2009). Light microscopy images were captured at 4x magnification and subjectively evaluated for visual evidence of tissue damage. Appendix C displays representative light microscopy images acquired at 4x magnification of tracheal epithelial specimens from the A) control condition, B) 30-minute time-dose, C) 60-minute time-dose, and D) 120-minute time-dose. Double-headed arrows represent the apical epithelial surface facing the lumen. Visual examination of H&E stains of tracheal epithelia revealed relatively intact epithelium in the control condition and 30-minute time-dose. The apical surface of the epithelium (double-headed arrows) is less pronounced in the 60-minute and 120-minute time-doses. In particular, H&E staining in the 120-minute time-dose shows evidence of the epithelial surface detaching from the remaining tissue. While the results are limited and conclusions cannot be made at this time, future research is warranted to consider the influence of airflow damage to the vocal folds. It is possible that the effect of airflow rate may contribute to vocal fold epithelial damage or apoptotic events. If this hypothesis is supported, additional care would need to be taken to differentiate damage caused by the biomechanical forces versus aerodynamic forces during vibration exposure. To expand the work in the current study, future research is warranted to quantify the rate of apoptotic cell death in the tracheal epithelium.

Statistical Analysis

All statistical analyses were performed using IBM SPSS Statistics for Windows v. 23.0 (IBM Corp., 2015, Armonk, NY). To address research aims 1 and 3, a series of one-way between subjects ANOVAs were computed to determine the main effect of increasing time-doses of vibration exposure on the means of TUNEL staining, epithelial cell nuclei area, TNF-α gene

transcript levels, and TNF-α protein expression. Significant main effects were followed up with post-hoc comparisons using the Tukey's Honestly Significant Difference (HSD) test. To address research aim 2, a series of Pearson product-moment correlation coefficients were computed to investigate the correlations between total extrapolated cycle-doses of vibration exposure and the means of TUNEL staining and epithelial cell nuclei area. For all analyses, statistical significance was determined by an alpha level of $p < 05$.

CHAPTER V

RESULTS

Pre-Hypothesis Testing

Prior to presenting the results related to this study's three hypothesis-driven aims, described briefly are analyses that focused on *in vivo* phonation, extrapolated cycle-doses, normality tests, and intra-rater reliability.

In Vivo Phonation

Table 8 displays baseline electrical stimulation (mA), airflow rate (mL/s), and subglottal pressure (cm/H_2O) to evoke *in vivo* phonation for individual animals (N = 20) in the control, 30-minute, 60-minute, and 120-minute phonation time-doses. Two separate one-way between subjects ANOVAs revealed no significant differences in electrical stimulation, $F(3, 16) = 1.06$, $p = .393$ and subglottal pressure, $F(3, 16) = 1.29$, $p = .313$ across conditions. Airflow was delivered at a constant rate of 85.03 mL/s across conditions.

Table 8

Baseline Electrical Stimulation, Airflow Rate, and Subglottal Pressure in Control and Experimental Conditions

Animal	Electrical Stimulation (mA)	Airflow Rate (mL/s)	Subglottal Pressure (cm/H_2O)
		Control[a]	
130676	2.20	85.03	10.00
130678	2.40	85.03	7.00
130654A	1.40	85.03	8.00
130656	2.40	85.03	5.00
130651A	1.00	85.03	8.00
		30-Minute Time-Dose[a]	
130616	0.90	85.03	6.00
130673	1.70	85.03	10.00
130651	1.20	85.03	9.00
130674	2.40	85.03	8.00
130650A	1.00	85.03	8.00
		60-Minute Time-Dose[a]	
130675	0.80	85.03	8.00
130649	0.70	85.03	6.00
130650	1.20	85.03	7.00
130652	2.30	85.03	7.00
130655A	1.10	85.03	6.00
		120-Minute Time-Dose[a]	
130615	1.10	85.03	8.00
130625	2.00	85.03	5.00
130623	2.00	85.03	7.00
130624	2.40	85.03	8.00
130653A	1.00	85.03	5.00

Note. [a] $n = 5$.

Six separate one-way repeated measures ANOVAs were used to evaluate the chronological effect of 15-minute time intervals on vocal intensity (dB sound pressure level) and F_0 (Hz) in the experimental conditions only (N = 15). Results showed no significant difference in vocal intensity across time interval in the 30-minute, $F(2) = 1.87$, $p = .216$, 60-minute, $F(4)$, = 1.68, $p = .204$, and 120-minute phonation time-doses, $F(8) = 0.90$, $p = .527$ (Figure 14). There was no significant difference in F_0 across time interval in the 30-minute, $F(2) = 1.19$, $p = .354$, 60-minute, $F(4) = 0.49$, $p = .741$, and 120-minute phonation time-doses, $F(8) = 1.18$, $p = .342$ (Figure 15). Table 9 shows the means and standard deviations of vocal intensity and F_0 across 15-minute time intervals in the experimental conditions.

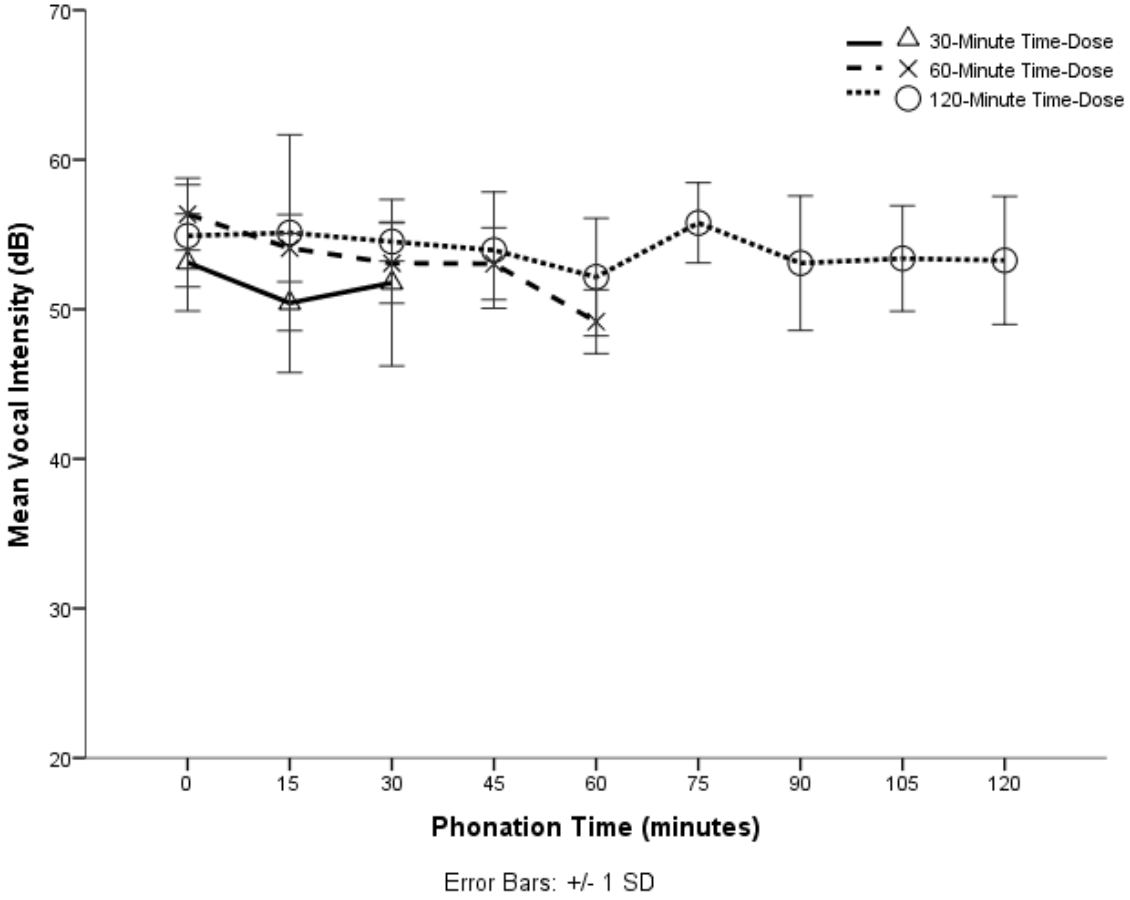

Figure 14. Mean Vocal Intensity (dB) Across 15-Minute Time Intervals in Experimental Conditions. No differences were observed in vocal intensity values across chronological time intervals. Triangles represent mean vocal intensity for 30-minute time-doses, multiplication symbols represent mean vocal intensity for 60-minute time-doses, and circles represent mean vocal intensity for 120-minute time-doses. Error bars represent standard deviations of the means.

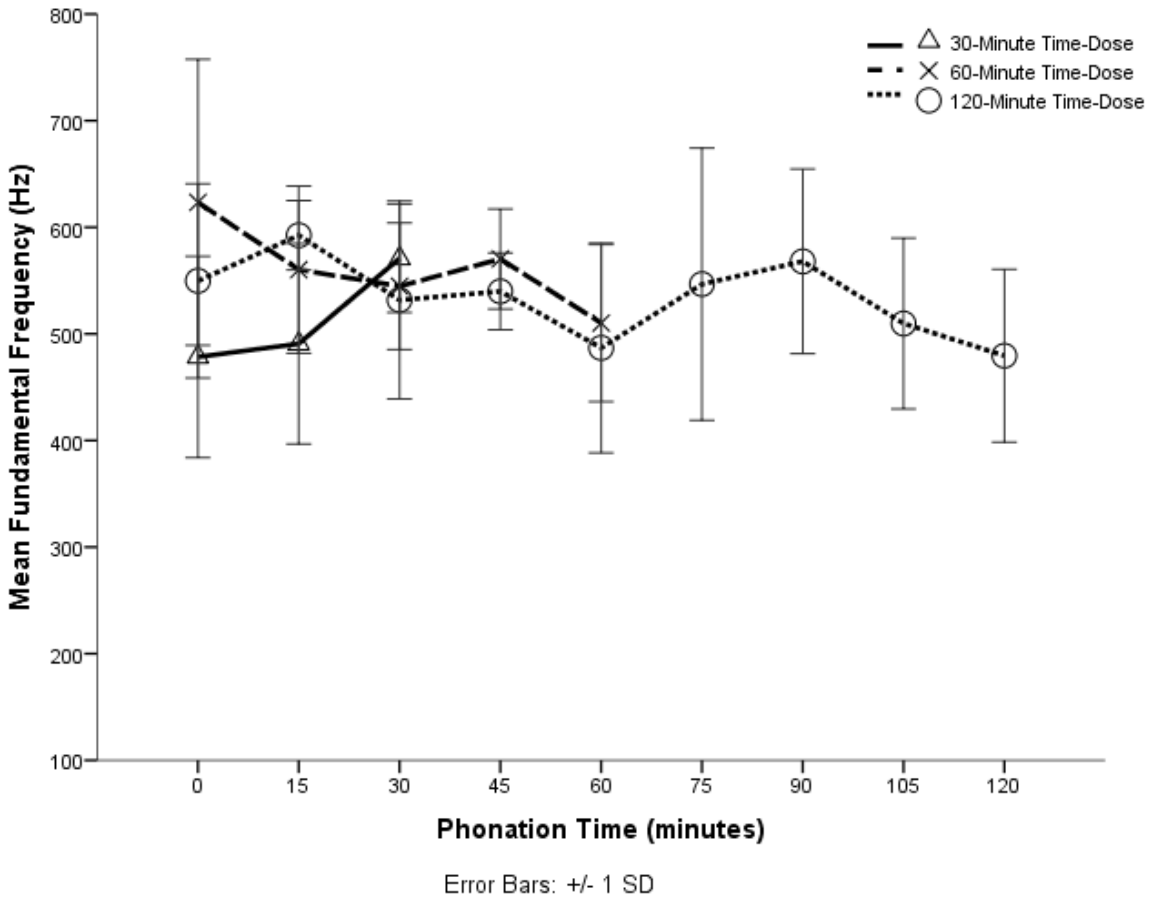

Figure 15. Mean Fundamental Frequency (Hz) Across 15-Minute Time Intervals in Experimental Conditions. No differences were observed in fundamental frequency values across chronological time intervals. Triangles represent mean fundamental frequency for 30-minute time-doses, multiplication symbols represent mean fundamental frequency for 60-minute time-doses, and circles represent mean fundamental frequency for 120-minute time-doses. Error bars represent standard deviations of the means.

Table 9

Mean Vocal Intensity and Fundamental Frequency Across 15-Minute Time Intervals in Experimental Conditions

Time Interval (min)	Fundamental Frequency (Hz)	Vocal Intensity (dB)
	30-Minute Time-Dose[a]	
0	526.67 (65.78)	49.91 (5.58)
15	462.17 (109.97)	53.05 (3.87)
30	551.18 (70.39)	52.36 (3.84)
	60-Minute Time-Dose[a]	
0	593.67 (68.83)	51.31 (2.87)
15	530.75 (115.50)	52.79 (1.93)
30	586.50 (99.82)	54.56 (1.75)
45	539.39 (86.34)	54.21 (2.76)
60	558.45 (66.83)	52.86 (5.58)
	120-Minute Time-Dose[a]	
0	565.23 (105.47)	51.08 (3.48)
15	538.73 (101.76)	54.29 (3.03)
30	555.42 (54.99)	54.62 (1.54)
45	534.01 (57.94)	54.85 (6.84)
60	563.07 (36.45)	56.09 (4.04)
75	546.59 (79.47)	53.15 (4.25)
90	512.85 (126.41)	54.52 (2.85)
105	553.12 (70.76)	53.69 (4.01)
120	436.03 (81.45)	53.89 (3.19)

Note. Standard deviations of the means are in parentheses. [a] $n = 5$. $N = 15$.

Vocal intensity and F_0 were averaged across chronological time intervals for each time-dose of 30 minutes, 60 minutes, and 120 minutes. As shown in Table 10, mean vocal intensity was 51.77 dB (*SD* = 4.40) in the 30-minute time-dose, 53.15 dB (*SD* = 3.22) for the 60-minute time-dose, and 54.02 dB (*SD* = 3.79) for the 120-minute time-dose. Mean F_0 was 513.34 Hz (*SD* = 87.27) for the 30-minute time-dose, 561.75 Hz (*SD* = 85.48) for the 60-minute time-dose, and 533.87 Hz (*SD* = 84.89) for the 120-minute time-dose. Two separate one-way between subjects ANOVAs revealed no significant differences in vocal intensity, $F(2, 82) = 2.08$, $p = .131$ and F_0, $F(2, 82) = 1.64$, $p = .200$ across conditions.

Table 10
Means of Collapsed Vocal Intensity and Fundamental Frequency Across Animals in Experimental Conditions

Time-Dose	Fundamental Frequency (Hz)	Vocal Intensity (dB)
30 Minutes[a]	513.34 (87.27)	51.77 (4.40)
60 Minutes[b]	561.75 (85.48)	53.15 (3.22)
120 Minutes[c]	533.88 (84.89)	54.02 (3.79)

Note. Standard deviations of the means are in parentheses. [a] *n* data points = 15. [b] *n* data points = 25. [c] *n* data points = 45.

Extrapolated Cycle-Doses

An extrapolation calculation was performed to estimate the total cycle-doses of vocal fold vibration exposure in the experimental conditions only (N = 15). Table 11 provides the mean total extrapolated cycle-doses in the 30-minute, 60-minute, and 120-minute phonation time-doses. As expected, a between subjects one-way ANOVA revealed a significant main effect of time-dose on extrapolated cycle doses, $F(2, 12) = 301.86$, $p = .000$ (Figure 16). Post-hoc comparisons using the Tukey's HSD test showed that mean total extrapolated cycle-doses were significantly higher in the 120-minute time-dose (M = 1,248,123.76, SD = 69,382.02) compared to the 60-minute (M = 758,364.12, SD = 55,773.18; $p = .000$) and 30-minute time-doses (M = 415,803.78, SD = 27,774.83; $p = .000$). Extrapolated cycle-doses were significantly higher in the 60-minute time-dose compared to the 30-minute time-dose ($p = .000$).

Table 11
Mean Total Extrapolated Cycle-Doses of Vibration Exposure in Experimental Conditions

Time-Dose	Total Extrapolated Cycle-Dose
30 Minutes[a]	415,803.78 (27,774.83)
60 Minutes[b]	758,364.12 (55,773.18)
120 Minutes[c]	1,248,123.76 (69,382.02)

Note. Standard deviations of the means are in parentheses. [a] n data points = 15. [b] n data points = 25. [c] n data points = 45.

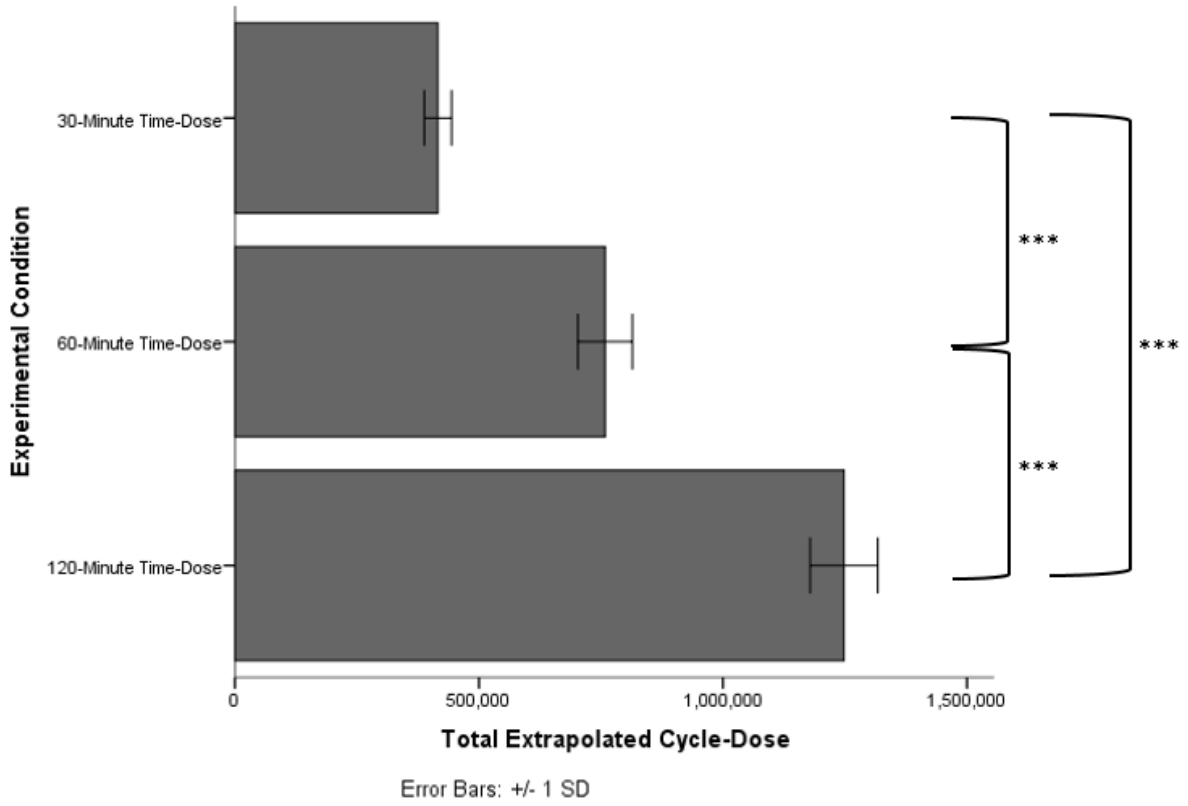

Figure 16. Mean Total Extrapolated Cycle-Doses of Vibration Exposure Across Experimental Time-Doses. Mean total cycle-doses were significantly greater in the 120-minute time-dose compared to the 60-minute and 30-minute time-doses, and the 60-minute time-dose was significantly greater compared to the 30-minute time-dose. Error bars represent standard deviations of the means and *** indicates $p < .001$.

Normality Tests

Five separate Shapiro-Wilk *W* tests were used to determine the normality of the data. All tested variables met the assumption of normality based on nonsignificant tests for the dependent variables of TUNEL staining, $W(5) = .89$, $p = .336$, epithelial cell nuclei area, $W(5) = .86$, $p = .224$, TNF-α gene expression, $W(5) = .96$, $p = .826$, TNF-α protein expression, $W(5) = .86$, $p = .244$, and the independent variable of extrapolated cycle-doses, $W(5) = .98$, $p = .920$.

Intra-Rater Reliability

Three different statistical tests were used to assess the intra-rater reliability for the dependent measurements of TUNEL staining, epithelial cell nuclei area, and TNF-α protein expression. First, three separate paired samples *t*-tests were used to confirm nonsignificant differences between the original measurement and repeated measurements on 10% of the images (i.e., measurement 1 versus measurement 2). In addition, three separate Pearson product-moment correlation coefficients were performed to investigate the strength of linear associations between measurement 1 versus measurement 2. Finally, three separate single measures intraclass correlation coefficients were used to investigate the amount of agreement between measurement 1 versus measurement 2.

Table 12 provides the results for intra-rater reliability. There were no significant differences between measurement 1 and measurement 2 for epithelial cell nuclei area, $t(5) = -1.45$, $p = .207$ and TNF-α protein expression, $t(5) = .58$, $p = .585$. However, there was a significant difference between measurement 1 and measurement 2 for TUNEL staining, $t(5) = 7.50$, $p = .001$. Measurement 1 and measurement 2 were strongly and positively correlated for TUNEL staining, $r(4) = .82$, $r^2 = .67$, $p = .046$, epithelial cell nuclei area, $r(4) = .96$, $r^2 = .92$, $p = .002$, and TNF-α protein expression, $r(4) = .92$, $r^2 = .85$, $p = .009$. The intraclass correlation

coefficient was good for TUNEL staining, ICC = .71, 95% confidence interval (-.10, .95), excellent for epithelial cell nuclei area, ICC = .94, 95% confidence interval (.66, .99), and excellent for TNF-α protein expression, ICC = .91, 95% confidence interval (.51, .99). Figure 17 shows scatterplots of measurement 1 versus measurement 2 for the dependent variables of TUNEL staining, epithelial cell nuclei area, and TNF-α protein expression. Overall, intra-rater reliability measurements indicate acceptable repeatability.

Table 12

Intra-Rater Reliability for Measurement 1 versus Measurement 2

	Measurement 1		Measurement 2		$t(5)$	p	r	r^2	Single Measures ICC
Variable	*M*	*SD*	*M*	*SD*					
TUNEL[a] (bits)	361.99	65.27	237.17	37.26	7.50	.001	0.82	0.67	0.71
Cell Nuclei Area[a] (px^2)	56,435.83	19,772.06	60,036.76	16,461.32	-1.45	.207	0.96	0.92	0.94
TNF-α Protein[a] (bits)	258.65	62.63	252.86	54.23	0.58	.585	0.92	0.85	0.91

Note. [a] $n = 6$. ICC = intraclass correlation coefficient.

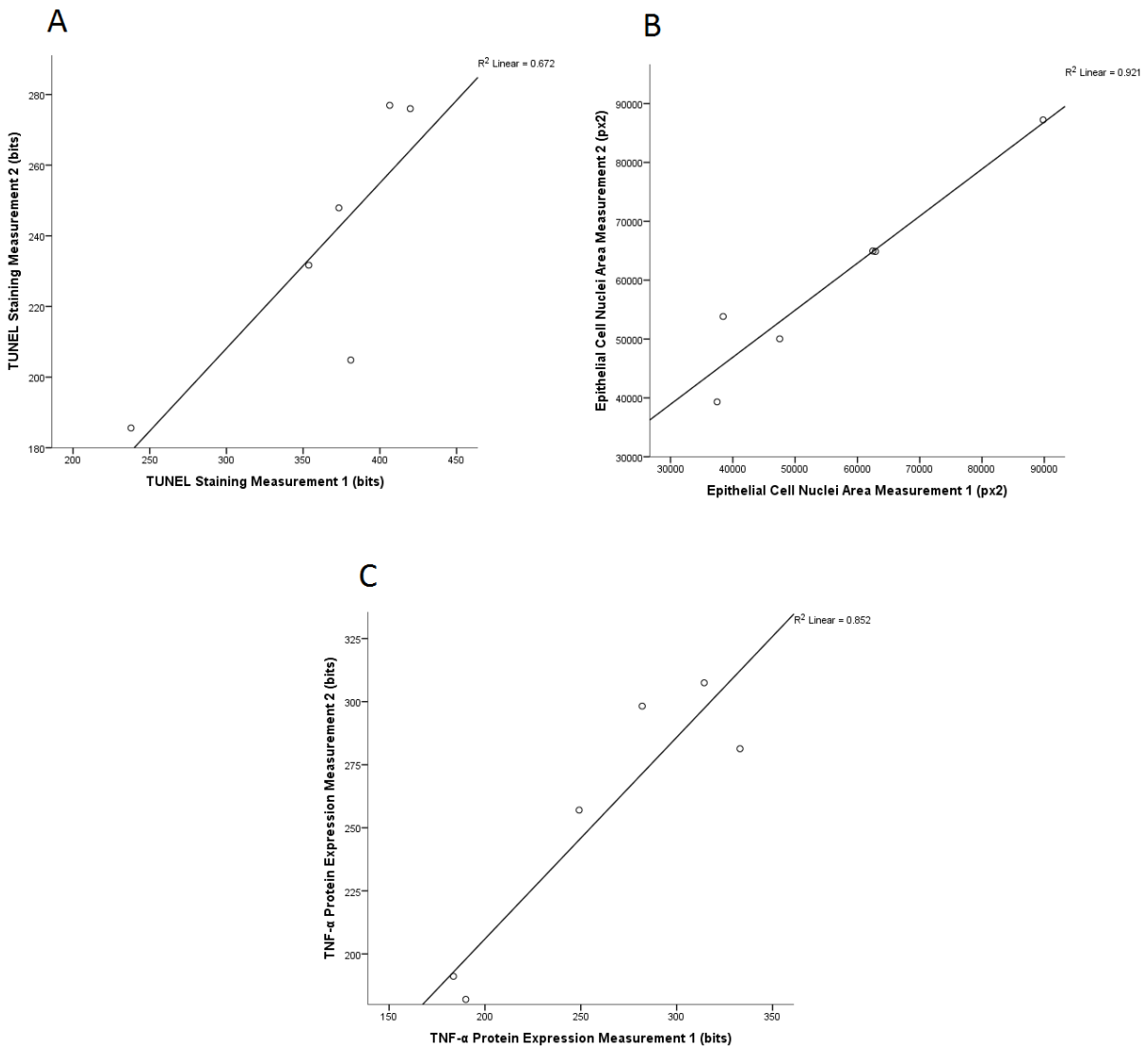

Figure 17. Intra-Rater Reliability for Dependent Variables. Scatterplots are shown for measurement 1 (x-axis) versus measurement 2 (y-axis) for A) TUNEL staining (bits), B) epithelial cell nuclei area (px^2), and C) TNF-α protein expression (bits). All scatterplots demonstrate positive correlations that indicate acceptable repeatability.

Research Aim 1

The purpose of Aim 1 was to measure the effects of increasing time-doses of vibration exposure on apoptotic cell death in the true vocal fold epithelium.

Hypothesis 1A: Effect of Increasing Time-Doses of Vibration Exposure on TUNEL Staining

Figure 18 displays representative fluorescent TUNEL-stained vocal fold tissue specimens in the control (Figure 18A), 30-minute (Figure 18B), 60-minute (Figure 18C), and 120-minute phonation time-doses (Figure 18D) acquired at 40x magnification. Table 13 displays the means, standard deviations, and confidence intervals of mean intensity of TUNEL staining (bits) across control and experimental conditions. Descriptively, mean intensity of TUNEL tended to sequentially increase with longer time-doses of vibration exposure.

A one-way between subjects ANOVA was computed to investigate the effect of increasing time-doses of vibration exposure on the mean intensity of TUNEL staining in the control, 30-minute, 60-minute, and 120-minute phonation time-doses. There was a significant main effect of time-dose on the mean intensity of TUNEL, $F(3, 16) = 4.41$, $p = .019$. Post-hoc comparisons using the Tukey's HSD test indicated that the mean intensity of TUNEL staining in the vocal fold epithelium of animals receiving 120-minute time-doses ($M = 375.74$, $SD = 90.62$) was significantly higher than animals receiving 120 minutes of vocal fold approximation alone (control) ($M = 228.00$, $SD = 45.10$; $p = .02$). No significant differences were observed between any other conditions. Specimens serving as the positive and negative controls are shown in Figure 19. The positive control confirmed that the TUNEL protocol successfully induced cleavage of genomic DNA, as evidenced by extensive labeling of TUNEL in the majority of cells in a rabbit tonsil specimen (Figure 19). The negative control confirmed that there was no presence of TUNEL staining in a true vocal fold tissue section that was exposed to the

120-minute phonation time-dose (Figure 19B). Figure 20 shows the mean intensity of TUNEL staining across control and experimental conditions.

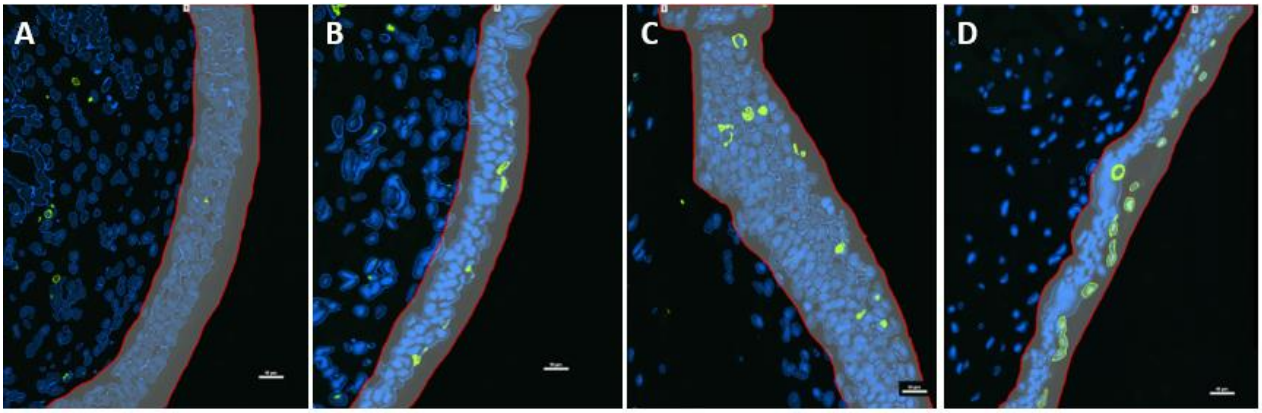

Figure 18. Fluorescent Stained True Vocal Fold Tissue Specimens using TUNEL Method. The outlined regions of interest show the apical cell surface (right) of the true vocal fold epithelium in the A) control, B) 30-minute, C) 60-minute, and D) 120-minute phonation time-doses. Images were acquired at 40x magnification.

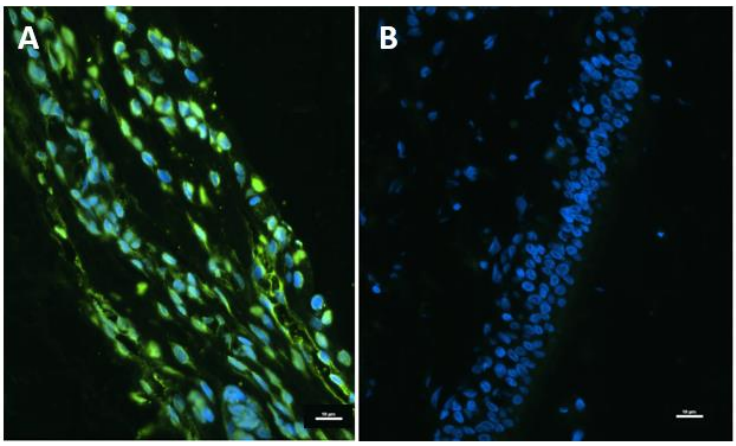

Figure 19. Positive and Negative Controls of Fluorescent Stained Tissue Specimens using TUNEL Method. TUNEL staining of the apical cell surface (right) is shown of a A) paraffin section of rabbit tonsil as the positive control and B) paraffin section of rabbit true vocal fold epithelium exposed to the 120-minute phonation time-dose as the negative control. Images were acquired at 40x magnification.

Table 13

Mean Intensity of TUNEL Staining (bits) Across Control and Experimental Conditions

Condition	*n*	*M* (*SD*)	95% CI
Control	5	228.00 (45.10)	[172.00, 284.01]
30-Minute Time-Dose	5	267.85 (49.87)	[205.94, 329.78]
60-Minute Time-Dose	5	333.86 (84.10)	[229.44, 438.28]
120-Minute Time-Dose	5	375.74 (90.62)	[263.22, 488.25]

Note. CI = confidence interval.

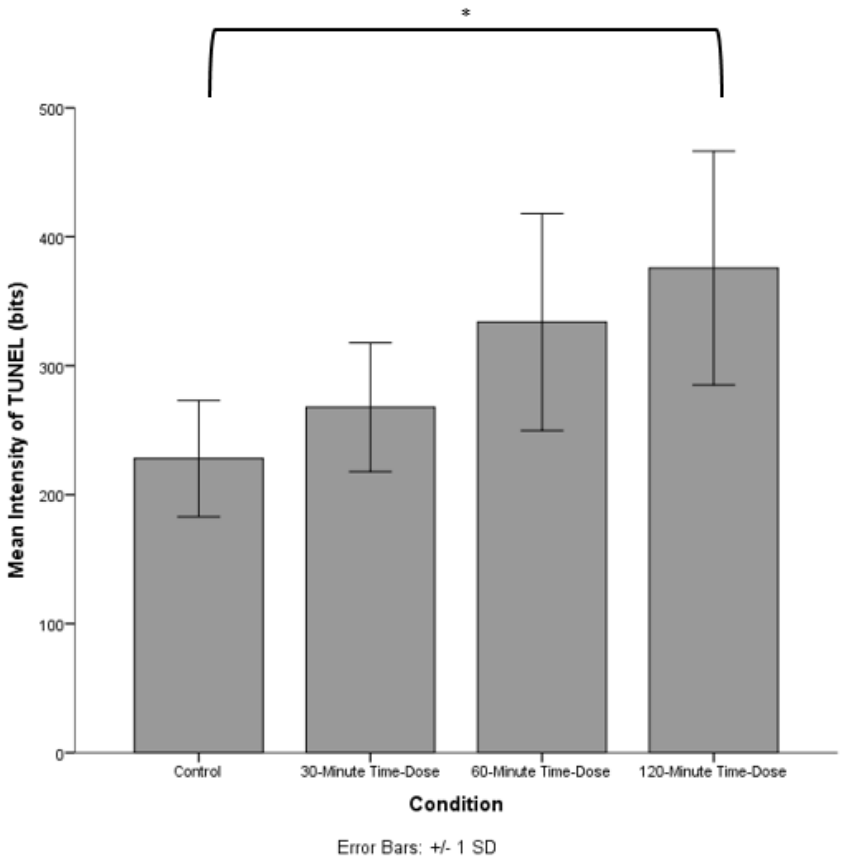

Figure 20. Mean Intensity of TUNEL Staining (bits) Across Control and Experimental Conditions. TUNEL staining was significantly greater in the 120-minute time-dose than the control condition. Error bars represent standard deviations of the means and * indicates $p < .05$.

Hypothesis 1B: Effect of Increasing Time-Doses of Vibration Exposure on Mean Area of Epithelial Cell Nuclei

Figure 21 displays representative TEM images of vocal fold tissue specimens in the control (Figure 21A), 30-minute (Figure 21B), 60-minute (Figure 21C), and 120-minute phonation time-doses (Figure 21D) acquired at 4400x magnification. Table 14 displays the means, standard deviations, and confidence intervals of the mean area of epithelial cell nuclei across control and experimental conditions. Descriptively, mean area of epithelial cell nuclei tended to sequentially decrease with longer time-doses of vibration exposure. However, the smallest mean area of epithelial cell nuclei was in the vocal fold epithelium of animals receiving 120 minutes of vocal fold approximation alone (control). A one-way between subjects ANOVA was computed to investigate the effect of increasing time-doses of vibration exposure on the mean area of epithelial cell nuclei in the control, 30-minute, 60-minute, and 120-minute phonation time-doses. Results revealed no significant main effect of time-dose on the mean area of epithelial cell nuclei, $F(3, 16) = 1.56$, $p = .239$. Figure 22 shows the mean area of epithelial cell nuclei across control and experimental conditions.

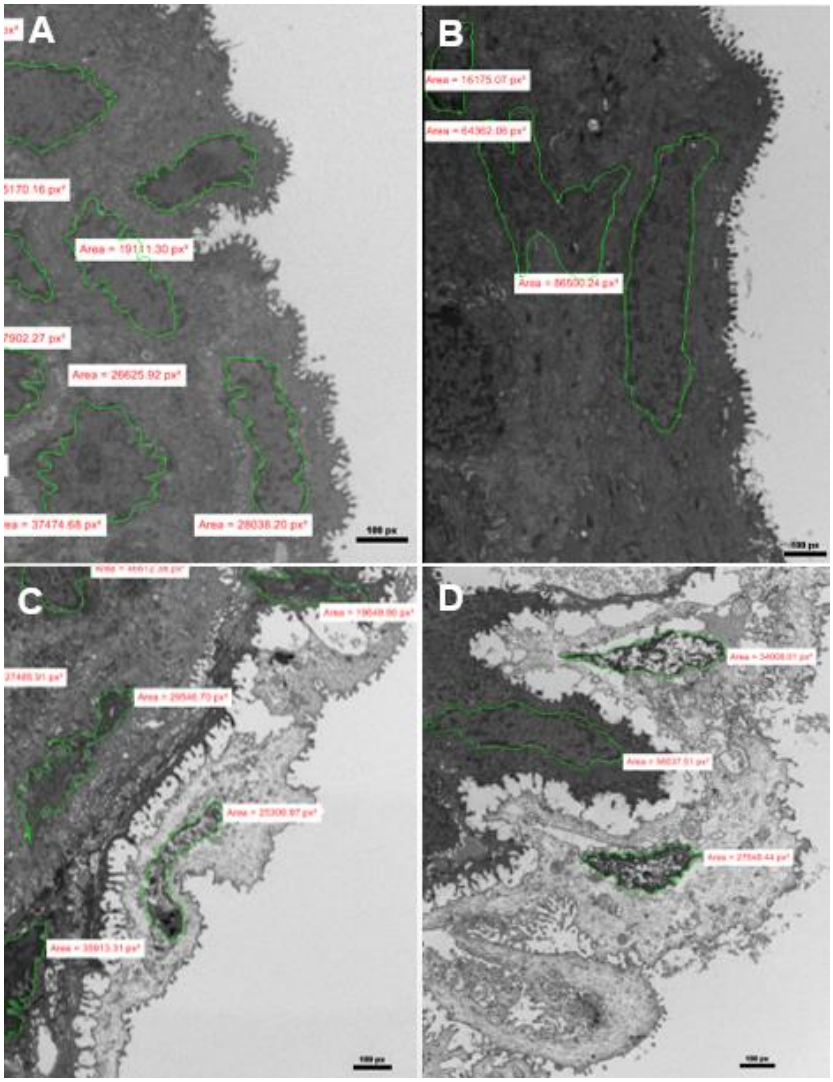

Figure 21. Analysis of Mean Area of True Vocal Fold Epithelial Cell Nuclei by Transmission Electron Microscopy. The apical cell surface of the vocal fold epithelium is shown on the right. The outlined regions of interest show the areas of cell nuclei with corresponding measures in px^2 in the A) control, B) 30-minute, C) 60-minute, and D) 120-minute phonation time-doses. Images were acquired at 4400x magnification.

Table 14

Mean Area of Epithelial Cell Nuclei (px^2) Across Control and Experimental Conditions

Condition	*n*	*M* (*SD*)	95% CI
Control	5	36,178.68 (11,787.77)	[21542.23, 50815.12]
30-Minute Time-Dose	5	56,183.10 (21,836.45)	[29069.56, 83296.63]
60-Minute Time-Dose	5	46,679.62 (14,911.62)	[28164.39, 65194.84]
120-Minute Time-Dose	5	39,721.15 (12,717.24)	[23930.62, 55511.68]

Note. CI = confidence interval.

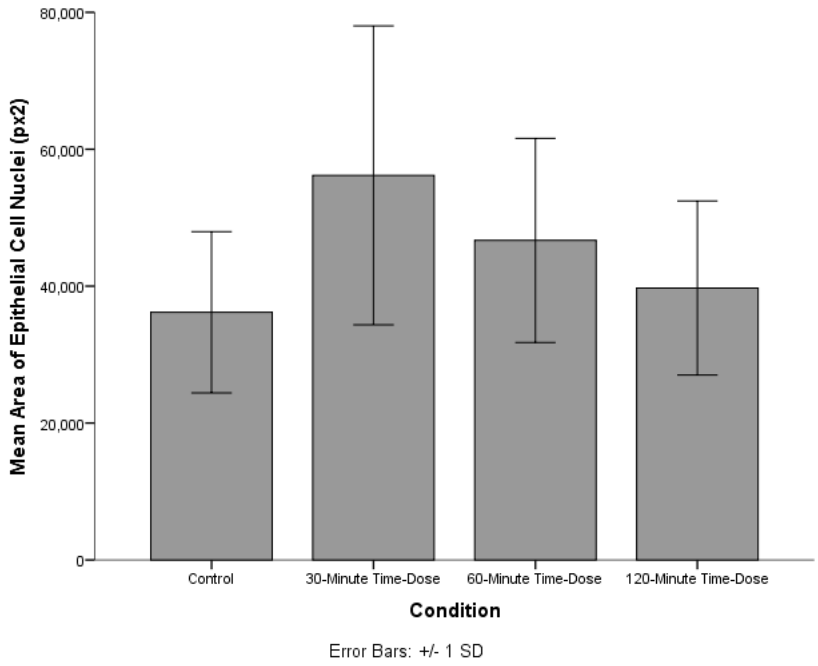

Figure 22. Mean Area of Epithelial Cell Nuclei (px^2) Across Control and Experimental Conditions. Area of cell nuclei did not significantly differ across the conditions. Error bars represent standard deviations of the means.

Research Aim 2

The purpose of Aim 2 was to determine the relationship between extrapolated cycle-doses of vibration exposure and apoptotic cell death in the true vocal fold epithelium.

Hypothesis 2A: Relationship between Increasing Cycle-Doses of Vibration Exposure and TUNEL Staining

A Pearson product-moment correlation coefficient was computed to investigate the relationship between extrapolated cycle-doses of vibration exposure and the mean intensity of TUNEL staining. Results revealed no significant correlation between extrapolated cycle-doses and the mean intensity of TUNEL staining, $r(13) = .51$, $r^2 = .26$, $p = .055$. Figure 23 displays a scatterplot of total extrapolated cycle-doses and TUNEL staining.

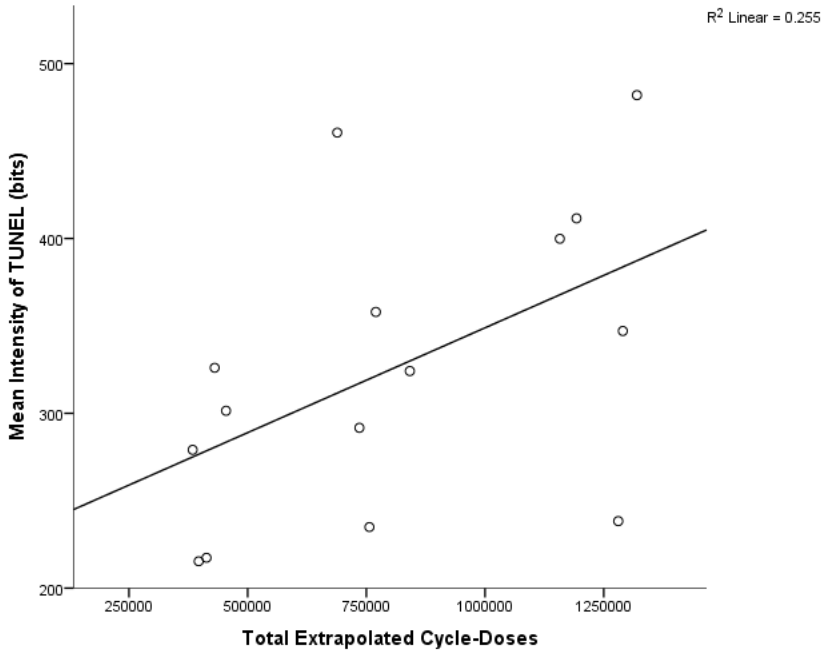

Figure 23. Scatterplot of Total Extrapolated Cycle-Doses of Vibration Exposure and Mean Intensity of TUNEL Staining (bits). There was no significant relationship between extrapolated cycle-doses (x-axis) and TUNEL staining (y-axis).

Hypothesis 2B: Relationship between Increasing Cycle-Doses of Vibration Exposure and Mean Area of Epithelial Cell Nuclei

A Pearson product-moment correlation coefficient was computed to investigate the relationship between extrapolated cycle-doses of vibration exposure and the mean area of epithelial cell nuclei. Results revealed no significant correlation between extrapolated cycle-doses and the mean area of epithelial cell nuclei, $r(13) = -0.40$, $r^2 = .16$, $p = .137$. Figure 24 displays a scatterplot of total extrapolated cycle-doses and mean area of epithelial cell nuclei.

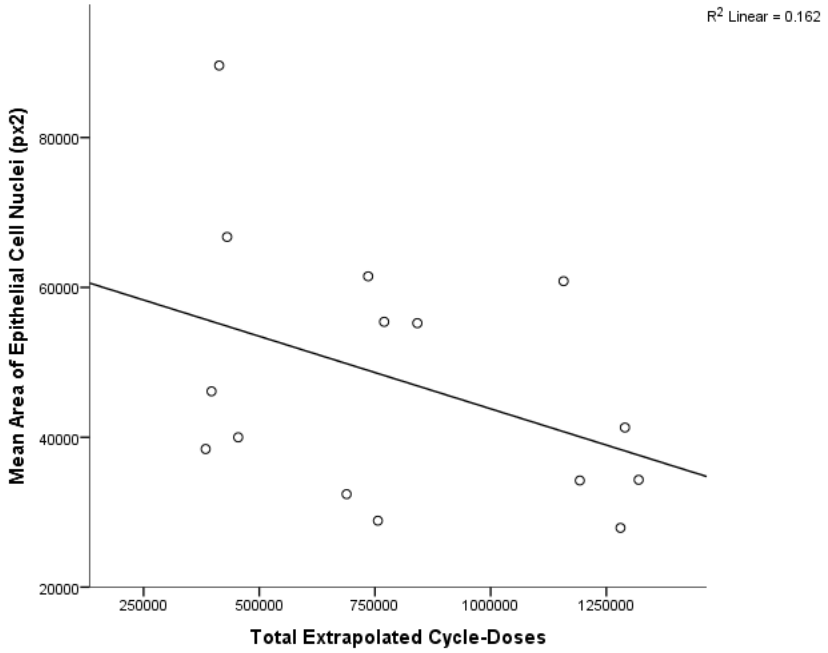

Figure 24. Scatterplot of Total Extrapolated Cycle-Doses of Vibration Exposure and Mean Area of Epithelial Cell Nuclei (px^2). There was no significant relationship between extrapolated cycle-doses (x-axis) and area of epithelial cell nuclei (y-axis).

Research Aim 3

The purpose of Aim 3 was to measure the effects of increasing time-doses of vibration exposure on gene and protein expression of the pro-inflammatory cytokine TNF-α in the true vocal fold epithelium.

Hypothesis 3A: Effect of Increasing Time-Doses of Vibration Exposure on Gene Transcript Levels of TNF-α

Table 15 displays the means, standard deviations, and confidence intervals of the mRNA expression ratios of TNF-α across control and experimental conditions. Descriptively, the TNF-α mRNA expression ratio (M = 1.46) was highest in the vocal fold epithelium of animals receiving 30 minutes of vibration exposure. The same TNF-α mRNA expression ratio (M = 1.27) was observed in the vocal fold epithelium of animals receiving 60-minute time-dose of vibration exposure and animals receiving 120 minutes of vocal fold approximation alone (control). A one-way between subjects ANOVA was computed to investigate the effect of increasing time-doses of vibration exposure on the gene transcript levels of TNF-α in the control, 30-minute, 60-minute, and 120-minute phonation time-doses. Results revealed no significant main effect of time-dose on the gene transcript levels of TNF-α, $F(3, 15) = 2.18$, $p = .133$. Figure 25 shows a boxplot of median mRNA expression ratios of TNF-α across control and experimental conditions.

Table 15

Mean Log-Transformed mRNA Expression Ratios of TNF-α Across Control and Experimental Conditions

Condition	*n*	*M* (*SD*)	95% CI
Control	4	1.27 (0.06)	[1.18, 1.36]
30-Minute Time-Dose	5	1.46 (0.12)	[1.30, 1.61]
60-Minute Time-Dose	5	1.27 (0.19)	[1.03, 1.51]
120-Minute Time-Dose	5	1.22 (0.19)	[0.98, 1.46]

Note. CI = confidence interval.

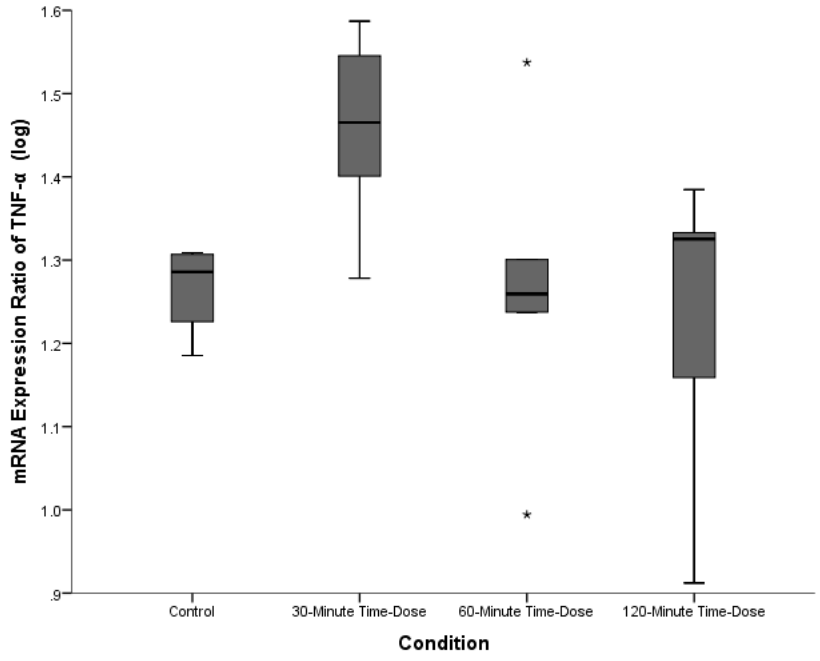

Figure 25. Log-Transformed mRNA Expression Ratios of TNF-α Across Control and Experimental Conditions. Thick horizontal black lines display the median, bars above the horizontal black lines display the upper quartile, and bars below the horizontal black lines display the lower quartile. Error bars display maximum and minimum values. Asterisks represent outlier values. TNF-α gene expression did not significantly differ across conditions.

Hypothesis 3B: Effect of Increasing Time-Doses of Vibration Exposure on Mean Intensity of TNF-α Protein Expression

Figure 26 displays representative fluorescent stained vocal fold tissue specimens of TNF-α protein expression in the control (Figure 26A), 30-minute (Figure 26B), 60-minute (Figure 26C), and 120-minute phonation time-doses (Figure 26D) acquired at 40x magnification. Table 16 displays the means, standard deviations, and confidence intervals of mean intensity of TNF-α protein expression (bits) across control and experimental conditions. Descriptively, mean intensity of TNF-α protein expression tended to sequentially increase from the vocal fold epithelium of animals receiving 120 minutes of vocal fold approximation alone (control) to animals receiving 30 minutes of vibration exposure to 60 minutes of vibration exposure.

A one-way between subjects ANOVA was computed to investigate the effect of increasing time-doses of vibration exposure on the mean intensity of TNF-α protein expression in the control, 30-minute, 60-minute, and 120-minute phonation time-doses. Results revealed no significant main effect of time-dose on TNF-α protein expression, $F(3, 16) = 0.62$, $p = .61$. Specimens serving as the positive and negative controls are shown in Figure 27. The positive control confirmed that TNF-α protein was expressed, as evidenced by extensive labeling of TNF-α in the majority of cells in a rabbit tonsil specimen (Figure 27A). The negative control confirmed that there was no expression of TNF-α in a true vocal fold tissue section that was exposed to the 120-minute phonation time-dose (Figure 27B). Figure 28 shows the mean intensity of TNF-α protein expression across control and experimental conditions.

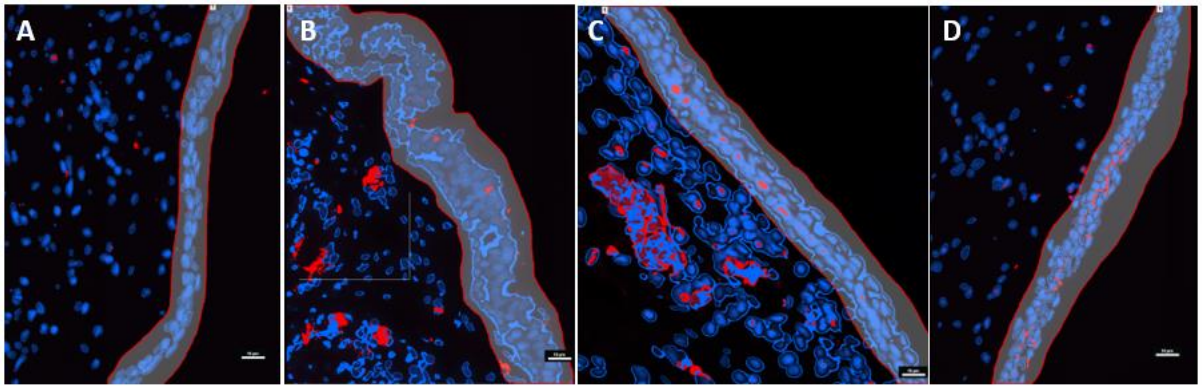

Figure 26. Fluorescent Stained True Vocal Fold Tissue Specimens of TNF-α Protein Expression. The outlined regions of interest show the apical cell surface (right) of the true vocal fold epithelium in the A) control, B) 30-minute, C) 60-minute, and D) 120-minute phonation time-doses. Images were acquired at 40x magnification.

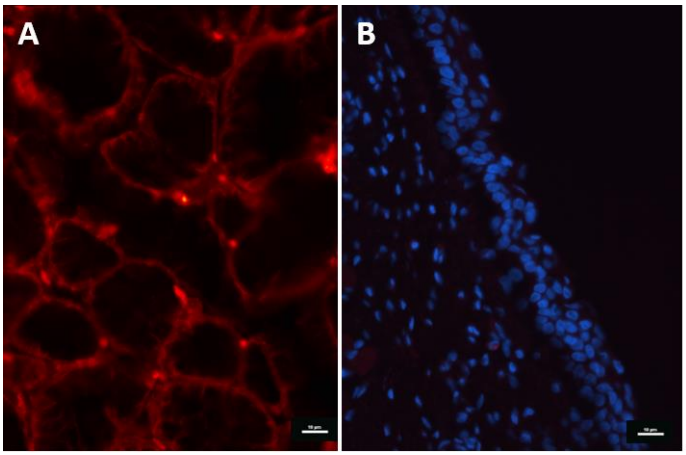

Figure 27. Positive and Negative Controls of Fluorescent Stained Tissue Specimens of TNF-α Protein Expression. TNF-α protein staining of the apical cell surface (right) is shown of a A) paraffin section of rabbit tonsil as the positive control and B) paraffin section of rabbit true vocal fold epithelium exposed to the 120-minute phonation time-dose as the negative control. Images were acquired at 40x magnification.

Table 16

Mean Intensity of TNF-α Protein Expression Across Control and Experimental Conditions

Condition	*n*	*M* (*SD*)	95% CI
Control	5	256.91 (57.00)	[186.13, 327.70]
30-Minute Time-Dose	5	278.70 (67.63)	[194.72, 362.68]
60-Minute Time-Dose	5	330.31 (130.15)	[168.70, 491.92]
120-Minute Time-Dose	5	293.72 (78.32)	[196.47, 390.97]

Note. CI = confidence interval.

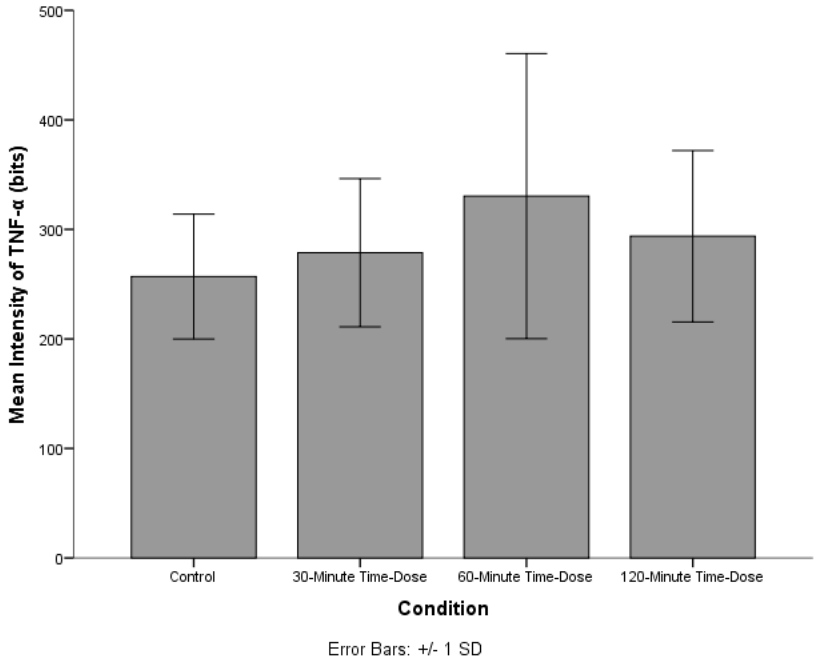

Figure 28. Mean Intensity of TNF-α Protein Expression (bits) Across Control and Experimental Conditions. TNF-α protein expression did not significantly differ across conditions. Error bars represent standard deviations of the means.

Post-Hoc Analysis

After presenting the results related to the primary research aims, several post-hoc analyses were performed to further evaluate the data. Described briefly are analyses that focused on the relationships between apoptosis signaling and TNF-α levels.

Post-Hoc Analysis 1: Relationship between TUNEL Staining and TNF-α Protein Expression

A Pearson product-moment correlation coefficient was computed to investigate the relationship between the mean intensity of TUNEL staining and the mean intensity of TNF-α protein expression. Results revealed that the mean intensity of TUNEL staining was positively correlated with the mean intensity of TNF-α protein expression, $r(18) = .53$, $r^2 = .28$, $p = .017$. As TUNEL staining increased, TNF-α protein expression also increased. Figure 29 displays a scatterplot of TUNEL staining and TNF-α protein expression.

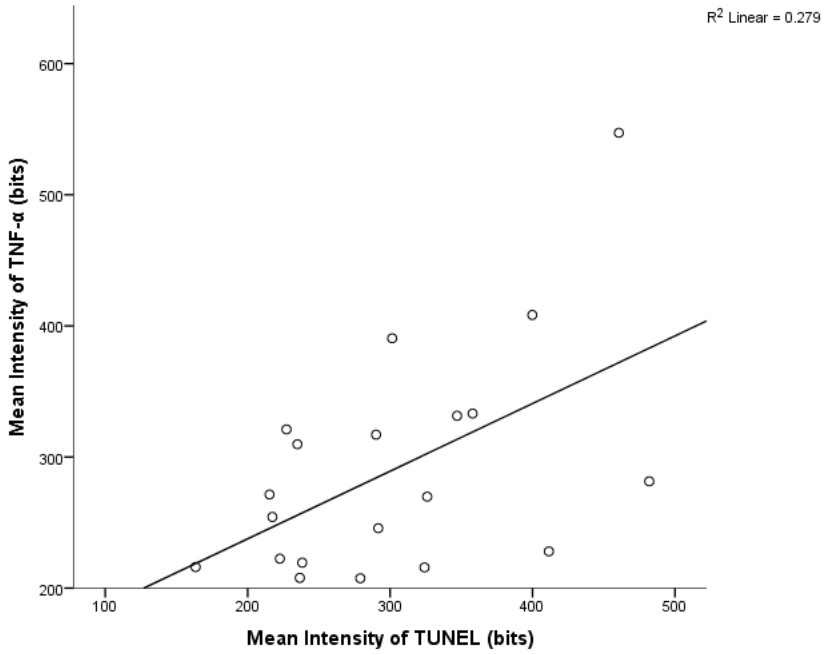

Figure 29. Scatterplot of Mean Intensity of TUNEL Staining (bits) and Mean Intensity of TNF-α Protein Expression (bits). There was a positively correlation between TUNEL staining (x-axis) and TNF-α protein expression (y-axis).

Post-Hoc Analysis 2: Relationship between TUNEL Staining and Gene Transcript Levels of TNF-α

A Pearson product-moment correlation coefficient was computed to investigate the relationship between the mean intensity of TUNEL staining and the gene transcript levels of TNF-α. Results revealed no significant correlation between the mean intensity of TUNEL staining and TNF-α gene expression, $r(17) = -.30$, $r^2 = .09$, $p = .209$.

Post-Hoc Analysis 3: Relationship between TNF-α Gene and Protein Expression

A Pearson product-moment correlation coefficient was computed to investigate the relationship between TNF-α gene expression and TNF-α protein expression. Results revealed no significant correlation between the gene transcript levels of TNF-α and the mean intensity of TNF-α protein expression, $r(17) = -.05$, $r^2 = .00$, $p = .856$.

CHAPTER VI

DISCUSSION

Overview

The work in this dissertation addressed three research aims. First, the purpose of this study was to measure the effects of increasing time-doses of *in vivo* vibration exposure on apoptotic cell death in the vocal fold epithelium. The next research objective was to investigate the relationship between extrapolated cycle-doses of *in vivo* vibration exposure and apoptotic cell death in the vocal fold epithelium. Lastly, this study evaluated the effects of increasing time-doses of *in vivo* vibration exposure on gene transcript levels and protein expression of the pro-inflammatory cytokine TNF-α in the vocal fold epithelium. Chapter VI concludes this dissertation with a summary of the major findings from the three research aims and additional commentary.

Although it has been established that vibration leads to apoptosis in the vocal fold epithelium (Novaleski et al., accepted for publication), it remains unknown whether this is a static response or if increasing vibration exposure leads to greater apoptosis. Thus, this study was the first known attempt to quantify the rate of apoptosis signaling in vocal fold epithelial cells with increasing durations and extrapolated cycle-doses of vibration exposure. Overall, results revealed that 120 minutes of acute exposure to vibration is an apoptosis-inducing stimulus in the vocal fold epithelium. Specifically, the vocal folds of animals exposed to 120 minutes of vibration exposure had significantly higher expression of apoptosis as measured by the TUNEL method. Findings also showed a positive relationship between TUNEL staining and TNF-α

protein expression in the vocal fold epithelium. That is, as TUNEL staining increased in the vocal folds in response to vibration exposure, protein expression of TNF-α also increased.

Research Aim 1

The purpose of research aim 1 was to measure the effects of increasing time-doses of vibration exposure on apoptotic cell death in the true vocal fold epithelium. Two common techniques were used to detect apoptosis. First, TUNEL method detects free 3'-OH DNA ends of nuclear condensed chromatin generated by apoptotic cells. This technique enzymatically detects internucleosomal DNA cleavage, which is a hallmark characteristic of apoptosis when an endogenous endonuclease is activated (Bortner, Oldenburg, & Cidlowski, 1995). When DNA fragmentation occurs, TUNEL-positive cells indicate that these cells are committed to die via the apoptosis signaling pathway. Conversely, TEM is a method that provides high-resolution images and is considered the gold standard technique for characterizing the morphological features of apoptosis (Elmore, 2007; Martinez et al., 2010). TEM can capture important high-quality images as evidence of apoptosis taking place that TUNEL staining is unable to detect. As a result, both TUNEL and TEM are complementary approaches to examine multiple aspects of apoptotic cell death.

Different results were observed between the outcome measures of TUNEL and TEM. TUNEL method demonstrated that the longest studied time-dose (i.e., 120 minutes) of vibration exposure led to significantly increased intensity of immunofluorescent staining compared to vocal fold approximation alone for the same time duration. In contrast, TEM images detected no differences in the quantified area of epithelial cell nuclei across experimental and control conditions. Rather, vocal folds that underwent approximation demonstrated the smallest

epithelial cell nuclei area. Both of these findings agree with previous literature which reported that the vocal fold expresses TUNEL-labeled cells after biomechanical vibration, and that condensed chromatin and apoptotic bodies were observed after biomechanical vibration and approximation (Novaleski et al., accepted for publication). The present study enhances the previous literature by objectively quantifying apoptotic cell death according to the intensity of immunofluorescent staining for TUNEL and area of cell nuclei. Additionally, this study provides evidence of a statistically meaningful difference in TUNEL staining between vibratory and control conditions.

Despite that the research design included additional phonation time-dose conditions of 30 and 60 minutes, no time-dose response of *in vivo* vibration exposure was observed for TUNEL method and TEM imaging. Thus, acutely increasing time durations that the vocal folds are exposed to biomechanical vibration does not sequentially signal greater degrees of apoptosis. Accumulated voicing times, as measured by time-dose, do not necessarily predict how many vocal fold epithelial cells are programmed to die by apoptosis. It may perhaps be more accurate to propose that a specific threshold of accumulated voicing time is needed to induce apoptosis and subsequently detect DNA fragmentation. Based on the present results, it appears that a minimum of 120 minutes of *in vivo* vocal fold vibration is the necessary stimulus for apoptosis to increase using the TUNEL method. The biomechanical forces caused by 120 minutes of vibration exposure in the vocal folds might serve as an internal signal for epithelial cells to self-organize by undergoing apoptosis. Interestingly, it is recognized that apoptotic cell death may have been initiated prior to the 120-minute time-dose (e.g., between 60 minutes and 120 minutes). Conversely, very early stages of apoptosis may have begun prior to the detection of DNA fragmentation, which might indicate that there is a possible temporal delay in measuring

apoptosis. A systematic study would be useful to determine the influence of the length of time between vibration exposure and delayed laryngeal tissue excision on apoptosis signaling.

The area of epithelial cell nuclei in TEM images failed to differ with increasing time-doses of vibration exposure. Similar to a previous standardized rating task of TEM images (Novaleski et al., accepted for publication), these results indicate that vocal fold epithelial cells do not shrink in size in response to vibration. Moreover, cell shrinking is not a common morphological feature after vibration for up to 120 minutes. Indeed, Novaleski and colleagues (accepted for publication) observed differences in epithelial cell nuclei size between a non-blinded qualitative analysis and rating task of TEM images. Moreover, describing TEM images alone may be a less accurate method of measuring cell structures and processes.

Other known limitations of TEM imaging should be addressed. First, because TEM relies on high-resolution imaging techniques, researchers are able to examine only small portions of tissue specimens (Williams & Carter, 2009). In other words, the sampling capability of TEM is poor. Another disadvantage of TEM is that artifacts are common because three-dimensional images are viewed only two-dimensionally in transmission. TEM images also lack sensitivity to the depth of specimens, as transmission images are averaged through the specimen thickness (Williams & Carter, 2009). Thus, caution must be used when interpreting the structures observed in TEM images. Considering the limitations of TEM in lieu of the current study, the quantitative measurement of nuclei area should not be considered an accurate three-dimensional view of vocal fold epithelial cells. To more accurately evaluate the shape of vocal fold epithelial

cells as it relates to apoptosis, it is recommended that future research focus on alternative imaging techniques such as atomic force microscopy[54] (Lee et al., 2015).

Beyond the quantified area of epithelial cell nuclei, subjective evaluation of TEM images revealed multiple morphological characteristics of cells. Notably, some images showed the formation of apoptotic bodies, but no inflammatory cells such as macrophages and fibroblasts were identified. Although it was difficult to determine, there were instances in which apoptotic bodies appeared to be inside another cell. This speculation is based on similarities in expectations of epithelial shape and consistent morphology compared to surrounding epithelial cells. Based on this qualitative observation, it may be possible that during apoptotic cell death in the vocal fold epithelium, neighboring epithelial cells engulf the dying epithelial cells as a more efficient means of removal.

Interestingly, the control condition demonstrated the smallest epithelial cell nuclei area but the least expression of TUNEL staining. It is possible that the physical movement caused by vocal fold approximation signals an early sign of apoptosis, cellular shrinking. Conversely, DNA fragmentation as measured by the TUNEL method, is a later stage of apoptosis that was not detected at the time of immediate tissue excision. In anticipation of further tissue damage, perhaps vocal fold epithelial cells signal apoptotic cell death in response to any movement. Moreover, it may be that the apoptotic cascade can be delayed or interrupted before the epithelial cells are destined to die by apoptosis and before DNA begins to fragment. As such, it is speculated that the smaller area of epithelial cell nuclei may be the aftermath of an initial but subsequently interrupted strategy to signal cell death.

[54] Atomic force microscopy is a technique that provides three-dimensional images of surface morphology of tissues. Lee and colleagues (2015) previously used atomic force microscopy to measure the changes in thickness collagen fibrils after acute vocal fold injury in rabbits.

In addition to TUNEL and TEM measurements, several attempts were made to stain vocal fold tissue specimens for caspase-3 activity. While TUNEL method is a sensitive measure of DNA fragmented cells, it can inappropriately identify necrotic cells as apoptotic cells (Grasl-Kraupp et al., 1995). For this reason, caspase-3 assay was selected as an additional measurement of apoptosis. When activated by apoptosis, caspases act together as a cascade in the cleavage of proteins rather than random destruction of proteins, making caspase-3 an excellent biochemical marker of apoptosis (Martinez et al., 2010). The assay stains for activation of the main caspase effector of the apoptotic cascade, caspase-3 (Gown & Willingham, 2002). Such a measure would have provided increased confidence that apoptotic cell death occurred. Unfortunately, the primary antibodies and procedures that were used in this study showed nonspecific staining for caspase-3. A probable reason is because the antibodies failed to be optimized for rabbit tissue.

On the other hand, it is speculated that perhaps successful staining of caspase-3 would not have provided any additional useful information. Despite the observation of TUNEL staining, it is possible that staining for caspase-3 activity may not have increased. This might be because caspase-3 activation is transient and the optimal time point may have been missed in the selected time-doses. In contrast, TUNEL detects the cleavage of DNA, which is a long-lasting effect that marks the end stages of cell death. Thus, TUNEL appears to be a more sensitive assay to detect apoptosis. Future investigations are necessary to consider alternative measurements of apoptosis to validate the finding that TUNEL staining increases after 120 minutes of vibration exposure compare to 120 minutes of vocal fold approximation alone. In particular, caspase-3 may be better suited in optimized vocal fold tissue from a different species (e.g., murine).

Research Aim 2

The objective of research aim 2 was to determine the relationship between extrapolated cycle-doses of vibration exposure and apoptotic cell death in the true vocal fold epithelium. Extrapolated cycle-doses of vibration exposure were selected to more accurately identify the biomechanical stresses that the vocal folds underwent during the *in vivo* phonation procedure. In contrast to the independent variable of time-dose that relies on measuring accumulated voicing time in minutes (i.e., 30, 60, 120), cycle-dose provides a closer estimation of the total number of vibratory cycles over time based on the phonatory output parameter of mean F_0. Cycle-dosing adds a new parameter to this *in vivo* animal model, as the extrapolation procedure takes into account both mean F_0 values and time duration of vibration exposure. Compared to time-dose, it is hypothesized that cycle-dose is a measurement that better represents the degree of biomechanical stresses that the vocal folds are exposed to. Thus, cycle-dose might serve as an alternative independent variable to correlate structural and functional vocal fold tissue changes in the current model.

First, this study revealed that extrapolated cycle-doses are closely related to the selected phonation time-doses. As expected, total extrapolated cycle-doses sequentially increased as time-doses increased. Stated another way, the vocal folds were exposed to a higher number of cycles of biomechanical vibration with longer durations of phonation. Next, cycle-doses were not correlated with the outcome measures of TUNEL and TEM. Moreover, the total cycles of vocal fold vibration were not meaningfully related to apoptosis signaling. The accumulated number of estimated cycles of vocal fold vibration, as measured by cycle-dose, do not necessarily predict how many vocal fold epithelial cells are programmed to die by apoptosis. It

may be that because cycle-dose correlations were computed with animals only from the experimental phonation conditions (N = 15), the analyses may have been underpowered.

Cycle-dose measurements in the present study are notably different from vibration dosimetry during continuous speech in human participants. Because an accelerometer cannot to be attached to the neck of an animal during the surgical phonation procedure, cycle-dose was extrapolated and quantified from the output parameter of mean F_0 to estimate cycles of vibration. Given that extrapolation of the values is not an exact calculation of total cycles of vibration, the current method could be less accurate than using an accelerometer. In the future, it would be interesting to incorporate an additional dosimetry measure of distance-dose. Distance-dose is a metric of the estimated distance that the vocal folds travel during vibration, which would be based on the phonatory parameter of mean vocal intensity (dB). Additionally, it remains unknown which dosimetry measurement (i.e., time-dose, cycle-dose, distance-dose) best predicts apoptotic cell death or other tissue-level changes in the current *in vivo* animal model.

Research Aim 3

The objective of research aim 3 was to measure the effects of increasing time-doses of vibration exposure on gene and protein expression of the pro-inflammatory cytokine TNF-α in the true vocal fold epithelium. Results indicated that neither TNF-α gene transcript levels nor TNF-α protein expression differed by time-dose. That is, TNF-α gene and protein levels did not change in response to increasing time-doses of vibration exposure. However, post-hoc testing revealed an interesting relationship between TNF-α and apoptosis, as the expression of TUNEL was positively related to TNF-α protein expression. In particular, as the intensity of fluorescent TUNEL staining increased, the intensity of fluorescent TNF-α staining also increased. This

finding suggests that TNF-α protein expression in the vocal fold epithelium has a tendency to become upregulated in response to vibratory-induced fragmentation of DNA. Perhaps the process of DNA fragmentation sends a signal to upregulate TNF-α protein levels.

TNF-α is a protein that promotes inflammation and is activated in many inflammatory diseases (Dinarello, 2000; Rath & Aggarwal, 1999; Varfolomeev & Ashkenazi, 2004). In addition to inflammation, TNF-α is involved in cell proliferation and cell death. Previous studies reported that biomechanical trauma causes an upregulation of TNF-α protein expression in the vocal folds (King et al., 2013; Verdolini et al., 2003). The current study contradicts this observation, as TNF-α protein levels were not altered after *in vivo* vibration exposure. The discrepancy between the existing literature and the current study may be explained by differences in methodologies. Perhaps TNF-α protein levels become upregulated after loud phonation in human participants and diseased *in vitro* cultured fibroblasts, but are not influenced by the biomechanical stresses of *in vivo* animal phonation.

Moreover, the literature reveals discrepancies regarding the effect of TNF-α on cell death. While administering TNF-α to cultured human vocal fold fibroblasts might increase the rate of cell death and inhibit cell proliferation (Chen & Thibeault, 2010), it has also been reported that TNF-α does not induce cell death in vocal fold fibroblasts (Berchtold et al., 2013). The current study's findings appear to weakly support the preliminary notion that TNF-α might be related to the signaling of apoptotic cell death during DNA fragmentation. It remains unknown, however, whether TNF-α initiates apoptosis or whether apoptosis leads to alterations in TNF-α. In addition, it is possible that TNF-α protein was not being produced by the vocal fold epithelium. That is, the detected TNF-α levels may have likely been produced from the lamina propria. Because TNF-α is a pro-inflammatory cytokine, it would seem logical that TNF-α was

produced from inflammatory cells such as vocal fold fibroblasts, which likely proliferate in response to injury (Tateya, Tateya, Lim, Sohn, & Bless, 2006).

Both gene and protein expression of TNF-α were evaluated. To analyze the TNF-α gene expression profile, qRT-PCR used a ratio that compared a relative measure of DNA to a control gene. Although qRT-PCR does not allow for an exact quantitative measurement of DNA, it is beneficial because it produces multiple copies of DNA sequences with high accuracy and confirms if cDNA sequences are expressed in a tissue specimen (Bartlett, Jette, King, Schaser, & Thibeault, 2012). Given that there is no direct correlation between the degree that mRNA is expressed and degree that a protein is produced, TNF-α protein expression was also investigated to confirm the results of qRT-PCR. Moreover, results of this study demonstrated that protein expression and gene transcript levels of TNF-α were not correlated with one another.

While the present study provides evidence of a relationship between apoptosis and TNF-α in the vocal fold epithelium, it would be ideal to more directly link apoptosis to TNF-α. Based on the current results, we are unable to conclude that TNF-α induces apoptosis in the vocal folds. Therefore, future research is necessary to further investigate TNF-α-induced apoptosis in epithelial cells of the vocal folds. Specifically, *in vitro* vocal fold epithelial cell populations would serve as an excellent model to approach this line of research. As a preliminary step, the focus could be to determine if the administration of low, medium, and high doses of TNF-α to vocal fold epithelial cells in an *in vitro* culture model induces apoptotic cell death using a sensitive measurement of apoptosis (e.g., TUNEL method). If the direct treatment of TNF-α induces an apoptotic response in the cells, the next step could be to determine if the administration of blocking antibodies to the vocal fold tissue results in reduced rates of apoptosis after vibration exposure. This line of research would improve our current understanding of

potential signaling pathways that might be targeted for future clinical treatments following prolonged periods of vocal fold vibration in humans.

Additional Commentary

Animal models are important in voice science research. The current study relied on an established *in vivo* animal model of phonation. In humans, it is impossible to control the amount of trauma that the vocal folds are exposed to during vibration. There is a large degree of variability in the etiology and maintenance of human vocal fold diseases. Fortunately, the current *in vivo* rabbit phonation model allows for systematic control over the amount of vibration exposure to the vocal folds, providing a more programmatic approach to studying tissue-level changes to the vocal folds during vibration. Despite that rabbits and humans differ in the function and frequency of phonation, many basic biochemical processes such as apoptotic cell death are similar across species. Therefore, the *in vivo* model is an appropriate initial step toward improving our understanding of apoptosis, which will eventually be translated to apoptosis in healthy and diseased human vocal folds. While this animal model provides an interesting preliminary examination of cell death in response to biomechanical stimulation, perhaps alternative experimental models may be better suited for future research in this area. Specifically, the use of biomechanical reactors using *in vitro* cell culture populations may allow for greater control over the frequency of vibration. In addition, *in vitro* cells can readily be treated with antibodies and blocking agents to examine their effect on inhibiting cell death.

In further considering the translational promise of the current model, the *in vivo* phonation model might have the potential to be used to examine clinical paradigms in humans. An essential principle of behavioral voice therapy as a therapeutic intervention for voice

disorders is to implement voicing patterns that decrease vocal fold collision, which presumably reduced trauma to the tissue to promote healing. For instance, resonant voice therapy uses a barely adducted or abducted glottal configuration to encourage minimal vocal fold contact and improve voice production (Verdolini, Druker, Palmer, & Samawi, 1998). In theory, the current *in vivo* animal model paradigm has the potential to be used to address whether decreasing subglottal pressure by increasing the rate of controlled humidified airflow through the glottis results in decreased collision and ultimately, less structural vocal fold tissue damage. Moreover, the current model might have future clinical applications of manipulating phonatory variables *in vivo* to change glottal configurations that are common in interventions for voice disorders.

An interesting observation was that fluorescent TUNEL staining was expressed in both the apical and suprabasal domains of the vocal fold epithelium. In other words, there were no obvious patterns of staining throughout the stratified layers of the epithelium. This finding is consistent with work by Leydon, Bartlett, Roenneburg, and Thibeault (2011) who reported that proliferating vocal fold cells also localized in the basal and suprabasal epithelial layers following vocal fold injury. Similarly, there is evidence that vocal fold inflammatory cells proliferate along the length of the vocal fold (i.e., anterior, posterior, middle) in response to injury (Tateya et al., 2006). Given that some degree of cell proliferation was detected in surrounding regions of the vocal folds that were not directly injured, the methods in the present study relied on averaging the apoptosis assays at distinct regions along the length of the vocal fold. Despite the current approach, it is unclear if greater apoptosis signaling occurs in the middle portion of the vocal fold that is believed to be exposed to the greatest biomechanical trauma during vibration. Thus, a future research design is warranted to determine if there is a main effect of localization of apoptotic cells at the anterior, posterior, or middle regions of the vocal fold epithelium.

When detecting cell death, the morphological characteristics of apoptosis and necrosis frequently overlap. In certain circumstances, apoptosis and necrosis are isolated processes. In other situations, both types of cell death can co-occur or gradually evolve from one type of cell death to the other (Elmore, 2007). Research is necessary to further distinguish apoptosis from necrosis as a result of physiologic and phonotraumatic vibration exposure. There are likely differences in cell death signaling with different types of vocal fold vibration. Specifically, we believe that physiologic vibration (i.e., modal intensity phonation) leads primarily to apoptotic cell death (Novaleski et al., accepted for publication). However, up to 120 minutes of physiologic vibration exposure also revealed rare occurrences of necrosis (i.e., cellular and organelle swelling) (Novaleski et al., accepted for publication). We further predict that phonotraumatic vibration (i.e., raised intensity phonation) results in necrosis because it is a more severe form of damage. Similar to the intestinal epithelia, it is speculated that at least a portion of dying vocal fold epithelial cells eventually slough off (e.g., cell shedding) and subsequently enter the airway lumen.

It is recognized that caution should be used with interpreting the relationship between acute exposure to vocal fold vibration and cell death. That is, findings from this study are limited to only several outcome measures of cell death and the studied time points of 30, 60, and 120 minutes following vibration exposure. Although we are unable to acknowledge the precise link between cell death after biomechanical trauma, we speculate that there are multiple and complex cell signaling processes occurring simultaneously during the vocal fold wound healing cascade. For instance, additional cytokines (e.g., pro-apoptotic, pro-survival) may signal or inhibit apoptotic cell death. In fact, it may be possible that cell death is the result of faulty cell mechanisms that fail to function properly. The results of the current study cannot be interpreted

as a direct link between vibration exposure and cell death in the vocal folds. In the present *in vivo* model, an interesting observation is that several tissue specimens from the same animals consistently showed higher intensity staining compared to other animals, which reiterates the notion that there are likely multiple factors that can influence apoptotic cell death after vibration.

Although not studied in this dissertation, the tight intercellular junctional complex may be related to apoptotic cell death. Marchiando and colleagues (2011) observed that epithelial barrier integrity was maintained in the intestine following rearrangement of the tight and adherens junction proteins from the apical toward the basolateral cell membrane. Future research should determine if the tight junctions in the vocal fold epithelium relocate in a similar fashion to prevent compromise of the barrier. Apoptosis is activated by an intrinsic and extrinsic signaling pathway. Unfortunately, the methods in the current study are unable to determine which apoptosis signaling pathway occurs in response to *in vivo* vibration exposure. In the future, experiments with *in vitro* cell populations may provide a more direct answer to determining which pathways are activated or inactivated during vocal fold vibration.

The overall significance of apoptosis in the vocal folds ultimately has clinical application (see Chapter VII: Apoptosis and Vocal Fold Disease: Clinically Relevant Implications of Cell Death). The high frequency of cycles of vocal fold vibration places the epithelium at significant risk of biomechanical injury, and apoptotic cell death could be considered an emerging threat to the epithelial barrier. Thus, it is possible that irregular apoptosis could be involved, at least in part, in the pathogenesis of vocal fold disease. For instance, perhaps abnormally increased rates of apoptosis can lead to bacterial or pathogen invasion, while significantly reduced rates of apoptosis may lead to an excessive accumulation of cells that may develop into vocal fold epithelial hyperplasia or nodular formations. In the long-term arm of this research program,

apoptotic events may become useful biomarkers for the prevention, diagnosis, prognosis, and management of human vocal fold diseases.

Conclusion

The work in this dissertation sought to determine how vocal fold epithelial cells respond to time-doses and cycle-doses of vibration exposure. In addition, this was a preliminary attempt to better understand the relationship between the pro-inflammatory cytokine TNF-α and apoptotic cell death in the vocal fold epithelium. Collectively, findings suggest that 120 minutes of vibration exposure is the required time-dose stimulus to signal the apoptotic cascade in vocal fold epithelial cells. While this critical threshold of vibratory stresses sends a signal for epithelial cells in the vocal folds to die by apoptosis, vocal fold movement for 120 minutes may begin to initiate an earlier phase of apoptosis as measured morphologically by reduced epithelial cell nuclei size. In addition, this is the first attempt from our laboratory to consider the influence of cycle-dose of vibration exposure on apoptosis. The results of this study may serve as a foundation to more accurately characterize the function of vocal fold epithelial cell death, as well as a preliminary step toward determining the potential implications of cell death in vocal fold diseases of epithelial origin.

CHAPTER VII

APOPTOSIS AND VOCAL FOLD DISEASE[55]: CLINICALLY RELEVANT IMPLICATIONS OF CELL DEATH

Overview

Vocal fold diseases affecting the epithelium have a detrimental impact on voice outcomes. Chapter VII briefly reviews the role of apoptotic cell death on normal vocal fold epithelial regulation, implications of cell death on vocal fold wound healing, and a theoretical framework to describe how disorganized apoptosis may contribute to diseases of the vocal folds.

Introduction to Cell Death

Non-keratinized, stratified squamous epithelium comprises the surface cell layer of the membranous true vocal folds. It is believed that healthy vocal fold epithelium is necessary to maintain an optimal environment for periodic vibration (Murray & Thomson, 2012; Tse et al., 2015; Xuan & Zhang, 2014). As such, normal epithelium may be increasingly important in influencing normal voice quality. In contrast, disorganized vocal fold epithelium presents clinically in many voice disorders. Tissue-level changes to the vocal folds are indicative of abnormalities at the cellular level. Macroscopic tissue charges often present as clinical signs of vocal fold pathology (Gray, 2000) and auditory perceptual judgment of dysphonia (e.g., hoarseness). Common voice disorders related to the epithelium include laryngeal SCC, leukoplakia, keratosis, epithelial hyperplasia/thickening, human papilloma virus, and benign

[55] Portions of the work in Chapter VII will be prepared as a review article on apoptosis and vocal fold disease for future submission to a refereed journal.

lesions. Additionally, surgical and medical interventions for voice disorders can adversely interfere with the epithelial layer of the vocal folds. The most notable interventions impacting the epithelium are phonomicrosurgery to remove lesions and radiation therapy to treat head and neck cancer.

The vocal fold epithelium serves several important biological functions that contribute to maintaining a healthy environment for normal vibratory function. Among these functions, the epithelial layer serves as a barrier to protect against external threats to assist with regulating the vocal fold tissue. To promote a strong barrier against insults, an established property of many epithelial tissues is rapid cell turnover (Hooper, 1956; Pellettieri & Sanchez Alvarado, 2007). Cell turnover involves three primary phases of cell death, division, and renewal (Pellettieri & Sanchez Alvarado, 2007). During turnover, differentiated cells are regularly replaced with proliferating cells to maintain tissue morphology and function (Denecker et al., 2001). Specifically, cell death terminates epithelial cells from the apical cell surface (Hooper, 1956).

The most commonly studied type of programmed cell death is apoptosis. Apoptosis is a regulated mechanism that determines which cells are eliminated (Ashkenazi & Dixit, 1998; Denecker et al., 2001; Elmore, 2007). The primary function of cell death is to assist with maintaining tissue homeostasis throughout the development of an organism, such as balancing the rates of cell proliferation and cell death. For instance, cell death serves a physiologic role in normal states by eliminating an excessive number of differentiated epithelial cells that are rapidly replaced with new cells. Therefore, there is substantial benefit to apoptosis during cell turnover, as this systematic approach to removing cells could prevent further damage or faulty cell growth.

Although rapid cell turnover is a common feature of epithelial tissue and that cell death serves a physiologic role in normal states, irregular rates of apoptosis (e.g., excessive, deficient) occur in disease or trauma (Elmore, 2007; Meresman et al., 2000). For instance, increased rates of apoptosis can lead to gaps in the epithelial surface layer. Such gaps may significantly increase the permeability of the epithelial barrier and increase the barrier's susceptibility to outside damage (Gitter, Bendfeldt, Schulzke, & Fromm, 2000; Watson et al., 2009). Irregularities in cell death lead to adverse consequences in cancer, autoimmune disease, and neurological disease (Ashkenazi & Dixit, 1998; Cory & Adams, 2002). Common stimuli that trigger cell death include biomechanical trauma, toxic agents, heat, radiation, hypoxia, and ischemia (Denecker et al., 2001; Elmore, 2007).

Cell Death in Vocal Fold Disease

Understanding the function of apoptosis during wound healing in the vocal folds has implications for diseases of the vocal folds. Apoptosis is indicated in several clinical voice disorders. The most notable vocal fold disease involving apoptosis is laryngeal SCC. Cancer involves simultaneous interactions of uncontrolled cell proliferation and reduced apoptosis (Evan & Vousden, 2001). As such, incessant proliferating cells invade and destroy tissue. Primary tumor and resection biopsies from patients with laryngeal squamous cell carcinoma and epithelial hyperplasia show evidence of apoptosis (Hellquist, 1997; Hirvikoski et al., 1999). These results indicate that apoptosis may be a potentially useful clinical biomarker to predict the survival rate for laryngeal cancer.

A common treatment approach for laryngeal SCC is radiation therapy. Radiation treatment, which may or may not be combined with chemotherapy or surgical intervention,

logically targets the abnormal reduction in apoptotic cell death by causing many cells to die (Johns et al., 2012). Unfortunately, radiation-induced fibrosis often leads to serious complications by perturbing the elasticity required during vocal fold vibration.

Additionally, apoptosis may be involved in benign vocal fold lesions. In contrast to directly detecting apoptosis in the vocal folds, researchers often alluded to apoptosis by describing morphological features consistent with cell death. As an example, benign vocal folds lesions have been characterized by desquamating epithelial cells, shrinking nuclei, and altered chromatin (Dikkers et al., 1993; Kotby et al., 1988; Martins et al., 2011). Such descriptions strongly suggest that apoptosis has implications in the development or maintenance of benign vocal fold lesions.

It is believed that benign vocal fold lesions develop because of too much vibration exposure that eventually reaches a critical threshold of injury. However, this rationale does not explain why only some voice users (e.g., teachers, singers) develop vocal pathology, while others do not. The following section describes a proposed theoretical model which suggests that phonotraumatic vibration exposure may be the result of cell signaling miscommunication, via changes in the normal rate of apoptosis, that could lead to poor wound healing and eventual lesion development.

Theoretical Framework

When a tissue is subjected to injury, the body responds by initiating the wound healing cascade. Wound healing is a complex process that requires a particular series of overlapping events. It is critical for an individual phase to be completed efficiently in order to allow the next phase of wound healing to begin. Such promptness will determine the overall success of a

healed wound. Poor clinical outcomes result when wounds are open for longer durations, as the wound remains persistently inflamed (Greenhalgh, 1998). The wound healing cascade involves an inflammatory, proliferation, and maturation phase. An inflammatory response results in a cessation of blood flow to the wound and increased production of essential inflammatory cell types including neutrophils, macrophages, and lymphocytes (Greenhalgh, 1998). These cells localize to the wounded area to remove contaminants and initiate re-epithelialization (Branski, Verdolini, Sandulache, Rosen, & Hebda, 2006). Next is the proliferation phase, in which there is an upregulation of fibroblasts and increase in collagen production to assist with regaining strength to the structure. It is during this phase when granulation tissue develops. Finally, the maturation phase involves an equal balance between collagen and collagenase production. For several months, there is an increase in vascularity and cellularity. Over time, however, this decreases toward the final stage of repair in which the wound evolves into acellular scar tissue (Greenhalgh, 1998).

Biomechanically-induced forces increase apoptosis. Common mechanical forces trigger apoptosis and other types of cell death in corneal epithelium, intestinal epithelium, cardiovascular system, and neuronal cells (Que & Gores, 1996; Ren & Wilson, 1997; Serbest et al., 2006; Watson et al., 2009; Wernig & Xu, 2002). There is increasing evidence that apoptosis plays a critical role during the wound healing cascade, as it is important to hold a steady balance between cell death and proliferation (Boccafoschi, Sabbatini, Bosetti, & Cannas, 2010; Hooper, 1956; Wernig & Xu, 2002). Apoptosis is believed to be primarily responsible for removing inflammatory cells that are no longer necessary. Removing inflammatory cells reduces the time that the tissue remains inflamed, thereby accelerating the wound healing response and signaling the next stage of cell proliferation (Ellis et al., 1991; Rai et al., 2005). Thus, apoptosis promotes

optimal healing outcomes by reducing excessive scarring and fibrosis (Ellis et al., 1991; Elmore, 2007; Greenhalgh, 1998).

Physiologic Vibration

The first component of the theoretical model reasons that the biomechanical stresses during vibration exposure signal an inflammatory response. This initial construct is based on observations in human vocal folds. Within many normal vocal fold tissues, it has been observed that mild inflammation is present (Gray, 2000). This consistent state of irritation indicates that the vocal folds are capable of regular repair from vibratory-induced injury (Catten, Gray, Hammond, Zhou, & Hammond, 1998). It is very likely that key inflammatory cells in the vocal fold lamina propria are regularly activated in response to vibration exposure. To localize to the site of injury and begin to repair wounded vocal fold tissue, there is likely an increase in cell proliferation of vocal fold fibroblasts, myofibroblasts, neutrophils, and macrophages. If necessary, re-epithelialization can occur at the wound site.

The next step of the theoretical model suggests that as the vocal folds gradually recover from inflammation, the body signals inflammatory cells to undergo apoptotic cell death. Apoptosis itself is not associated with an inflammatory response and is efficient in terms of energy production. Therefore, apoptosis is considered an ideal method for cells to die. While it is possible that necrosis may be involved in wound healing, necrosis would be considered a form of wasted energy (Greenhalgh, 1998). Because cell proliferation increases the number of inflammatory cells, it is reasonable to believe that proliferation also produces new epithelial cells. Thus, apoptosis can eliminate the excessive number of differentiated epithelial cells that are being replaced with new cells.

The final theoretical step purports that during episodes of apoptosis, tight junction proteins subsequently remodel to expand the length of the epithelial barrier to maintain it. This notion is based on previous research in the small intestinal epithelium, in which the rearrangement of the tight intercellular junctional complex during apoptosis may serve to protect the epithelial barrier (Madara, 1990; Marchiando et al., 2011). It is possible that tight junction proteins gradually lose the capability to remodel at a sufficient rate. The change in phenotype of the apical junctional complex may result in enlarged epithelial surface gaps. There is little concern about the emergence of surface gaps in the epithelium because of the increased rate of cell proliferation. In essence, dead cells removed from the epithelial surface are replaced with an appropriate number of newly generated cells. This balance between cell proliferation and cell death is critical to the maintenance of tissue homeostasis during physiologic vibration exposure.

This theory suggests that there is no significant threat to the vocal folds during regular vibratory-induced injury for two primary reasons. First, apoptosis removes inflammatory cells relatively quickly and efficiently. In addition, epithelial surface gaps are resealed almost immediately after being formed because of the equilibrium between proliferation and death. This theory is based on the idea that vocal fold tissue undergoes regular cycles of inflammation and recovery during normal, physiologic vibration exposure. This is a potential explanation for why the majority of the population can produce voice without significant disturbances in voice quality.

Phonotraumatic Vibration

During wound healing, it is critical to hold a steady balance between cell proliferation and death. For example, autoimmune diseases result in an excessive rate of apoptosis of immune cells, leading to the inability to effectively protect against infections (Greenhalgh, 1998). The

balance between both mechanisms of cell turnover is fundamental in understanding health and disease (Boccafoschi et al., 2010; Wernig & Xu, 2002). In particular, proliferation and death must occur at a reasonably similar rate to properly maintain tissue homeostasis (Hooper, 1956). The proposed theoretical framework takes this concept into consideration to describe what cellular interactions occur during phonotraumatic vibration exposure and the development of vocal pathology.

It has previously been speculated that vibration exposure is on a continuum that eventually reaches a critical threshold of injury (Branski et al., 2006). It is believed by some scientists and clinicians that benign vocal fold disease develops because of too much exposure to vibration in terms of duration and magnitude. Unfortunately, this rationale does not explain why some people develop pathology and why some do not. However, the current theoretical model suggests that phonotraumatic vibration is the result of cell signaling miscommunication. Signaling disruption suggests that vocal fold cells are unable to effectively communicate that inflammatory cells have increased and therefore, cannot properly initiate apoptotic cell death to begin. Perhaps a signal for apoptosis is accidentally turned off. As a result, there is a significant decrease in the rate of apoptosis and inflammatory cells cannot be eliminated quickly enough to reach the next stage of wound healing. This cell signaling problem can lead to poor wound healing and the development of vocal fold scar tissue or benign lesions.

The theory reasons that there may be a substantial change in the rate of apoptosis from physiologic to phonotraumatic vibration. While vibration typically involves a sufficient rate of apoptosis during normal wound healing, it is believed that vocal fold disruption is the result of significantly reduced apoptosis. The chronic non-healing state is subjected to further biomechanical stresses during phonotraumatic vibration. Rather than progressing from

granulation to scar, irregularities in apoptosis could eventually evolve into benign nodular formations (i.e., vocal fold nodules) and subsequent scar tissue (Greenhalgh, 1998; Rai et al., 2005).

During the cell proliferation stage, it is critical for cells to be continually removed to maintain a balance during cell turnover. Apoptosis is involved in tissue changing from granulation to scar (Rai et al., 2005). Granulation tissue needs to reduce its cellular components to properly evolve into scar tissue. As such, interruption in the proliferation phase may delay the development of granulation tissue. If there is no epithelial covering (i.e., re-epithelialization), inflammation will persist, resulting in prolonged wound healing and a chronic non-healing state. In addition, if there is a delay in signaling the downregulation of fibroblasts and myofibroblasts, apoptosis is also disrupted. This can lead to a problem of excessive scar formation (Greenhalgh, 1998). In comparison to previous beliefs about phonotraumatic vibration, the above theory of cell signaling miscommunication better explains the pathogenesis of vocal pathology.

Conversely, abnormalities in apoptotic cell death may perhaps predict that particular individuals have a greater susceptibility for developing voice disorders. If this were the case, biomarkers for apoptosis would potentially be useful for clinical prediction and prevention by identifying which professional voice users (e.g., teachers, singers) are more likely to develop future voice problems. Therefore, preventative strategies could be implemented among such identified individuals, who would benefit from early education about proper vocal health and voice care.

REFERENCES

Aggarwal, B. B., Gupta, S. C., & Kim, J. H. (2012). Historical perspectives on tumor necrosis factor and its superfamily: 25 years later, a golden journey. *Blood, 119*(3), 651-665.

Al-Sadi, R., Khatib, K., Guo, S., Ye, D., Youssef, M., & Ma, T. (2011). Occludin regulates macromolecule flux across the intestinal epithelial tight junction barrier. *Am J Physiol Gastrointest Liver Physiol, 300*(6), G1054-1064.

ApopTag Fluorescein In Situ Apoptosis Detection Kit (2012).

Ashkenazi, A., & Dixit, V. M. (1998). Death receptors: Signaling and modulation. *Science, 281*(5381), 1305-1308.

Awan, S. N. (2001). *The voice diagnostic protocol: A practical guide to the diagnosis of voice disorders*. Gaithersburg, MD: Pro-Ed/Aspen Publishers.

Bartlett, R. S., Gaston, J. D., Yen, T. Y., Ye, S., Kendziorski, C., & Thibeault, S. L. (2015). Biomechanical screening of cell therapies for vocal fold scar. *Tissue Eng Part A, 21*(17-18), 2437-2447.

Bartlett, R. S., Jette, M. E., King, S. N., Schaser, A., & Thibeault, S. L. (2012). Fundamental approaches in molecular biology for communication sciences and disorders. *J Speech Lang Hear Res, 55*(4), 1220-1231.

Behrman, A., Sulica, L., & He, T. (2004). Factors predicting patient perception of dysphonia caused by benign vocal fold lesions. *Laryngoscope, 114*(10), 1693-1700.

Berchtold, C. M., Coughlin, A., Kasper, Z., & Thibeault, S. L. (2013). Paracrine potential of fibroblasts exposed to cigarette smoke extract with vascular growth factor induction. *Laryngoscope, 123*(9), 2228-2236.

Boccafoschi, F., Sabbatini, M., Bosetti, M., & Cannas, M. (2010). Overstressed mechanical stretching activates survival and apoptotic signals in fibroblasts. *Cells Tissues Organs, 192*(3), 167-176.

Bortner, C. D., Hughes, F. M., Jr., & Cidlowski, J. A. (1997). A primary role for K+ and Na+ efflux in the activation of apoptosis. *J Biol Chem, 272*(51), 32436-32442.

Bortner, C. D., Oldenburg, N. B., & Cidlowski, J. A. (1995). The role of DNA fragmentation in apoptosis. *Trends Cell Biol, 5*(1), 21-26.

Bradley, R. M. (2000). Sensory receptors of the larynx. *Am J Med, 108 Suppl 4a*, 47s-50s.

Branski, R. C., Rosen, C. A., Verdolini, K., & Hebda, P. A. (2004). Markers of wound healing in vocal fold secretions from patients with laryngeal pathology. *Ann Otol Rhinol Laryngol, 113*(1), 23-29.

Branski, R. C., Rosen, C. A., Verdolini, K., & Hebda, P. A. (2005). Biochemical markers associated with acute vocal fold wound healing: A rabbit model. *J Voice, 19*(2), 283-289.

Branski, R. C., Verdolini, K., Sandulache, V., Rosen, C. A., & Hebda, P. A. (2006). Vocal fold wound healing: A review for clinicians. *J Voice, 20*(3), 432-442.

Brenner, D., Blaser, H., & Mak, T. W. (2015). Regulation of tumour necrosis factor signalling: Live or let die. *Nat Rev Immunol, 15*(6), 362-374.

Bruning, T., Bartsch, R., Bolt, H. M., Desel, H., Drexler, H., Gundert-Remy, U., . . . van Thriel, C. (2014). Sensory irritation as a basis for setting occupational exposure limits. *Arch Toxicol, 88*(10), 1855-1879.

Bucca, C. B., Bugiani, M., Culla, B., Guida, G., Heffler, E., Mietta, S., . . . Brussino, L. (2011). Chronic cough and irritable larynx. *J Allergy Clin Immunol, 127*(2), 412-419.

Catten, M., Gray, S. D., Hammond, T. H., Zhou, R., & Hammond, E. (1998). Analysis of cellular location and concentration in vocal fold lamina propria. *Otolaryngol Head Neck Surg, 118*(5), 663-667.

Chen, X., & Thibeault, S. L. (2010). Role of tumor necrosis factor-alpha in wound repair in human vocal fold fibroblasts. *Laryngoscope, 120*(9), 1819-1825.

Cohen, S. M., Kim, J., Roy, N., Asche, C., & Courey, M. (2012). Direct health care costs of laryngeal diseases and disorders. *Laryngoscope, 122*(7), 1582-1588.

Cory, S., & Adams, J. M. (2002). The Bcl2 family: Regulators of the cellular life-or-death switch. *Nat Rev Cancer, 2*(9), 647-656.

de Medeiros, A. M., Assuncao, A. A., & Barreto, S. M. (2012). Absenteeism due to voice disorders in female teachers: A public health problem. *Int Arch Occup Environ Health, 85*(8), 853-864.

Denecker, G., Vercammen, D., Declercq, W., & Vandenabeele, P. (2001). Apoptotic and necrotic cell death induced by death domain receptors. *Cell Mol Life Sci, 58*(3), 356-370.

Dikkers, F. G., Hulstaert, C. E., Oosterbaan, J. A., & Cervera-Paz, F. J. (1993). Ultrastructural changes of the basement membrane zone in benign lesions of the vocal folds. *Acta Otolaryngol, 113*(1), 98-101.

Dinarello, C. A. (2000). Proinflammatory cytokines. *Chest, 118*(2), 503-508.

Dowdall, J. R., Sadow, P. M., Hartnick, C., Vinarsky, V., Mou, H., Zhao, R., . . . Rajagopal, J. (2015). Identification of distinct layers within the stratified squamous epithelium of the adult human true vocal fold. *Laryngoscope, 125*(9), E313-319.

Durkes, A., & Sivasankar, M. P. (2015). In vivo investigation of acidified pepsin exposure to porcine vocal fold epithelia. *Laryngoscope*.

Edinger, A. L., & Thompson, C. B. (2004). Death by design: Apoptosis, necrosis and autophagy. *Curr Opin Cell Biol, 16*(6), 663-669.

Ellis, R. E., Yuan, J. Y., & Horvitz, H. R. (1991). Mechanisms and functions of cell death. *Annu Rev Cell Biol, 7*, 663-698.

Elmore, S. (2007). Apoptosis: A review of programmed cell death. *Toxicol Pathol, 35*(4), 495-516.

Evan, G. I., & Vousden, K. H. (2001). Proliferation, cell cycle and apoptosis in cancer. *Nature, 411*(6835), 342-348.

Fiers, W., Beyaert, R., Declercq, W., & Vandenabeele, P. (1999). More than one way to die: Apoptosis, necrosis and reactive oxygen damage. *Oncogene, 18*(54), 7719-7730.

Fisher, K. V., Telser, A., Phillips, J. E., & Yeates, D. B. (2001). Regulation of vocal fold transepithelial water fluxes. *J Appl Physiol (1985), 91*(3), 1401-1411.

Ganz, T. (2002). Epithelia: Not just physical barriers. *Proc Natl Acad Sci U S A, 99*(6), 3357-3358.

Gaston, J., Quinchia Rios, B., Bartlett, R., Berchtold, C., & Thibeault, S. L. (2012). The response of vocal fold fibroblasts and mesenchymal stromal cells to vibration. *PLoS One, 7*(2), e30965.

Gates, R., Forrest, L. A., & Obert, K. (2013). *The owner's manual to the voice: A guide for singers and other professional voice users*. New York, NY: Oxford University Press.

Ge, P. J., French, L. C., Ohno, T., Zealear, D. L., & Rousseau, B. (2009). Model of evoked rabbit phonation. *Ann Otol Rhinol Laryngol, 118*(1), 51-55.

Gitter, A. H., Bendfeldt, K., Schulzke, J. D., & Fromm, M. (2000). Leaks in the epithelial barrier caused by spontaneous and TNF-alpha-induced single-cell apoptosis. *Faseb j, 14*(12), 1749-1753.

Gown, A. M., & Willingham, M. C. (2002). Improved detection of apoptotic cells in archival paraffin sections: Immunohistochemistry using antibodies to cleaved caspase 3. *J Histochem Cytochem, 50*(4), 449-454.

Gray, S., & Titze, I. (1988). Histologic investigation of hyperphonated canine vocal cords. *Ann Otol Rhinol Laryngol, 97*(4 Pt 1), 381-388.

Gray, S. D. (2000). Cellular physiology of the vocal folds. *Otolaryngol Clin North Am, 33*(4), 679-698.

Greenhalgh, D. G. (1998). The role of apoptosis in wound healing. *Int J Biochem Cell Biol, 30*(9), 1019-1030.

Gregory, C. D., & Devitt, A. (2004). The macrophage and the apoptotic cell: An innate immune interaction viewed simplistically? *Immunology, 113*(1), 1-14.

Hellquist, H. B. (1997). Apoptosis in epithelial hyperplastic laryngeal lesions. *Acta Otolaryngol Suppl, 527*, 25-29.

Hirano, M. (1974). Morphological structure of the vocal cord as a vibrator and its variations. *Folia Phoniatr (Basel), 26*(2), 89-94.

Hirvikoski, P., Kumpulainen, E., Virtaniemi, J., Pirinen, R., Salmi, L., Halonen, P., . . . Kosma, V. M. (1999). Enhanced apoptosis correlates with poor survival in patients with laryngeal cancer but not with cell proliferation, bcl-2 or p53 expression. *Eur J Cancer, 35*(2), 231-237.

Hooper, C. E. (1956). Cell turnover in epithelial populations. *J Histochem Cytochem, 4*(6), 531-540.

Imaizumi, M., Thibeault, S. L., & Leydon, C. (2014). Classification for animal vocal fold surgery: Resection margins impact histological outcomes of vocal fold injury. *Laryngoscope, 124*(11), E437-444.

Ishizaka, K., & Flanagan, J. L. (1972). Synthesis of voiced sounds from a two-mass model of the vocal cords. *Bell System Technical Journal, 51*(6), 1233–1268.

Jiang, J., Lin, E., & Hanson, D. G. (2000). Vocal fold physiology. *Otolaryngol Clin North Am, 33*(4), 699-718.

Jiang, J., Verdolini, K., Aquino, B., Ng, J., & Hanson, D. (2000). Effects of dehydration on phonation in excised canine larynges. *Ann Otol Rhinol Laryngol, 109*(6), 568-575.

Jiang, J. J., & Titze, I. R. (1994). Measurement of vocal fold intraglottal pressure and impact stress. *J Voice, 8*(2), 132-144.

Jiao, H., Wang, Z., Liu, Y., Wang, P., & Xue, Y. (2011). Specific role of tight junction proteins claudin-5, occludin, and ZO-1 of the blood-brain barrier in a focal cerebral ischemic insult. *J Mol Neurosci, 44*(2), 130-139.

Johns, M. M., Kolachala, V., Berg, E., Muller, S., Creighton, F. X., & Branski, R. C. (2012). Radiation fibrosis of the vocal fold: From man to mouse. *Laryngoscope, 122 Suppl 5*, S107-125.

Khan, M. M. (2008). *Immunopharmacology*. New York. NY: Springer Publishing.

Khosla, S., Murugappan, S., Paniello, R., Ying, J., & Gutmark, E. (2009). Role of vortices in voice production: Normal versus asymmetric tension. *Laryngoscope, 119*(1), 216-221.

Kimura, K., Teranishi, S., Kawamoto, K., & Nishida, T. (2011). Protective effect of dexamethasone against hypoxia-induced disruption of barrier function in human corneal epithelial cells. *Exp Eye Res, 92*(5), 388-393.

King, S. N., Chen, F., Jette, M. E., & Thibeault, S. L. (2013). Vocal fold fibroblasts immunoregulate activated macrophage phenotype. *Cytokine, 61*(1), 228-236.

King, S. N., Guille, J., & Thibeault, S. L. (2015). Characterization of the leukocyte response in acute vocal vold injury. *PLoS One, 10*(10), e0139260.

King, S. N., Hanson, S. E., Chen, X., Kim, J., Hematti, P., & Thibeault, S. L. (2014). In vitro characterization of macrophage interaction with mesenchymal stromal cell-hyaluronan hydrogel constructs. *J Biomed Mater Res A, 102*(3), 890-902.

Klemuk, S. (2008). Rheometers, bioreactors, and vocalization forces: Using basic science investigations to help the voices of teachers. *Perspectives on Voice and Voice Disorders, 18*(3), 119-225.

Kojima, T., Valenzuela, C. V., Novaleski, C. K., Van Deusen, M., Mitchell, J. R., Garrett, C. G., . . . Rousseau, B. (2014). Effects of phonation time and magnitude dose on vocal fold epithelial genes, barrier integrity, and function. *Laryngoscope, 124*(12), 2770-2778.

Kojima, T., Van Deusen, M., Jerome, W. G., Garrett, C. G., Sivasankar, M. P., Novaleski, C. K., & Rousseau, B. (2014). Quantification of acute vocal fold epithelial surface damage with increasing time and magnitude doses of vibration exposure. *PLoS One, 9*(3), e91615.

Kotby, M. N., Nassar, A. M., Seif, E. I., Helal, E. H., & Saleh, M. M. (1988). Ultrastructural features of vocal fold nodules and polyps. *Acta Otolaryngol, 105*(5-6), 477-482.

Kreiman, J., & Sidtis, D. (2011). *Foundations of voice studies: An interdisciplinary approach to voice production and perception*. San Diego, CA: Wiley-Blackwell.

Lalaoui, N., Lindqvist, L. M., Sandow, J. J., & Ekert, P. G. (2015). The molecular relationships between apoptosis, autophagy and necroptosis. *Semin Cell Dev Biol, 39*, 63-69.

Lee, Y. C., Kim, H. J., Kim, K. S., Choi, S., Kim, S. W., Park, H. K., & Eun, Y. G. (2015). Investigation of nanostructural changes following acute injury using atomic force microscopy in rabbit vocal folds. *Microsc Res Tech, 78*(7), 569-576.

Levendoski, E. E., Leydon, C., & Thibeault, S. L. (2014). Vocal fold epithelial barrier in health and injury: A research review. *J Speech Lang Hear Res, 57*(5), 1679-1691.

Leydon, C., Bartlett, R. S., Roenneburg, D. A., & Thibeault, S. L. (2011). Localization of label-retaining cells in murine vocal fold epithelium. *J Speech Lang Hear Res, 54*(4), 1060-1066.

Leydon, C., Sivasankar, M., Falciglia, D. L., Atkins, C., & Fisher, K. V. (2009). Vocal fold surface hydration: A review. *J Voice, 23*(6), 658-665.

Li, N. Y., Heris, H. K., & Mongeau, L. (2013). Current understanding and future directions for vocal fold mechanobiology. *J Cytol Mol Biol, 1*(1), 001.

Li, N. Y., Verdolini, K., Clermont, G., Mi, Q., Rubinstein, E. N., Hebda, P. A., & Vodovotz, Y. (2008). A patient-specific in silico model of inflammation and healing tested in acute vocal fold injury. *PLoS One, 3*(7), e2789.

Lim, X., Tateya, I., Tateya, T., Munoz-Del-Rio, A., & Bless, D. M. (2006). Immediate inflammatory response and scar formation in wounded vocal folds. *Ann Otol Rhinol Laryngol, 115*(12), 921-929.

Long, J. L. (2010). Tissue engineering for treatment of vocal fold scar. *Curr Opin Otolaryngol Head Neck Surg, 18*(6), 521-525.

Lungova, V., Verheyden, J. M., Herriges, J., Sun, X., & Thibeault, S. L. (2015). Ontogeny of the mouse vocal fold epithelium. *Dev Biol, 399*(2), 263-282.

Macara, I. G., Guyer, R., Richardson, G., Huo, Y., & Ahmed, S. M. (2014). Epithelial homeostasis. *Curr Biol, 24*(17), R815-825.

Madara, J. L. (1990). Maintenance of the macromolecular barrier at cell extrusion sites in intestinal epithelium: Physiological rearrangement of tight junctions. *J Membr Biol, 116*(2), 177-184.

Majno, G., & Joris, I. (1995). Apoptosis, oncosis, and necrosis: An overview of cell death. *Am J Pathol, 146*(1), 3-15.

Marcelino, F. C., & Oliveira, D. T. (2005). Histopathological changes of vocal folds induced by chronic pollutant exposure: An experimental study. *J Voice, 19*(4), 529-533.

Marchiando, A. M., Graham, W. V., & Turner, J. R. (2010). Epithelial barriers in homeostasis and disease. *Annu Rev Pathol, 5*, 119-144.

Marchiando, A. M., Shen, L., Graham, W. V., Edelblum, K. L., Duckworth, C. A., Guan, Y., . . . Watson, A. J. (2011). The epithelial barrier is maintained by in vivo tight junction expansion during pathologic intestinal epithelial shedding. *Gastroenterology, 140*(4), 1208-1218.e1201-1202.

Martinez, M. M., Reif, R. D., & Pappas, D. (2010). Detection of apoptosis: A review of conventional and novel techniques. *Analytical Methods, 2*(8), 996-1004.

Martini, F. H. (1998). *Fundamentals of anatomy and physiology* (4th ed.). Upper Saddle River, NJ: Prentice Hall, Inc.

Martins, R. H., Defaveri, J., Custodio Domingues, M. A., de Albuquerque, E. S. R., & Fabro, A. (2010). Vocal fold nodules: Morphological and immunohistochemical investigations. *J Voice, 24*(5), 531-539.

Martins, R. H., Defaveri, J., Domingues, M. A., & de Albuquerque e Silva, R. (2011). Vocal polyps: Clinical, morphological, and immunohistochemical aspects. *J Voice, 25*(1), 98-106.

Maximow, A. A., & Bloom, W. (1952). *A textbook for histology* (6th ed.). Philadelphia, PA: W.B. Saunders Company.

McInnes, I. B. (2013). *Cytokines* (Firestein, S. E. Gabriel, I. B. McInnes, & J. R. O'Dell, Ed. 9th ed.). Philadelphia, PA: Elsevier Saunders.

Mehta, D. D., Van Stan, J. H., Zanartu, M., Ghassemi, M., Guttag, J. V., Espinoza, V. M., . . . Hillman, R. E. (2015). Using ambulatory voice monitoring to investigate common voice disorders: Research update. *Front Bioeng Biotechnol, 3*, 155.

Meresman, G. F., Vighi, S., Buquet, R. A., Contreras-Ortiz, O., Tesone, M., & Rumi, L. S. (2000). Apoptosis and expression of Bcl-2 and Bax in eutopic endometrium from women with endometriosis. *Fertil Steril, 74*(4), 760-766.

Murray, P. R., & Thomson, S. L. (2012). Vibratory responses of synthetic, self-oscillating vocal fold models. *J Acoust Soc Am, 132*(5), 3428-3438.

National Institute on Deafness and Other Communication Disorders (NIDCD) 2012-2016 Strategic Plan. Retrieved from https://www.nidcd.nih.gov/about/plans/2012-2016/Pages/2012-2016-Strategic-Plan.aspx

Novaleski, C. K., Mizuta, M., & Rousseau, B. (accepted for publication). Evaluation of dying vocal fold epithelial cells by ultrastructural features and TUNEL method. *Cells Tissues Organs*.

Panayiotidis, M. I., Bortner, C. D., & Cidlowski, J. A. (2006). On the mechanism of ionic regulation of apoptosis: Would the Na+/K+-ATPase please stand up? *Acta Physiol (Oxf), 187*(1-2), 205-215.

Patel, R. R., Walker, R., & Sivasankar, P. M. (2015). Spatiotemporal quantification of vocal fold vibration after exposure to superficial laryngeal dehydration: A preliminary study. *J Voice*, doi: 10.1016/j.jvoice.2015.07.009. [Epub ahead of print].

Pellettieri, J., & Sanchez Alvarado, A. (2007). Cell turnover and adult tissue homeostasis: From humans to planarians. *Annu Rev Genet, 41*, 83-105.

Que, F. G., & Gores, G. J. (1996). Cell death by apoptosis: Basic concepts and disease relevance for the gastroenterologist. *Gastroenterology, 110*(4), 1238-1243.

Rai, N. K., Tripathi, K., Sharma, D., & Shukla, V. K. (2005). Apoptosis: A basic physiologic process in wound healing. *Int J Low Extrem Wounds, 4*(3), 138-144.

Rath, P. C., & Aggarwal, B. B. (1999). TNF-induced signaling in apoptosis. *J Clin Immunol, 19*(6), 350-364.

Ren, H., & Wilson, G. (1997). The effect of a shear force on the cell shedding rate of the corneal epithelium. *Acta Ophthalmol Scand, 75*(4), 383-387.

Rodriguez-Boulan, E., & Macara, I. G. (2014). Organization and execution of the epithelial polarity programme. *Nat Rev Mol Cell Biol, 15*(4), 225-242.

Ross, M. H., Kaye, G. I., & Pawlina, W. (2003). *Histology: A text and atlas* (4th Ed.). Baltimore, MD: Lippincott Williams & Wilkins.

Rousseau, B., Suehiro, A., Echemendia, N., & Sivasankar, M. (2011). Raised intensity phonation compromises vocal fold epithelial barrier integrity. *Laryngoscope, 121*(2), 346-351.

Roy, N., Merrill, R. M., Gray, S. D., & Smith, E. M. (2005). Voice disorders in the general population: Prevalence, risk factors, and occupational impact. *Laryngoscope, 115*(11), 1988-1995.

Sbarbati, A., Merigo, F., Benati, D., Tizzano, M., Bernardi, P., & Osculati, F. (2004). Laryngeal chemosensory clusters. *Chem Senses, 29*(8), 683-692.

Serbest, G., Horwitz, J., Jost, M., & Barbee, K. (2006). Mechanisms of cell death and neuroprotection by poloxamer 188 after mechanical trauma. *Faseb j, 20*(2), 308-310.

Solomon, N. P., Glaze, L. E., Arnold, R. R., & van Mersbergen, M. (2003). Effects of a vocally fatiguing task and systemic hydration on men's voices. *J Voice, 17*(1), 31-46.

Story, B. H., & Titze, I. R. (1995). Voice simulation with a body-cover model of the vocal folds. *J Acoust Soc Am, 97*(2), 1249-1260.

Strieter, R. M., Kunkel, S. L., & Bone, R. C. (1993). Role of tumor necrosis factor-alpha in disease states and inflammation. *Crit Care Med, 21*(10 Suppl), S447-463.

Swanson, E. R., Ohno, T., Abdollahian, D., Garrett, C. G., & Rousseau, B. (2010). Effects of raised-intensity phonation on inflammatory mediator gene expression in normal rabbit vocal fold. *Otolaryngol Head Neck Surg, 143*(4), 567-572.

Tao, C., Jiang, J. J., & Zhang, Y. (2006). Simulation of vocal fold impact pressures with a self-oscillating finite-element model. *J Acoust Soc Am, 119*(6), 3987-3994.

Tateya, I., Tateya, T., Lim, X., Sohn, J. H., & Bless, D. M. (2006). Cell production in injured vocal folds: A rat study. *Ann Otol Rhinol Laryngol, 115*(2), 135-143.

Thibeault, S. L., & Duflo, S. (2008). Inflammatory cytokine responses to synthetic extracellular matrix injection to the vocal fold lamina propria. *Ann Otol Rhinol Laryngol, 117*(3), 221-226.

Titze, I. R. (1994). Mechanical stress in phonation. *J Voice, 8*(2), 99-105.

Titze, I. R., & Hunter, E. J. (2015). Comparison of vocal vibration-dose measures for potential-damage risk criteria. *J Speech Lang Hear Res, 58*(5), 1425-1439.

Titze, I. R., Hunter, E. J., & Svec, J. G. (2007). Voicing and silence periods in daily and weekly vocalizations of teachers. *J Acoust Soc Am, 121*(1), 469-478.

Titze, I. R., Svec, J. G., & Popolo, P. S. (2003). Vocal dose measures: Quantifying accumulated vibration exposure in vocal fold tissues. *J Speech Lang Hear Res, 46*(4), 919-932.

Tizzano, M., Cristofoletti, M., Sbarbati, A., & Finger, T. E. (2011). Expression of taste receptors in solitary chemosensory cells of rodent airways. *BMC Pulm Med, 11*, 3.

Van Den Berg, J. (1958). Myoelastic-aerodynamic theory of voice production. *J Speech Hear Res, 1*(3), 227-244.

Varfolomeev, E. E., & Ashkenazi, A. (2004). Tumor necrosis factor: An apoptosis JuNKie? *Cell, 116*(4), 491-497.

Verdolini Abbott, K., Li, N. Y., Branski, R. C., Rosen, C. A., Grillo, E., Steinhauer, K., & Hebda, P. A. (2012). Vocal exercise may attenuate acute vocal fold inflammation. *J Voice, 26*(6), 814.e811-813.

Verdolini, K., Druker, D. G., Palmer, P. M., & Samawi, H. (1998). Laryngeal adduction in resonant voice. *J Voice, 12*(3), 315-327.

Verdolini, K., Rosen, C. A., Branski, R. C., & Hebda, P. A. (2003). Shifts in biochemical markers associated with wound healing in laryngeal secretions following phonotrauma: A preliminary study. *Ann Otol Rhinol Laryngol, 112*(12), 1021-1025.

Walensky, L. D. (2006). BCL-2 in the crosshairs: Tipping the balance of life and death. *Cell Death Differ, 13*(8), 1339-1350.

Watson, A. J., Duckworth, C. A., Guan, Y., & Montrose, M. H. (2009). Mechanisms of epithelial cell shedding in the Mammalian intestine and maintenance of barrier function. *Ann N Y Acad Sci, 1165*, 135-142.

Welham, N. V., Lim, X., Tateya, I., & Bless, D. M. (2008). Inflammatory factor profiles one hour following vocal fold injury. *Ann Otol Rhinol Laryngol, 117*(2), 145-152.

Wernig, F., & Xu, Q. (2002). Mechanical stress-induced apoptosis in the cardiovascular system. *Prog Biophys Mol Biol, 78*(2-3), 105-137.

Williams, D. B., & Carter, C. B. (2009). *Transmission electron microscopy: A textbook for materials science* (2nd Ed.). New York, NY: Springer Science.

Wilson, S. E., & Kim, W. J. (1998). Keratocyte apoptosis: Implications on corneal wound healing, tissue organization, and disease. *Invest Ophthalmol Vis Sci, 39*(2), 220-226.

Xuan, Y., & Zhang, Z. (2014). Influence of embedded fibers and an epithelium layer on the glottal closure pattern in a physical vocal fold model. *J Speech Lang Hear Res, 57*(2), 416-425.

You, K., Xu, X., Fu, J., Xu, S., Yue, X., Yu, Z., & Xue, X. (2012). Hyperoxia disrupts pulmonary epithelial barrier in newborn rats via the deterioration of occludin and ZO-1. *Respir Res, 13*, 36.

Zhuang, P., Sprecher, A. J., Hoffman, M. R., Zhang, Y., Fourakis, M., Jiang, J. J., & Wei, C. S. (2009). Phonation threshold flow measurements in normal and pathological phonation. *Laryngoscope, 119*(4), 811-815.

Appendix A

Institutional Animal Care and Use Committee Protocol M/14/207 Approval Letter

December 18, 2014
IACUC New Protocol

Approval Letter

Principal Investigator:	Rousseau, Bernard
Protocol ID#:	M/14/207
Title:	Apoptosis Signaling In Vocal Fold Epithelium In Response To Acute Phonotrauma....

The request of the new protocol referenced above has been approved by the Institutional Animal Care and Use Committee. The life of this protocol is three years. If there are modifications to this protocol, please present the changes to IACUC for approval prior to implementing them.

Type of Review:	New Protocol
Date Approved:	12/18/2014
Next Review:	12/18/2015 (due for continuing review)
Expiration Date:	12/18/2017

Appendix B

Light Microscopy Images of Immunohistochemical Caspase-3 Staining of Vocal Fold Epithelium

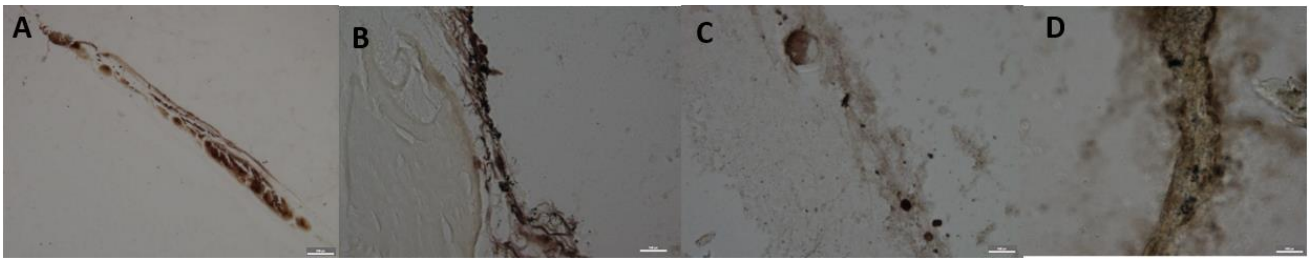

Appendix C

Hematoxylin and Eosin Staining of Paraffin Sections of Tracheal Epithelium